Bypassing androgen pathway dependence in advanced prostate cancer

Eric Gregory Bluemn

A dissertation

submitted in partial fulfillment of the

requirements for the degree of

Doctor of Philosophy

University of Washington

2012

Reading Committee:

Peter Nelson, Chair

William Grady

Marshall Horwitz

Program Authorized to Offer Degree:

Molecular and Cellular Biology

University of Washington

Abstract

Bypassing androgen pathway dependence in advanced prostate cancer.

Eric Gregory Bluemn

Chair of the Supervisory Committee:
Professor
Peter S. Nelson

Continued reliance of castration-resistant prostate cancer (CRPC) on androgen receptor (AR) signaling has spurred the development of novel, potent antiandrogen therapeutics. The clinical use of successively more potent antiandrogens will likely generate CRPC that is independent of AR-driven pathways for survival. This is corroborated by an increase in AR-null neuroendocrine-like prostate cancers (NEPCa) following extended androgen deprivation therapy (ADT). However, there are currently no models of epithelial-like Androgen Pathway-Independent Prostate Cancer (APIPC) that have been generated from previously AR-positive models. We took a two-step approach to study APIPC in more detail: **Aim 1)** Utilize high-throughput functional genomics to screen for genes/pathways regulating ligand-independent CRPC growth and **Aim 2)** Develop a cell-line model of APIPC from an AR-positive cell line through Total Androgen Pathway Suppression, and identify the emergent growth pathway sufficient for androgen pathway-independent growth. In **Aim 1** we identified a protein phosphatase 2A (PP2A) regulatory subunit (PPP2R2C) as a suppressor of CRPC growth. Using *in vitro* molecular biology we demonstrated that loss of PPP2R2C promotes non-AR-mediated castration-resistant growth in previously androgen-dependent cell lines. We also found that PPP2R2C expression is downregulated in primary and metastatic prostate tumors compared to benign prostate epithelia. Furthermore, investigation of retrospective outcomes from patients surgically treated for primary prostate cancer indicated that low PPP2R2C expression is associated with a poor prognosis. **Aim 2** successfully led to the

development of an APIPC model cell line that does not express AR or androgen-regulated genes, and relies on an autocrine growth pathway for androgen-free survival. Furthermore, it does not express markers of neuroendocrine prostate cancer, a well-defined AR-null prostate cancer variant. By analyzing a panel of human metastases, we were able to identify a subset of tumors that also do not express AR, androgen-regulated genes, or markers of neuroendocrine prostate cancer. These data suggest that metastatic prostate tumors can compensate for total loss of androgen receptor signaling by deregulating alternative growth and survival pathways *in vitro* and *in vivo.* Our results identify signaling pathways that may be targeted to inhibit the development of AR-null disease.

TABLE OF CONTENTS

List of Figures

List of Tables

Acknowledgements

The following body of work has been a collaborative effort, and could not have been completed without guidance and assistance from many individuals. My graduate advisor, Peter Nelson, has played a tremendous role in managing both the development of this project and my development as a scientist. By challenging my ideas but also allowing me to hold autonomy over my projects, Pete has taught me to function independently as a researcher. I am extremely grateful for the resources, time, and effort that he has invested in my training over the past five years. Other members of the Nelson lab, including Daniella Bianchi, Ilsa and Roger Coleman, James Dean, Ruthy Dumpit, Ryan Gordon, Susana Hernandez Lopez, Jared Lucas, and Sophie Spencer directly contributed technical assistance and expertise. Their contributions and support have impacted both my scientific development and the successful completion of these projects.

Several collaborators also deserve acknowledgement. Carla Grandori and James Annis at the University of Washington Quellos High Throughput Screening Core were very helpful in designing and performing high-throughput siRNA screening experiments. Brigham Mecham's expertise in analyzing high-throughput datasets has been immensely helpful, and his patience in explaining statistical methods to molecular biologists was much appreciated. Other investigators provided cell lines and patient tissue including Robert Vessella (University of Washington), Christopher Porter (Virginia Mason), and Paul Rennie (University of British Columbia). Without their contributions these projects would not have been possible. I am also very grateful for the advice and time investment received from my thesis committee members: William Grady, Marshall Horwitz, David Morris, Valera Vasioukhin.

Financial support for this work was graciously provided by the University of Washington Medical Scientist Training Grant and a Department of Defense Prostate Cancer Pre-Doctoral Fellowship (W81XWH-10-1-0133).

Dedication

To my mother.
I could not have completed this work without your love, patience, and support.

Chapter 1: Overview of metastatic prostate cancer resistance to androgen receptor targeted therapeutics.

Introduction

Prostate cancer is the second leading cause of cancer death in American men and mortality remains high despite improvements in therapy (1). While the majority of primary prostate tumors are treated successfully via radical prostatectomy or external beam radiotherapy, some tumors progress to invasive and disseminated disease. Patients with metastatic prostate cancer are treated with androgen deprivation therapy (ADT), through either chemical or surgical castration. ADT initially results in a median 2-3 years regression of disease, however metastatic tumors uniformly recur in a castrate-resistant (CR) form (2). Castration-resistant prostate cancer (CRPC) is generally incurable with existing treatment approaches.

Because ADT is initially effective and there is copious evidence supporting the re-expression of androgen-regulated signaling in CRPC, most investigational therapies have focused on developing a more potent blockade of androgen receptor (AR) transcriptional activity and the synthesis of androgenic ligands (2). Recent studies have provided important insights that involve deciphering AR signaling and regulation, identifying mechanisms of intratumoral androgen maintenance, and the development of novel therapies directed toward the AR pathway. These and other conceptual advances support the exploration of new mechanisms by which prostate tumors may escape androgen dependence when challenged with aggressive selection against AR-mediated signaling.

AR Signaling in CRPC

AR signaling is critical to the development of the normal prostate and in the progression from primary to metastatic disease. Continued reliance on AR signaling for survival is a hallmark of CRPC, demonstrated by re-expression of androgen regulated genes (ARGs) after castration (2) and the susceptibility of tumors refractory to conventional ADT to more potent androgen pathway inhibitors (3-

5). Therefore, discovering mechanisms of AR expression and AR-driven transcription in tumor cells treated with ADT is imperative.

Androgen deprivation therapy. Androgen signaling in CRPC is inhibited by 1) preventing steroid hormone production and 2) direct inhibition of the AR with small molecules. First-line hormonal therapy focuses on inhibiting testicular androgen production via surgical removal of the testes (bilateral orchiectomy) or by treating patients with supraphysiologic doses of gonadotropin-releasing hormone designed to inhibit upstream mediators of testosterone production via negative feedback mechanisms (6, 7).

To treat recurrent AR-dependent CRPC, small molecule inhibitors were developed that directly target AR and enzymes involved in steroid hormone production. Bicalutamide is a non-steroidal AR antagonist that has been shown to improve symptoms and increase survival in men with CRPC (8). Unfortunately, bicaluatmide is a relatively weak AR inhibitor and can act as an AR agonist in some situations (9). Also, the testes are not the only site of androgen production – the adrenal glands produce a significant amount of weak androgens, which are thought to bind AR and stimulate ARG transcription. Extra-testicular steroid hormone production has been targeted with non-specific CYP17 enzyme inhibitors such as ketoconazole, resulting in a very modest decrease in serum androgens (10). Continued AR-dependent growth and incomplete inhibition of AR activity and ligand production has led investigators to pursue more potent inhibitors targeting the AR and steroidogenesis pathways, discussed in more detail below.

Regulation of AR Expression. AR is commonly overexpressed in CRPC, an observation partly explained by genomic amplification of the AR locus: AR genomic amplification and overexpression is found in ~60% of CRPC tumors (11). Alternative mechanisms for AR upregulation were recently identified (Figure 1). Analysis of androgen-dependent (AD) prostate cancer cell lines identified an AR-regulated enhancer element located within the second intron of AR. Low AR signaling activates the

enhancer and results in upregulated AR expression. Restoration of AR signaling causes AR to bind the enhancer and recruit lysine-specific demethylase 1 (LSD1). LSD1 represses transcription, demonstrating a negative feedback program that limits endogenous AR expression in normal tissues (12). However, when AD prostate cancer cell lines are grown under castrate-levels of androgen, low AR transcriptional activity results in upregulated AR expression. Increased AR maintains residual ARG expression.

Tumor suppressor loss also stimulates AR expression in prostate cancer. Two independent studies identified widespread genomic loss of retinoblastoma (Rb) in primary tumors (~5%) and CRPC (35%) (11), with a loss of Rb protein in 74% of CRPC (13). Loss of normal Rb function enhanced LNCaP xenograft growth in castrate mice. Upon further investigation, this survival benefit was not mediated by losing classical Rb tumor suppressor function, but through an alternate mechanism that upregulated E2F1 expression. In Rb-deficient cells E2F1 is recruited to the AR regulatory locus resulting in increased AR expression and transcriptional activity, maintaining the AR transcriptional program (13).

Regulation of AR Transcriptional Activity. The activity and specificity of nuclear steroid hormone receptors is determined by cofactor binding (14). A recent large-scale genomic analysis of primary and metastatic tumors found a novel AR cofactor, NCOA2, to be upregulated in a subset of primary (8%) and metastatic tumors (37%). Follow-up experiments in LNCaP cells found that NCOA2 expression correlated with an increased AR transcriptional response to dihydrotestosterone (DHT**)**. NCOA2 overexpression in primary tumors correlated with a higher risk of recurrence, linking AR activity in primary tumors to future mortality (11).

In addition to globally increased AR activity, altered AR signaling in CRPC includes a change in transcriptional targets. The first published example of an alternative transcriptional program came from experiments comparing ARGs in the AD cell model LNCaP and its CR subline LNCaP-abl. Wang *et al* discovered that the androgen-regulated transcriptional program in LNCaP-abl was enriched for genes promoting M-phase progression, notably ubiquitin-conjugating enzyme E2C (UBE2C). UBE2C expression

was also found to be upregulated in clinical CRPC (15). Other studies have identified a shift towards pro-mitotic gene expression in conjunction with decreased AR signaling. However, the investigators hypothesized that increased mitosis resulted from a decrease in the pro-differentiation role of AR, and not a global change in the specific genes regulated by AR (12, 13).

AR Splice Variants. AR splice variants (ARVs) encoding ligand-binding-domain (LBD) deficient receptors are a newly discovered mechanism for ADT resistance. ARVs were initially discovered in the CWR22R xenograft line, and have since been identified in the VCaP cell line, LuCaP xenografts, the Myc-CaP mouse models of prostate cancer and clinical CRPC (15-18). While previous studies suggested that ARVs are able to function independently of full-length AR (AR^{FL}), work by Watson *et al* demonstrated that several ARVs were dependent on AR^{FL} heterodimerization for nuclear translocation and transcriptional activity, and could be inhibited by LBD-targeting antiandrogens (18).

Sun *et al* identified a previously undiscovered ARV in LuCaP xenografts, AR^{v567es}. AR^{v567es} is missing LBD exons 5-7, but retains the hinge region necessary for nuclear translocation (19) and is constitutively localized to the nucleus. In contrast to the activity of other known variants, AR^{v567es} is less dependent on AR^{FL} for transcriptional activity, and even upregulates AR^{FL} expression. Furthermore, LNCaP cells expressing exogenous AR^{v567es} co-expressed a subset of ARGs in a ligand-independent fashion, suggesting a mechanism for CR growth. There are also specific genes transcribed in LNCaP expressing exogenous AR^{v567es} that are not found in control LNCaP, suggesting a novel transcriptional program regulated by this AR variant (17, 20).

To date, two ARVs identified in human cancer (AR-V7, AR^{v567es}) and one identified in a mouse model (mAR-V4) significantly enhance ADT survival in prostate cell lines and are upregulated in response to castration (17, 18). Those ARVs dependent on AR^{FL} for transcriptional activity (AR-V7 and mAR-V4) are sensitive to AR^{FL} inhibitors (18). There are no published data regarding the sensitivity of AR^{v567es} to blockade with more potent antiandrogens. However, LBD-binding antiandrogens are unlikely to inhibit

the function of LBD-deficient ARV homodimers. Because AR^{v567es} translocates to the nucleus and transcribes ARGs in the absence of AR^{FL}, and is the most commonly expressed variant in clinical CRPC (17), it is necessary to develop therapeutics that effectively inhibit AR activity through a non-LBD mechanism.

Maintenance of Intratumoral Androgens

Extra-testicular androgen production occurs in adrenal glands and *de novo* in models of CRPC (21-24). The efficacy of steroid synthesis inhibitors in clinical trials supports the importance of extra-testicular ligand production in clinical disease (25) and there is emerging evidence suggesting that active steroid transport also plays a role in ADT resistance.

Androgen Synthesis. Two novel mechanisms of upregulating androgen biosynthesis were discovered by studying AD prostate cancer models. In one pathway, Lock *et al* investigated androgen-stimulated cholesterol-ester production in prostate cancer. They discovered that cholesterol-esters are broken down into cholesterol and fatty acid in response to ADT. Fatty acid is further converted to arachidonic acid (AA), which initiates a transcription program that increases steroid acute regulatory protein (StAR) expression. StAR co-localizes with CYP11A on the mitochondrial membrane and catalyzes the rate-limiting step in steroid biosynthesis: conversion of cholesterol to pregnenelone. Further investigation demonstrated increased expression of steroidogenic enzymes and *de novo* steroid synthesis in androgen-deprived LNCaP cells that were stimulated with exogenous AA (22).

Hyperinsulinemia, a clinically-observed side-effect of ADT, can activate an alternative intratumoral steroid biosynthesis pathway. Insulin treatment was sufficient to induce steroid biosynthesis in the three most widely-used AD prostate cancer cell lines. Following insulin stimulation, intracellular and secreted steroids were present in levels sufficient to induce ARG expression. Importantly, insulin upregulated the expression of StAR (23), similar to the result of AA stimulation (22), revealing a common, and potentially druggable target in intratumoral androgen synthesis.

Androgen Transport. Steroid hormones enter cells primarily via passive diffusion through the plasma membrane, but several studies now indicate that active transport by organic anion-transport polypeptides (OATP super-family, encoded by the SLCO gene family) contribute to ADT resistance. OATPs transport many known drugs, including steroid hormones (26). Therefore, it was clinically significant when mRNA profiling of CRPC tumors identified a subgroup of men whose tumors overexpressed SLCO family transporters. Further analysis of two independent patient cohorts indicated that SLCO2B1 and SLCO1B3 expression were associated with a shorter time to disease progression (27), and higher rates of prostate specific mortality (28).

The associations of SLCO2B1 and SLCO1B3 variants with higher mortality are clinically significant because they are both androgen transporters (29, 30), however SNP variants in each gene are associated with differential rates of steroid transport. Cell-line experiments showed contrasting levels of dihydroepiandosterone (DHEAS) transport between 3 SLCO2B1 SNP variants. Researchers also noted that SLCO1B3 SNP variants were not associated with shorter patient time to progression in isolation, but interacted with SLCO2B1 high-DHEAS transport SNP variants to decrease patient time to progression (27).

AR Interactions with oncogenic signaling pathways

Inactivation of the PTEN tumor suppressor is one of the most common abnormalities found in prostate cancers (11). PTEN inactivation de-regulates PI3K/AKT signaling and leads to the activation of multiple survival and proliferation pathways. The interaction between increased PI3K/AKT signaling and AR signaling is complex. While early studies suggested that AKT phosphorylation of AR repressed androgen-mediated transcription (31), most literature suggests that PI3K/ATK activation results in a net increase in proliferation and ARG expression (32). However, recent publications suggest a more complex feedback loop between PTEN, PI3K/AKT signaling, and AR activity**.**

Two independent reports using the PTEN conditionally-null mouse model incorporated PTEN/AKT-mediated AR-suppression into a feedback loop. While both groups found that PTEN deletion reduces AR expression, the mechanism varied. Carver *et al* proposed a model where AR activity was upregulated by HER kinase activation, and HER kinases were inhibited by AKT activity (33). Therefore, PTEN loss and increased AKT signaling inhibited HER kinases, decreasing AR activity (Figure 2). Previously published studies on HER kinase activation in human models of prostate cancer reported HER kinase activity *decreased* AR expression (34), yet clinical trials of HER inhibitors as monotherapy in CRPC has demonstrates a decrease in serum PSA in some patients (35, 36). This may be the result of reduced tumor burden or decreased AR activity. Clearly, the effect of HER kinase activity in prostate cancer is poorly understood and further investigation is needed.

A second model, proposed by Mullholland *et al*, suggests that PTEN deletion, independent of AKT, actively represses AR expression. Furthermore, a mouse model with a conditional deletion of AR in prostate epithelium caused an *increase* in PTEN-null cell proliferation (32). While proposing different mechanisms, the significant contribution of these publications is evidence that AKT activation combined with PTEN loss is sufficient for prostate tumor growth in the absence of robust AR signaling, and may actively repress the AR program. Thus, further reduction in AR activity by more potent ADT might select for tumors with activated PI3K/AKT/mTOR signaling and little or no residual AR activity.

AR Pathway-Directed Therapies

AR-dependent CRPC results from an incomplete response of metastatic tumors to current therapeutics designed to suppress AR ligands or directly interfere with AR activation. The development of more potent novel antiandrogens and androgen synthesis inhibitors is ongoing, and there are several new therapeutics in clinical trials.

Antiandrogens. Conventional AR antagonists offer incomplete inhibition of AR action, and exhibit partial agonist activity in the presence of mutated AR or high concentrations of inhibitor. More

potent inhibitors lacking agonist activity are necessary. A promising novel antiandrogen, MDV-3100, recently completed a Phase I/II trial in 140 patients with CRPC. Of patients treated, 56% experienced a >50% decrease in serum PSA, and imaging demonstrated that 22% of patients with soft tissue metastasis and 56% of patients with bony metastasis saw a stabilization of disease. Furthermore, there was no evidence of agonist activity and dose-related fatigue was the most common side effect (4).

Most AR antagonist development has targeted the C-terminal LBD, a domain that is lost in ARVs (17, 18). The AR N-terminal domain contains the DNA-binding elements common to both AR^{FL} and ARVs. Thus, inhibition of all AR forms could potentially be accomplished via N-terminal disruption. Anderson *et al* recently reported studies of a novel small-molecule N-terminal AR inhibitor, EPI-001. EPI-001 specifically binds the AR N-terminus and disrupts transcription and protein-protein interactions. Preliminary investigation showed that EPI-001 treatment caused decreased ARG expression and inhibited LNCaP xenograft growth in intact mice. Furthermore, EPI-001 inhibited LBD-deficient ARV activity (5). While not yet ready for clinical trials, EPI-001 is a significant discovery that will serve as a lead compound to identify other AR N-terminal inhibitors.

Androgen Synthesis Inhibitors. Recently, a Phase III trial was completed that demonstrated improved outcomes in patients treated with abiraterone acetate, an irreversible CYP17A inhibitor. 1195 patients previously treated with docetaxel received a combination of abiraterone/prednisone or placebo/prednisone. Overall survival was significantly increased in patients treated with abiraterone (14.8 months) versus patients treated with placebo (10.9 months). All other secondary endpoints (PSA response, time to PSA progression, progression-free survival) were also improved in the abiraterone treatment group. Furthermore, the side effect profile was limited to the effects of mineralocorticoid excess (25).

While abiraterone-resistant tumors have not yet been evaluated from men who relapsed during abiraterone treatment, mechanisms of resistance have been investigated *in vivo* using prostate cancer

xenografts. Reminiscent of AR-inhibitor trials, *in vivo* abiraterone resistance appears to occur via upregulation of the drug target, CYP17A, along with higher expression of ARV or mutated AR (21, 24). This underscores a continued reliance on AR-mediated transcriptional pathways, suggesting that combination therapy targeting the AR receptor and CYP17A might evoke a more prolonged therapeutic response. Alternatively, combination therapy may eliminate those cells still relying on AR-mediated signaling and promote the emergence of AR-pathway independent disease reliant on alternative growth and survival pathways.

Conclusions

The heterogeneous nature of CRPC makes treatment very challenging, although a common feature involves the activation and re-expression of the AR program following ADT. However, the molecular mechanisms resulting in ARG re-expression are diverse. Current literature suggests that tumors re-express ARGs following ADT by: 1) Upregulation of the targeted pathway (e.g. CYP17) or 2) Activation of an alternative pathway of resistance—of which there appear to be several, or 3) Both. It is important that future work focus on the development of additional ligand and synthesis inhibitors, in addition to investigating combination therapy between different ADT modalities (androgen synthesis inhibitors with more potent AR antagonists, for example). Targeting newly implicated ADT resistance mechanisms – such as ARVs, NCOA2, and StAR – in combination with existing therapy may act to further suppress CRPC.

A potential application of these results would be to tailor therapy to prostate cancer subtypes. For example, ADT use in primary prostate cancer has mixed results and is associated with significant morbidity (7). If clinicians used tumor biopsies to rationally select patients with AR-enhancing pathways for early ADT, perhaps subgroups could be identified who are likely to respond better to early ADT. Those patients expressing molecular signatures indicative of a poor ADT response might be better

treated with adjuvant chemotherapy or rationally-directed inhibitors of non-AR growth pathways (such as PI3K).

Finally, there is emerging experimental and clinical evidence of prostate tumors that completely escape dependence on AR (32, 33, 37). It is plausible that aggressive negative selection against AR-driven pathways – through combination of emerging treatments or the development of novel inhibitors - may select for truly androgen-pathway independent prostate tumors.

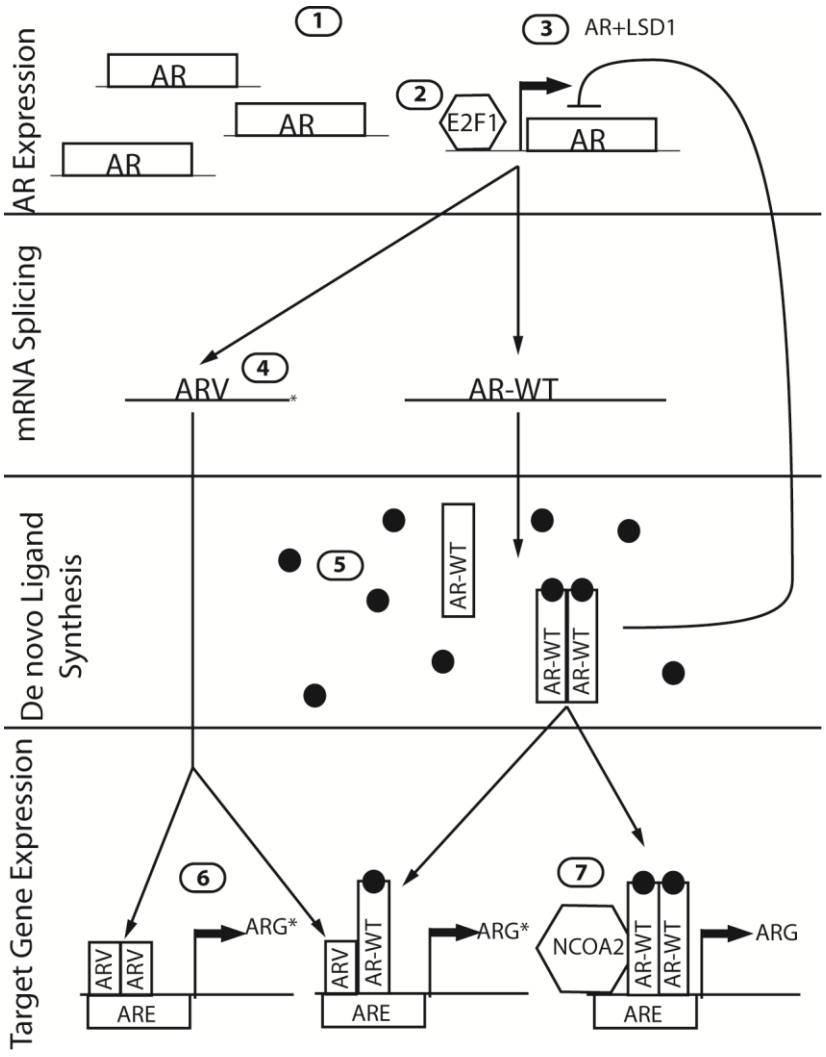

Figure 1: Mechanisms of AR pathway activation in CRPC. 1) AR gene amplification. 2) Rb increases E2F1 activity and AR transcription. 3) Low AR activity leads to increased AR expression via an enhancer element. Increased AR transcriptional activity recruits LSD1 to exert negative feedback on this pathway. 4) mRNA splicing generates LBD-deficient AR variants. 5) Extra-testicular ligand production maintains AR transcriptional activity. 6) ARVs induce ligand-independent expression of ARGs. ARG* represents the differential transcription program activated by some ARVs. 7) AR cofactors, such as NCOA2, amplify the magnitude of AR signaling.

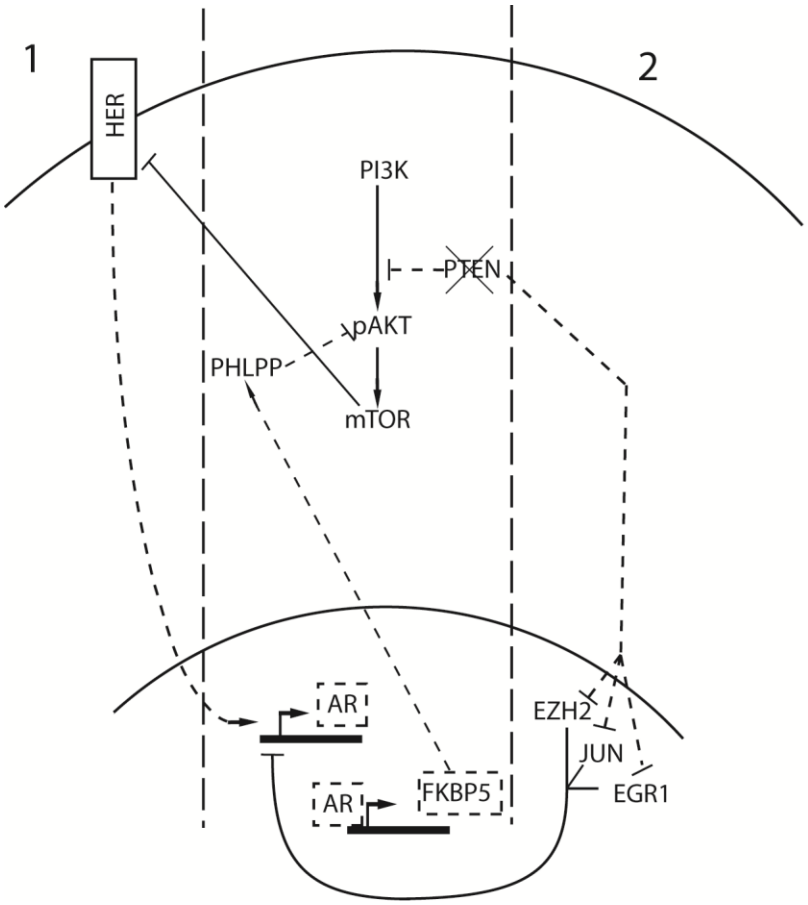

Figure 2: Feedback pathways of AR, PTEN, and PI3K. AR transcriptional activity represses PI3K signaling through the expression of FKBP5. FKBP5 facilitates the dephosphorylation of AKT by PHLPP. PTEN loss, common in prostate cancer, increases PI3K pathway activity and may also repress AR. Two prominent hypotheses explaining the mechanism of PI3K activity and AR repression are presented. 1) Carver *et al* hypothesize that HER kinases induce expression of AR, and increased PI3K signaling inhibits HER kinases in an mTOR-dependent fashion. This decreases AR expression (33). 2) Mullholland *et al* propose a mechanism by which PTEN negatively regulates the expression and activity of a number of proteins (EZH2, JUN, EGR1). PTEN loss deregulates these proteins, repressing AR expression (32). Dashed lines indicate pathways where activity is downregulated by PTEN loss.

Chapter 2: PPP2R2C downregulation promotes castration-resistant growth *in vitro* and is associated with increased prostate cancer-specific mortality.

Introduction

Recurrent castration-resistant prostate cancer (CRPC) continues to rely on androgen receptor (AR)-mediated transcriptional programs for growth and survival. However, there is mounting evidence that suggests alternative pathway activation may be sufficient for CRPC survival through mechanisms that are independent of AR-mediated transcription. This alternative signaling is highlighted in several recent *in vitro* and *in vivo* studies which have suggested that PI3K pathway activation is sufficient for CRPC survival in the absence of an active AR signaling pathway (32, 33). Furthermore, with clinical efforts focused on extinguishing AR activity, additional androgen pathway-independent resistance mechanisms are likely to emerge.

To identify additional genes and pathways that contribute to prostate cancer growth in the absence of AR signaling we performed *in vitro* high-throughput RNAi screening (HTRS) using a pre-arrayed "Druggable Genome" siRNA library. This siRNA library targets 6650 individual genes representing several major ontology classes including cellular kinases, phosphatases, transcription factors, and growth factor receptors. We hypothesized that a network of genes existed that, when lost, would confer a castration-resistant phenotype in prostate cancer cell lines previously dependent upon androgen-mediated signaling for growth and survival. To emphasize clinically-relevant tumor suppressors, HTRS results were cross-referenced with a gene expression dataset collected from benign and cancerous prostate tissue. This evaluation revealed that a subset of *protein phosphatase 2A* (PP2A) components were enriched in the HTRS experiments and downregulated in primary and metastatic prostate cancer.

PP2A is a highly conserved serine/threonine phosphatase that has a broad spectrum of biologic roles including the negative regulation of signal transduction, cell cycle progression, and gene expression (38,

39). The PP2A holoenzyme is comprised of a core dimer – consisting of a catalytic subunit (PPP2CA/PPP2CB) and a structural subunit (PPP2R1A/PPP2R1B) – which form a heterotrimeric complex with a "B" subunit. The B subunit originates from one of 18 genes grouped into four structurally unrelated families and is thought to dictate substrate specificity, cellular localization, and enzymatic activity of the PP2A complex (40).

Loss of PP2A activity is often a transforming event, which is perhaps most obvious in cells expressing the SV40 small t antigen (SV40ST) viral oncogene. SV40ST competes with B subunits to bind the PPP2C-PPP2R1 heterodimer(41); SV40ST binding is required for viral transformation(42). Additionally, non-viral mechanisms of PP2A inhibition are well documented in a wide variety of human cancers, and *de novo* inactivating mutations have been identified in each subunit class of the PP2A holoenzyme (38). In prostate cancer, decreased expression of the catalytic subunit PPP2CA and B-regulatory subunit PPP2R2A has been observed in some primary tumors (43, 44). Subsequent mechanistic studies revealed that loss of PPP2CA function was sufficient for castration-resistant growth *in vitro* (45).

By utilizing HTRS we identified additional PP2A family members that, when downregulated, induce *in vitro* castration-resistant growth in androgen-dependent prostate cancer cell lines. Loss of one B-regulatory subunit, PPP2R2C, was confirmed to function independently of AR-regulated pathways in subsequent follow-up experiments. In addition, investigation of a primary prostate cancer cohort revealed that PPP2R2C expression is decreased in prostate tumors, and loss of PPP2R2C protein expression is correlated with poor outcomes in clinical disease.

Results

High throughput RNAi screening identifies suppressors of castration-resistant growth.

In vitro HTRS was performed in two androgen-sensitive prostate cancer cell lines, LNCaP and VCaP. Briefly, cells were cultured in 384-well plates in media supplemented with charcoal-dextran stripped

fetal bovine serum (CSS) in order to simulate androgen deprivation therapy. Transfection of the Sigma Druggable Genome siRNA library was used to inhibit translation of 6650 individual genes (three equimolar siRNAs targeting a specific gene, one gene target per well), and cell number was estimated using Cell Titer-Glo luminescence reagent.

Raw luminescence signal intensity from the HTRS screen was transformed into Z-scores within each plate, and median standardized Z-scores for each gene were used in downstream analysis. Setting a significance threshold of $Z \geq 1.96$, we identified 380 siRNAs in LNCaP and 240 siRNAs in VCaP that induced castration-resistant growth; 42 siRNAs induced castration-resistant growth in both cell lines (Figure 3).

PPP2R2C and PPP2R1A are downregulated in primary and metastatic prostate cancer

To prioritize HTRS hits exhibiting potential tumor-suppressor expression patterns, we cross-referenced HTRS experimental results with a gene expression dataset collected from laser-capture microdissected benign prostate epithelia, primary prostate tumors, and CRPC metastases. Out of the 42 tumor suppressor genes identified in the *in vitro* HTRS, 14 genes were significantly downregulated in primary and metastatic prostate cancer compared to benign prostate epithelia. Two of these 14 genes were components of the PP2A complex, implicating PP2A phosphatase activity in the negative regulation of CRPC growth (Figure 4). Specifically, the mean expression of PPP2R2C in primary prostate cancer and metastatic tumors was 3.85-fold lower ($p=0.034$) and 5.69-fold lower ($p<0.001$) than benign prostate epithelia, respectively. PPP2R1A expression was also decreased in primary (1.06-fold, $p<0.001$) and metastatic prostate tumors (1.55-fold, $p<0.001$).

HTRS experimental results and microarray gene expression data were investigated for evidence of other PP2A components behaving as tumor suppressors. In contrast with existing reports (43, 44), PPP2CA and PPP2R2A were not downregulated in primary prostate cancer. However, PPP2CA was significantly

upregulated in metastatic disease (1.9-fold, p<0.001; Figure 5A). Furthermore, knockdown of PPP2CA or PPP2R2A did not induce significant castration-resistant growth in the HTRS experiments (Figure 5B).

PPP2R2C was selected for further investigation because of the following criteria: 1) Four of the 16 PP2A subunits that were tested in the HTRS experiments induced castration-resistant proliferation in at least one cell line (Figure 5B), 2) Knockdown of PPP2R2C induced significant castration-resistant proliferation in both cell lines, and 3) PPP2R2C was the HTRS hit found to be most downregulated in castration-resistant disease compared to benign epithelia.

Knockdown of PPP2R2C induces castration-resistant prostate cancer growth independent of androgen receptor activity.

Because the HTRS experiments were performed using an equimolar pool of three siRNA targeting each gene, we confirmed individual siRNA efficacy by transfecting LNCaP and VCaP with the deconvoluted pool of PPP2R2C siRNAs (#1-3). PPP2R2C knockdown in androgen-depleted LNCaP cells resulted in a 42% (siRNA #2, p<0.001) and 72% (siRNA #3, p<0.001) increase in growth compared to the scrambled control. PPP2R2C knockdown in androgen-depleted VCaP cells increased growth by approximately 33% (siRNA #2 and siRNA #3, p<0.001). PPP2R2C knockdown with siRNA #1 did not affect proliferation in either cell line (Figure 6A). Successful knockdown of PPP2R2C by gene-specific siRNA was confirmed by qRT-PCR. PPP2R2C expression in LCNaP showed a 6.6-fold and 5.9-fold knockdown by siRNA #2 and siRNA #3 (p<0.001), respectively (Figure 6C). qRT-PCR in transfected VCaP demonstrated a 11.3-fold by siRNA #2 and 9.4-fold knockdown by siRNA #3 (p<0.001) (Figure 6D). A decrease in PPP2R2C protein expression was confirmed by immunoblot (Figure 6E).

To assess the role of AR-regulated signaling in growth induced by PPP2R2C downregulation, LNCaP and VCaP cells cultured under androgen-depleted conditions were co-treated with PPP2R2C-specific siRNA and MDV3100, an AR inhibitor. MDV3100 treatment did not alter the effect of PPP2R2C knockdown in

LNCaP or VCaP (Figure 6B). Therefore, we concluded that loss of PPP2R2C must mediate *in vitro* castration-resistant prostate cancer proliferation through a non-AR mediated mechanism.

Because many mechanisms of castration-resistance function through ligand-independent upregulation of AR transcription and transcriptional activity, we also assessed the expression of AR and the canonical androgen regulated gene prostate-specific antigen (PSA) by qRT-PCR. AR expression was largely unaffected by PPP2R2C knockdown, with the exception of a 44% decrease in AR expression ($p<0.001$) when VCaP was transfected by PPP2R2C siRNA #2. LNCaP PSA expression decreased 25-30% in response to PPP2R2C knockdown ($p=0.04$), while PSA expression in VCaP did not change (Figure 6C, Figure 6D). This suggests that PPP2R2C knockdown does not induce growth by upregulating AR expression or increasing ligand-independent AR-mediated transcription.

PPP2R2C knockdown does not mediate growth through activation of cSRC, PI3K, or ERK1/2 signal transduction.

Previous experimentation in non-epithelial cancer models indicated that PPP2R2C may negatively regulate c-Src activity (46). In both *in vitro* and *in vivo* prostate cancer, increased c-Src activity is postulated to promote CRPC growth (47, 48). Therefore, we hypothesized that PPP2R2C knockdown mediated castration-resistant growth in LNCaP and VCaP cells by increasing c-Src phosphorylation. However, knockdown of PPP2RC did not result in c-Src phosphorylation changes (Figure 7A) and treatment with the c-Src inhibitor Dasatainib failed to inhibit castration-resistant growth induced by PPP2R2C knockdown (Figure 7B). Therefore, these data indicate that castration-resistant growth in LNCaP and VCaP cell lines following PPP2R2C knockdown is not mediated through c-Src activity.

Because PPP2R2C knockdown did not alter c-Src activity, we evaluated protein phosphorylation in alternative signal transduction pathways thought to influence CRPC growth. Specifically, we investigated the phosphorylation of AKT and *extracellular signal regulated kinase 1/2* (ERK1/2) (32, 49).

Knockdown of PPP2R2C did not result in observable changes in phospho-AKT or phospho-ERK1/2 when compared to the scrambled control siRNA (Figure 7A). To confirm that PPP2R2C knockdown did not induce growth through PI3K or ERK1/2 activation, cells were co-treated cells with small molecule inhibitors and siRNA targeting PPP2R2C. Inhibition of PI3K with LY294002, or MEK with U0126, failed to abrogate growth-induction mediated by PPP2R2C knockdown (Figure 7C, Figure 7D). Therefore, it appears that PPP2R2C knockdown deregulates a target distinct from PI3K, ERK1/2, or c-SRC signal transduction pathways.

Decreased PPP2R2C expression in primary tumors is correlated with disease relapse and PCSM.

Because PPP2R2C downregulation promotes *in vitro* castration-resistant growth, we hypothesized that PPP2R2C expression in primary prostate tumors might influence long-term disease outcome. To explore this hypothesis, IHC staining for PPP2R2C was performed on the Virginia Mason Prostate Cancer Survival Tissue Microarray (VM-TMA). The VM-TMA is composed of tissue from 100 patients treated for primary prostate cancer by surgical resection. Following surgery, patients were monitored for prostate cancer-specific clinical outcomes such as biochemical relapse, local recurrence, distant metastases, and PCSM. This TMA is a powerful and unique resource to assess PPP2R2C expression in primary prostate cancer, and to assess the impact of PPP2R2C expression on prostate cancer-specific morbidity and mortality.

IHC performed on the VM-TMA was evaluated for PP2R2C staining intensity by a genitourinary pathologist on a scale from 0-3, with a score of 0 representing no PPP2R2C staining and a score of 3 representing high-intensity nuclear staining (Figure 8). Consistent with the microarray expression data, we observed that PPP2R2C expression was higher in benign tissue (mean nuclear intensity = 2.04/3) than in primary prostate tumors (mean nuclear intensity = 1.74/3, p=0.001; Table 2). We analyzed the impact of nuclear PPP2R2C expression on prostate cancer morbidity and mortality using the Proc Mixed model in SAS (SAS 9.3, Cary, NC) adjusted for patient pre-surgical serum PSA levels and tumor stage at

the time of prostatectomy. While PPP2R2C expression was not correlated with the recurrence of local disease, lower PPP2R2C nuclear staining was significantly correlated with the risk of biochemical relapse ($p=0.006$) and the development of distant metastases ($p<0.001$). We also observed that PCSM was correlated with low PPP2R2C protein expression ($p=0.048$; Table 3). A logrank test comparing Kaplan-Meier survival curves for patients with tumors expressing high PPP2R2C (mean staining intensity ≥ 1) and those with low PPP2R2C (mean staining intensity <1) found them to be statistically different. Examination of these survival curves (Figure 9) revealed a survival advantage in those patients whose tumors expressed high levels of PPP2R2C ($p=0.045$).

Discussion

PP2A is a known tumor suppressor and loss of phosphatase activity or altered substrate specificity occurs in several human malignancies(38). Decreased PP2A activity is sufficient for castration-resistant growth in the LNCaP cell line, and PPP2CA expression is decreased in the castration-resistant LNCaP derivative C4-2b (45). However, complete loss of PPP2CA expression can be detrimental to cancer cell growth (41), suggesting that PPP2CA expression plays a dual role in promoting survival and negatively regulating proliferation. Considering that the SV40ST oncogene promotes cell transformation by inhibiting B-subunit binding without initiating apoptosis (42), it is likely that loss of select PP2A B-subunits could alter PP2A substrate specificity and promote tumorigenesis while avoiding the apoptotic effect of total PPP2CA loss. Knock-down of individual PP2A regulatory B-subunits has demonstrated differential effects on cell transformation (38, 41), an effect replicated these HTRS experiments (Figure 5B). Investigation into transforming B-subunit losses has demonstrated patterns of growth pathway deregulation similar to those observed during inhibition of PP2A catalytic activity and those induced by SV40ST oncogene expression (41).

Here, we provide the first *in vitro* data demonstrating that decreased expression of PPP2R2C promotes CRPC growth. Surprisingly, growth induction was not mediated by the upregulation of AR or androgen-

regulated genes, and growth was not inhibited by treatment with MDV3100. These data strongly suggest that PPP2R2C loss activates growth and survival pathways that bypass traditional ADT. Therefore, we expected to see PPP2R2C loss in a subset of clinical CRPC.

Decreased PPP2R2C expression in prostate tumors compared to benign epithelia was confirmed in two separate clinical datasets. Furthermore, multivariate regression analysis demonstrated a statistically significant association between decreased PPP2R2C expression, disease relapse, and increased PCSM. Kaplan-Meier survival estimates indicated that low PPP2R2C expression in primary tumors is associated with decreased long-term survival. To our knowledge, this is the first evidence suggesting that PPP2R2C loss is a risk factor in human malignancy and cancer-specific death.

The effect of PPP2R2C expression on PP2A substrate specificity is largely unknown. However, PPP2R2C has been shown to negatively regulate c-Src activity in osteosarcoma cells (46). Surprisingly, PPP2R2C downregulation did not alter c-Src pathway activity in prostate cell lines. This discrepancy may be due to tissue-specific differences in subcellular localization of the PP2A complex. In osteosarcoma cells, investigators detected perinuclear expression of PPP2R2C (46). In contrast, PPP2R2C demonstrated distinct nuclear localization in prostatic tissue (Figure 8).

Subsequent mechanistic studies will be required to identify specific PP2A targets mediated by PPP2R2C expression in prostatic tissue. Since PP2A directly regulates the activity of more than 50 kinases and other known proto-oncogenes (such as c-myc) (38, 39), this will likely require extensive proteomics-based experiments with an emphasis on deregulated survival and growth pathways found in clinical CRPC. Identification of small molecule inhibitors of the growth pathway(s) activated by PPP2R2C loss may prove useful as a therapeutic in men with CRPC, or as neoadjuvant therapy in men with downregulated PPP2R2C in primary disease.

Materials and Methods

Cell Culture and siRNA Transfection. LNCaP and VCaP cell lines were obtained from ATCC (Manassas, VA, USA) and maintained in phenol red-free RPMI1640 + 10% Fetal Bovine Serum (FBS) (Life Technologies, Grand Island, NY, USA) + 1%PenStrep (Life Technologies). One day prior to transfection cells were passaged in Optimem (Life Technologies) supplemented with 3% CSS onto Matrix Screen Mate tissue culture-treated 384 well plates (Thermo Scientific, Hudson, NH, USA) using the densities determined during the feasibility study on a on a FluidX XRD384 peristaltic liquid handler (Boston, MA, USA) in a total well volume of 50µL.

Experimental working plates were prepared by first stamping 10µM siRNA library stocks into dry 384 well Abgene 1055-384 well microarray plates (Thermo Scientific) using a Vario workstation (Cybio, Jena, Germany) equipped with a 25µL 384-well tip head. A sidecar plate containing UNI1 non-targeting control, Kif11, and assay specific controls (Sigma-Aldrich, St. Louis, MO, USA) was then replicated on each experimental working plate on the Cybio Vario workstation. Optimem and Lipofectamine RNAiMax (Life Technologies) were added to the experimental working plates on a FluidX XRD384 peristaltic liquid handler using predefined metrics determined via the Quellos HTS Feasibility assay. Transfections were carried out by adding 5µL for VCAP and 0.625µL for LNCAP respectively from each experimental working plate onto 3 replicate cell plates using the CyBio Vario workstation.

Cell viability was assessed after the 96-hour incubation with the addition of Cell Titer-Glo (Promega, Madison, WI, USA) on the FluidX 384 liquid handler. Luminescence was read using an Envision HTS multilabel reader (Perkin Elmer, Waltham, MA, USA).

Deconvoluted siRNA experiments were performed in 96-well plates using transfection conditions scaled-up from 384-well experiments in a total volume of 125µl. Kif11, UNI1 non-targeting control, and PPP2R2C-targeting siRNA were purchased from Sigma-Aldrich. 96 hours after transfection cell viability

was assessed by adding Cell Titer-Glo and measuring luminescence on a Synergy2 multiwell plate reader (BioTek, Winooski, VT, USA). siRNA sequences can be found in Table 4.

Dasatinib was purchased from Chemitek (Indianapolis, IN, USA), R1881 was purchased from PerkinElmer, U0126 was purchased from Cell Signaling Technology (Beverly, MA, USA), and LY294002 was purchased from Promega. MDV3100 was obtained as a gift from Medivation Inc (San Francisco, CA, USA).

Statistical analysis of siRNA experiments.

The data from the HTRS experiments were defined as the raw signal luminescence measured by the Envision HTS multilabel reader. For each sample, the raw intensities were transformed to Z-scores within each plate. The median standardized value for each gene was then used as an input for the downstream analysis. To downweight the influence of siRNAs undergoing large changes on the parameters used to define the Z-score transformation, the estimated means and variances were defined after removing the top and bottom 2.5% of the data within each plate.

Analysis of follow-up siRNA screens and qRT-PCR data was performed in Prism 4.0 software (GraphPad, La Jolla, CA, USA). Raw luminescence was normalized to the mean luminescence value of siUNI for each cell line. Treatment effect was measured by normalizing raw luminescence values in treatment groups to the median luminescence value in the vehicle-treated group. Statistical analysis was performed using an unpaired two-sided Student's T-test using Welch's correction to determine significance.

Statistical significance of PPP2R2C expression in gene expression microarray data and TMA nuclear intensity staining was performed using a Student's T-Test. Whereas, multivariate analysis assessing the association between PPP2R2C staining intensity and patient survival data was performed using the Proc-Mixed procedure in SAS (SAS Institute, Cary, NC, USA) adjusting for the random effects of pre-operative PSA and tumor stage. Kaplan-Meier survival estimates were generated with the Proc-Lifetest procedure

in SAS utilizing a logrank significance threshold of $p < .05$. Patients were grouped based on high PPP2R2C expression in primary tumors (mean nuclear staining intensity ≥ 1) and low PPP2R2C expression in primary tumors (mean nuclear staining intensity < 1).

Quantitative Real-Time PCR (qRT-PCR). RNA was isolated from cells 24 hours post-transfection using the RNeasy kit (Qiagen Inc, Valencia, CA) and cDNA was generated with Superscript II (Life Sciences) as per protocol. qRT-PCR reactions were performed in triplicate using an Applied Biosystems 7900 sequence detector with SYBR Green PCR master mix (Life Technologies). Primers were designed using PrimerQuest (IDT, San Diego, CA, USA), and all reactions were normalized to the expression of the housekeeping gene Rpl13a. A water negative control did not produce significant amplification product. PCR primer sequences can be found in Table 5. Statistical analysis was performed using an unpaired two-sided Student's T-test using Welch's correction to determine significance.

Gene Expression Microarrays. Agilent 44K whole human genome expression oligonucleotide microarrays (Agilent Technologies, Inc., Santa Clara, CA) were used to profile 14 human primary prostate tumors and 54 castration-resistant prostate metastases from eleven patients (the patient cohort is described in detail by Holcomb et al(50)). The tumor samples were laser-capture microdissected, and total RNA isolated and amplified as described previously (51). Probe labeling and hybridization was performed following the Agilent suggested protocols and fluorescent array images were collected using the Agilent DNA microarray scanner G2565BA. Agilent Feature Extraction software was used to grid, extract, and normalize data. The resulting data were then combined with a publicly available dataset consisting of 15 normal prostate samples from untreated cancer-free patients(52). Expression ratios were log2 scaled and mean-centered across each gene.

Protein Collection and Immunoblotting. Protein was collected from tissue culture by lysing adherent cells with a cell lysis buffer (1.5M Urea, 1%SDS, 1%NP-40, 2%Tween20, 250nM NaCl, PBS) supplemented

with 1x phosphatase inhibitors (PhosStop, Roche Diagnostics) and a 1x protease inhibitor cocktail (Complete Mini, Roche Diagnostics, Basel, Switzerland). Protein was quantified per protocol using a bicinchoninic acid assay (Thermo Scientific). Normalized cell lysates were loaded onto a 12% NuPAGE Bis-Tris gel (Life Technologies) in MES buffer. Protein was transferred to nitrocellulose membranes using a semi-dry transfer apparatus and Tris/CAPS buffer. Immunoblots were probed with primary antibodies targeting AKT (Cell Signaling Technology,#9272), phospho-AKT (Cell Signaling Technology, #4058), Erk1/2 (Sigma, M5670), diphosphorylated-Erk1/2 (Sigma, M9692), PP2R2C (Abnova, Taipei City, Taiwan; clone 6D1), Src(Cell Signaling Technology, #2110), and phospho-Src (Cell Signaling Technology, #2101). Horseradish-peroxidase conjugated secondary antibodies (Thermo Scientific) were used in conjugation with Supersignal West Pico Chemiluminescent substrate (Thermo Scientific) to visualize protein targets. Membranes were then stripped for 15 minutes in Stripping Buffer (Thermo Scientific) and re-probed with anti-Actin antibody (Santa Cruz Biotechnology, Santa Cruz, CA; sc-1616) as a loading control.

TMA Construction. Prostate specimens were collected from a cohort of one hundred men who underwent radical prostatectomy at Virginia Mason Medical Center in Seattle, WA between 1954 and 1997. Tissue specimens were formalin-fixed and embedded in paraffin following surgical resection. Patients were monitored for both biochemical recurrence (PSA>0.2 ng/ml following radical prostatectomy) and pathologic recurrence (pelvic disease, regional lymph node metastasis, distant metastasis, or PCSM). Tissue diagnosis or overt radiographic signs confirmed the presence of disease recurrence. To classify patients as developing prostate cancer-specific mortality, death certificates were obtained and prostate cancer had to be the first listed cause of death. Thirty-four patients were identified with known adverse outcomes of either distant metastasis or PCSM. These patients were matched by age, PSA and time since surgery at a 1:2 ratio with 66 patients who had undergone radical prostatectomy and had no evidence of recurrence. Fred Hutchinson Cancer Research Center's Internal

Review Office granted approval for the use of patient tissue samples and de-identified clinical data for research purposes according to the requirements of the Human Subjects Institutional Review Board guidelines (IRB #7624, Approval dates: 11/18/11-11/16/12).

Representative formalin-fixed, paraffin-embedded blocks of radical prostatectomy specimens were selected. A genitourinary pathologist reviewed hematoxylin and eosin-stained sections from representative FFPE blocks collected from each patient. Prostate cancer was confirmed and assigned a Gleason score. The H&E-stained sections were marked to identify the regions of cancer and benign glandular epithelia and three tissue microarrays (TMA) were constructed with 38 x 25 x 12 mm^3 paraffin recipient blocks utilizing a manual tissue arrayer (Beecher Instrument, Silver Spring, MD, USA). Patients were represented in the TMAs by four 0.6 mm diameter cores of tissue, one benign and three cancer, for a total of 400 biopsy cores.

Immunohistochemsitry. FFPE TMAs were deparraffinized and rehydrated. 3% Hydrogen peroxide was used to quench endogenous tissue peroxidases and an avidin/biotin blocking system (Dako, Glostrop, Denmark) was used to quench endogenous avidin/biotin. Antigen retrieval was performed with 10mM citrate buffer, pH=6.0 in a pressure cooker. Tissue was blocked with normal serum specific to the secondary antibody (horse) and the primary antibody for PPP2R2C (clone 6D1, Abnova) was applied for 30 min at room temp, followed by biotinylated anti-mouse secondary antibodies (Dako) and ABC reagent (Vector Laboratories, Burlingame, CA, USA). DAB (Dako) was used as the chromogen and the TMA was counterstained with Meyer's hematoxylin (Dako). PPP2R2C nuclear staining was assessed by a genitourinary pathologist and graded on a 0-3 scale, with a score of 3 representing intense nuclear staining.

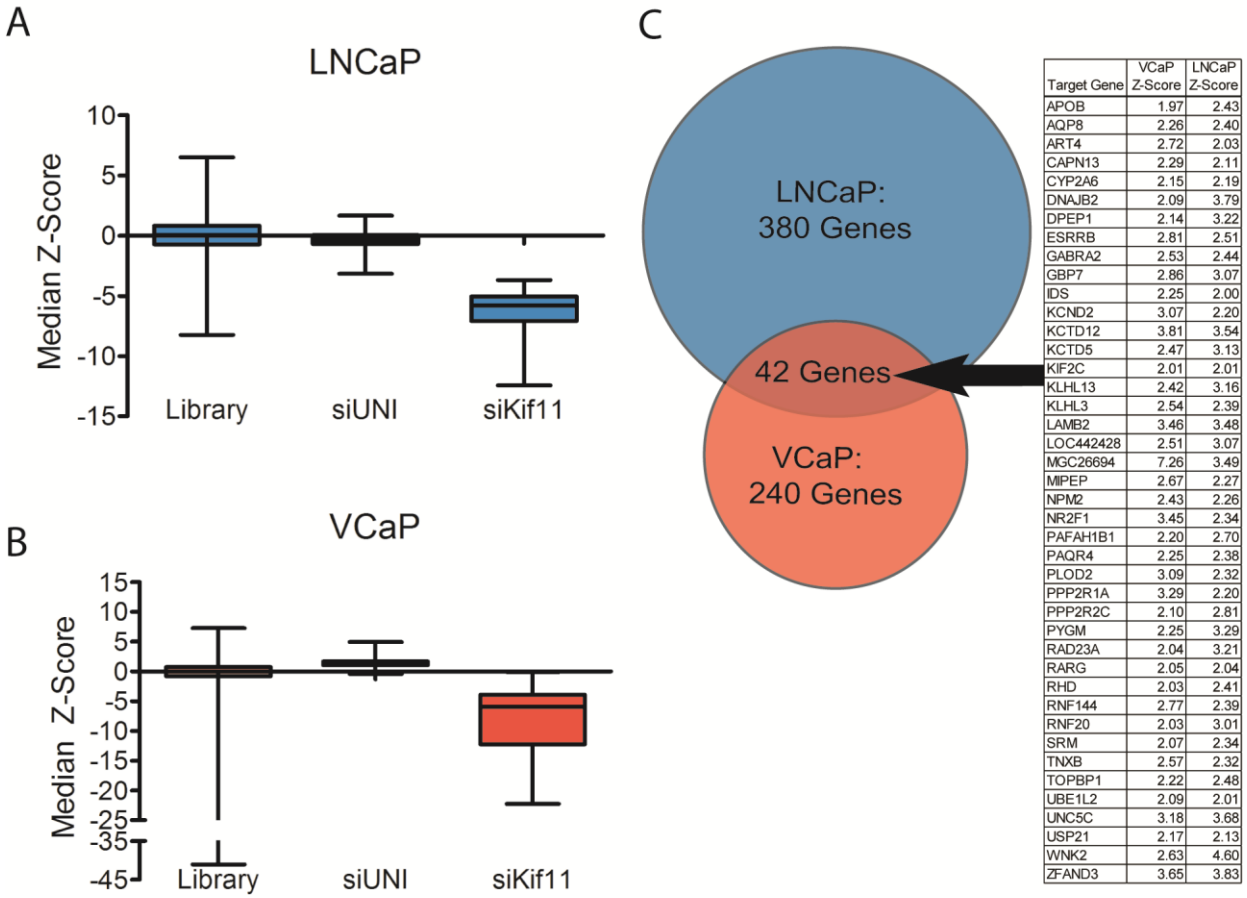

Target Gene	VCaP Z-Score	LNCaP Z-Score
APOB	1.97	2.43
AQP8	2.26	2.40
ART4	2.72	2.03
CAPN13	2.29	2.11
CYP2A6	2.15	2.19
DNAJB2	2.09	3.79
DPEP1	2.14	3.22
ESRRB	2.81	2.51
GABRA2	2.53	2.44
GBP7	2.86	3.07
IDS	2.25	2.00
KCND2	3.07	2.20
KCTD12	3.81	3.54
KCTD5	2.47	3.13
KIF2C	2.01	2.01
KLHL13	2.42	3.16
KLHL3	2.54	2.39
LAMB2	3.46	3.48
LOC442428	2.51	3.07
MGC26694	7.26	3.49
MIPEP	2.67	2.27
NPM2	2.43	2.26
NR2F1	3.45	2.34
PAFAH1B1	2.20	2.70
PAQR4	2.25	2.38
PLOD2	3.09	2.32
PPP2R1A	3.29	2.20
PPP2R2C	2.10	2.81
PYGM	2.25	3.29
RAD23A	2.04	3.21
RARG	2.05	2.04
RHD	2.03	2.41
RNF144	2.77	2.39
RNF20	2.03	3.01
SRM	2.07	2.34
TNXB	2.57	2.32
TOPBP1	2.22	2.48
UBE1L2	2.09	2.01
UNC5C	3.18	3.68
USP21	2.17	2.13
WNK2	2.63	4.60
ZFAND3	3.65	3.83

Figure 3: High throughput RNAi screening identifies suppressors of CRPC growth. 6650 siRNAs were used to knockdown experimental gene targets (Library) in LNCaP and VCaP. Positive controls for transfection, resulting in cell death (siKif11), and non-targeting scrambled control siRNA (siUNI) were included on each plate. Median Z-score values for experimental siRNAs and controls are plotted for LNCaP (A) and VCaP (B). (C) 380 siRNAs and 240 siRNAs induced castration-resistant growth above the significance threshold in LNCaP and VCaP, respectively. The 42 genes inducing castration-resistant growth in both cell lines are listed as gene symbols with the corresponding cell line-specific Z-score (Significance threshold: $Z \geq 1.96$).

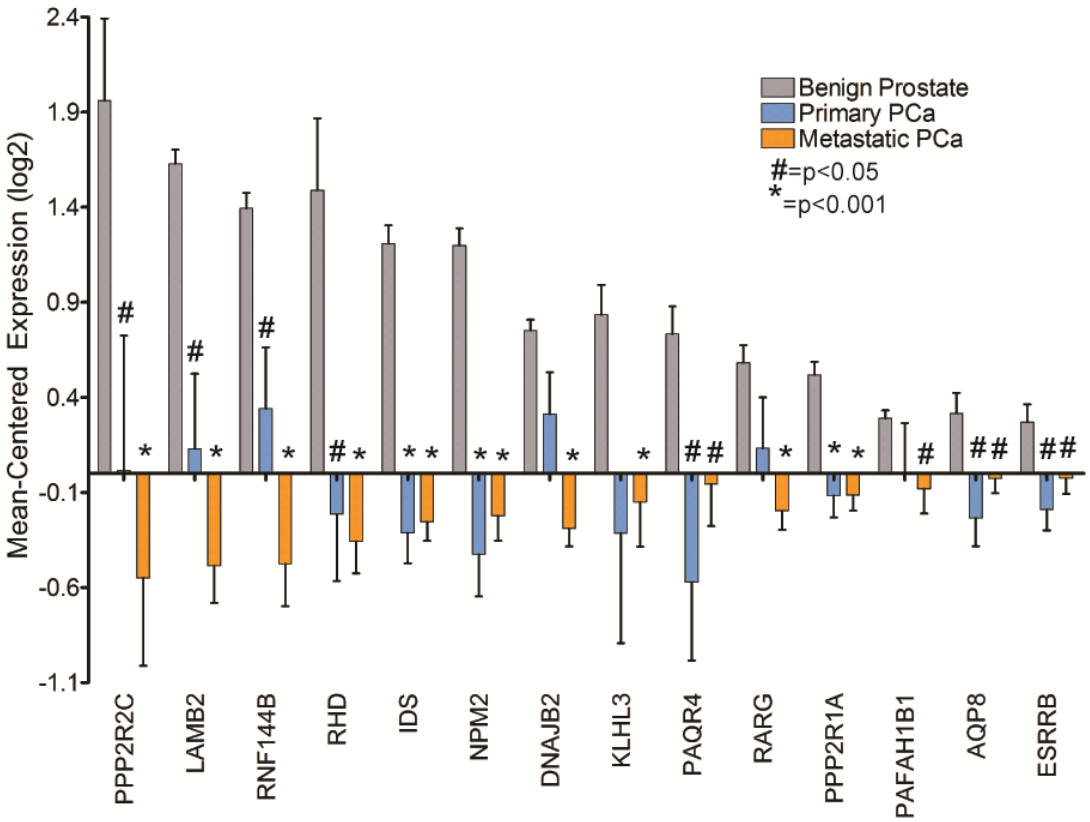

Figure 4: PPP2R2C is downregulated in primary and metastatic prostate cancer. Gene expression microarray data from 16 benign prostate samples, 15 primary tumors, and 55 metastases was cross-referenced with results from the HTRS experiments. Of the 42 positive hits identified in the HTRS experiments, 14 were significantly downregulated in primary tumors and CRPC metastases compared to benign prostate epithelia. PPP2R2C underwent the highest change in expression between benign epithelia and CRPC. Gene expression values were compared with a Student's T-test.

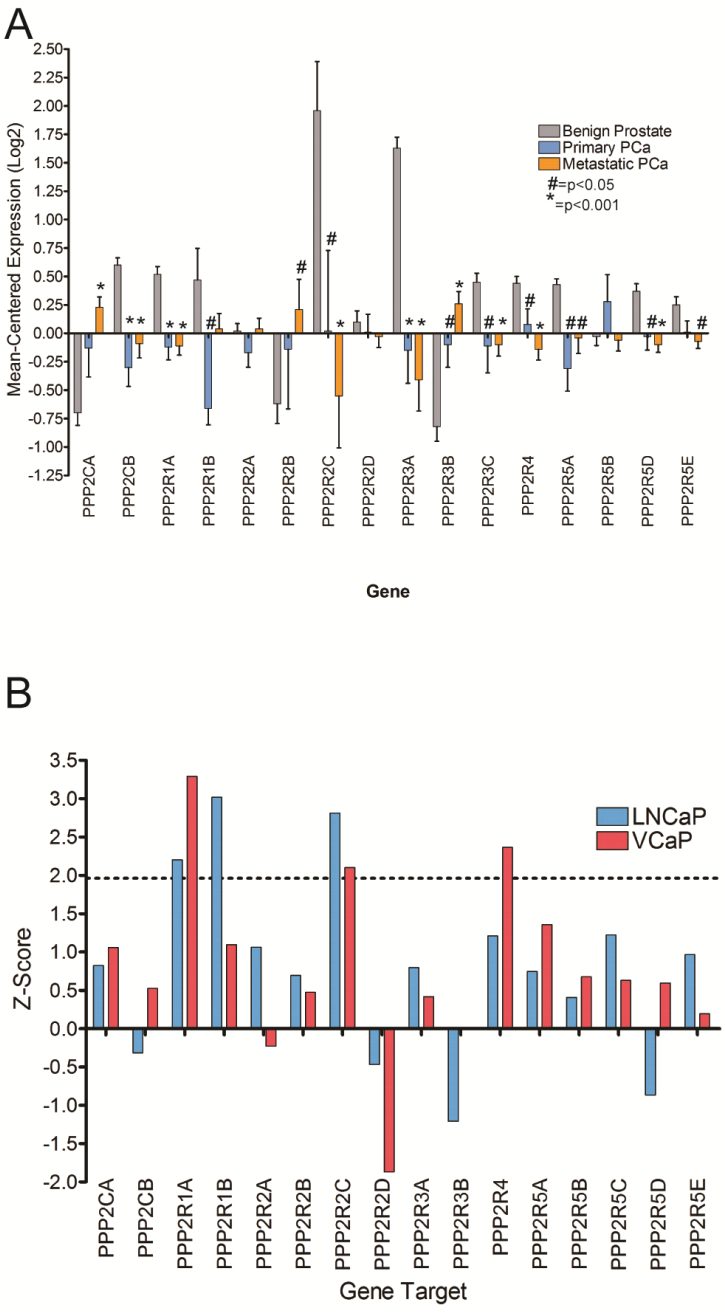

Figure 5: High throughput screening results and corresponding patient gene expression data for PP2A subunits. (A) PP2A subunit expression in benign prostate epithelia, primary prostate tumors, and CRPC metastases. Counter to previous reports [14, 15], PPP2CA and PPP2R2A are not downregulated in primary or metastatic prostate cancer; PPP2CA is significantly upregulated in prostate cancer metastases. (B) Knockdown of PPP2R1A and PPP2R2C are the only PP2A subunits to induce sufficient growth to reach the significance threshold in both cell lines. Knockdown of other PP2A B-regulatory subunits induced variable effects on proliferation.

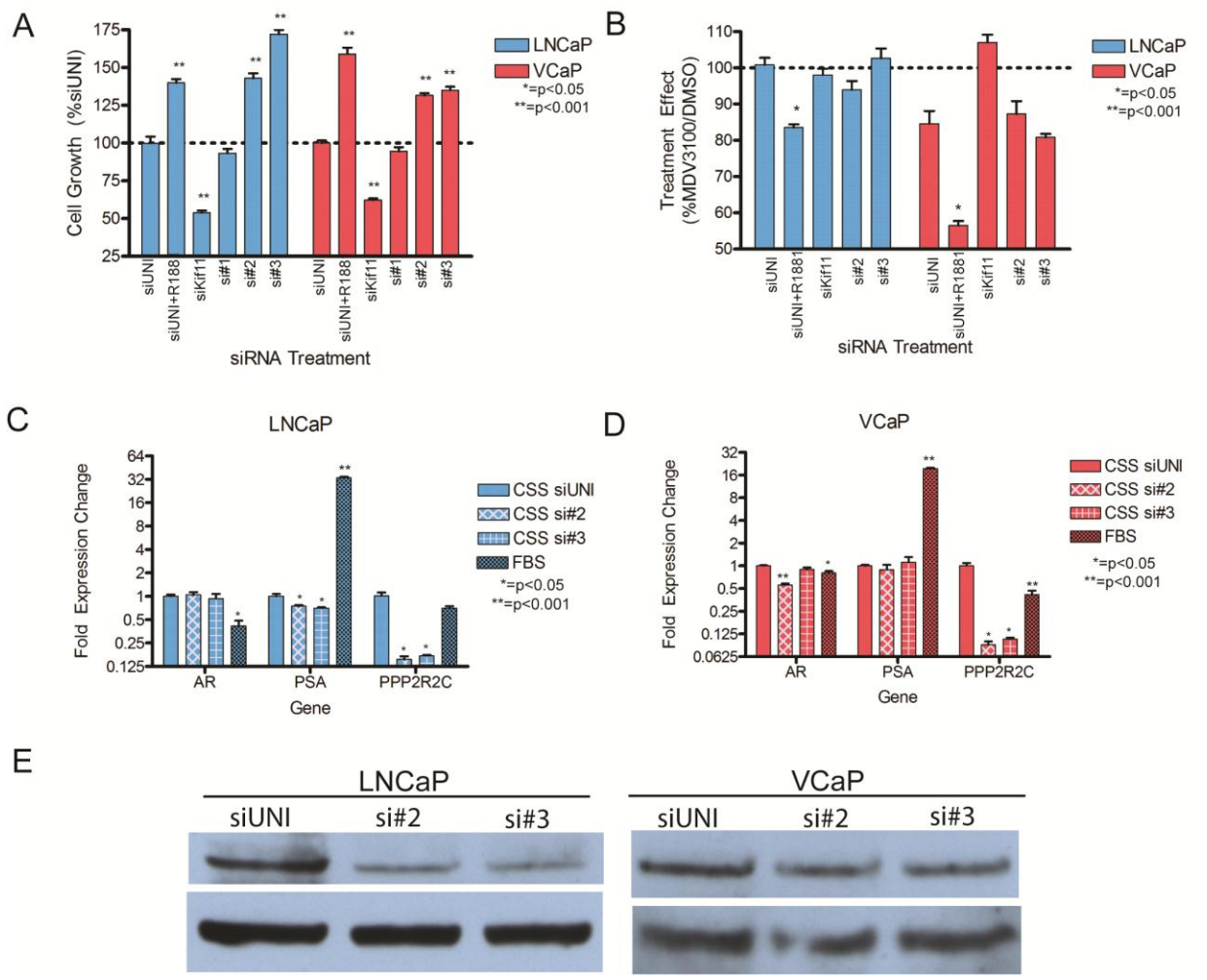

Figure 6: siRNA knockdown of PPP2R2C induces growth in LNCaP and VCaP through non-AR mediated pathways. (A) LNCaP and VCaP were transfected with the deconvoluted pool of PPP2R2C siRNAs (si#1-3), in addition to a scrambled control (siUNI) and a positive control for transfection (siKif11). siUNI + 1nM R1881 is a positive control for androgen-induced cell growth. siRNA #2 and siRNA #3 induced proliferation in LNCaP and VCaP. Raw luminescence values in each cell line were normalized to siUNI. Statistical comparisons between gene-specific siRNA versus siUNI were performed within each cell line. (B) LNCaP and VCaP were co-treated with 5µM MDV3100 and siRNA. While MDV3100 differentially inhibited R1881-driven proliferation, it did not have a differential effect on growth induced by PPP2R2C knockdown. Treatment effect was calculated by normalizing MDV3100-treated samples to the median luminescence value of the vehicle-treated control. Statistical comparisons between gene-specific siRNA versus siUNI were performed within each cell line. (C and D) qRT-PCR analysis of cDNA collected from LNCaP(C) and VCaP (D)demonstrates that siRNA #2 and siRNA #3 successfully knockdown PPP2R2C and do not increase the expression of AR or PSA. cDNA isolated from cells cultured in media supplemented with androgen replete fetal bovine serum was used as a positive control for androgen treatment. Statistical comparisons of gene expression were performed between siUNI and gene-specific siRNA within each cell line. (E) siRNA knockdown of PPP2R2C is verified via immunoblot.

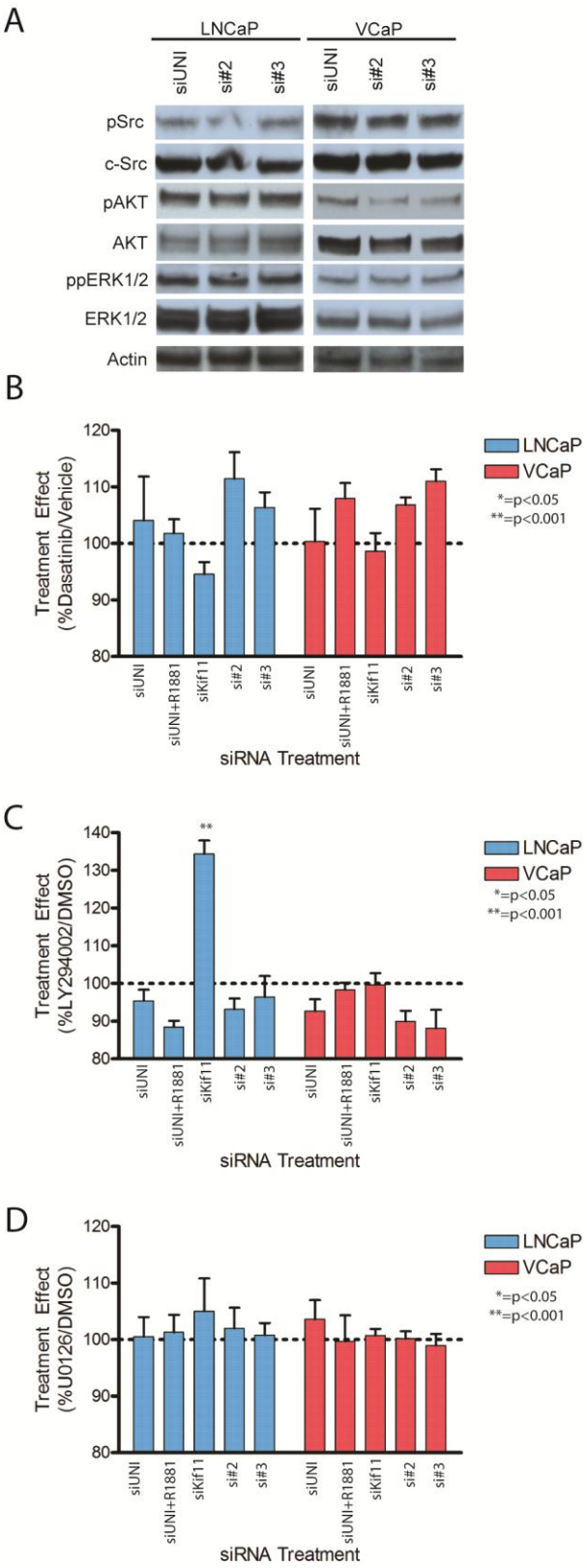

Figure 7: PPP2R2C knockdown does not activate c-Src, PI3K, or ERK1/2 signal transduction pathways. (A) PPP2R2C knockdown does not alter the phosphorylation status of Src, AKT, or ERK1/2 in LNCaP or VCaP cells cultured in androgen-depleted conditions. (B) Treatment with 1µM Dasatinib, a Src kinase inhibitor, does not significantly inhibit growth induced by PPP2R2C when compared to the scrambled control siRNA. (C) Treatment of LNCaP and VCaP with 2µM LY294002, a PI3K inhibitor, does not significantly inhibit growth induction by PPP2R2C knockdown. (D) Treatment of LNCaP and VCaP with 10µM U0126, an inhibitor of MEK, does not inhibit growth induced by PPP2R2C knockdown. Treatment effect was calculated by normalizing MDV3100-treated samples to the median luminescence value of the vehicle-treated control. Statistical comparisons between gene-specific siRNA versus siUNI were performed within each cell line.

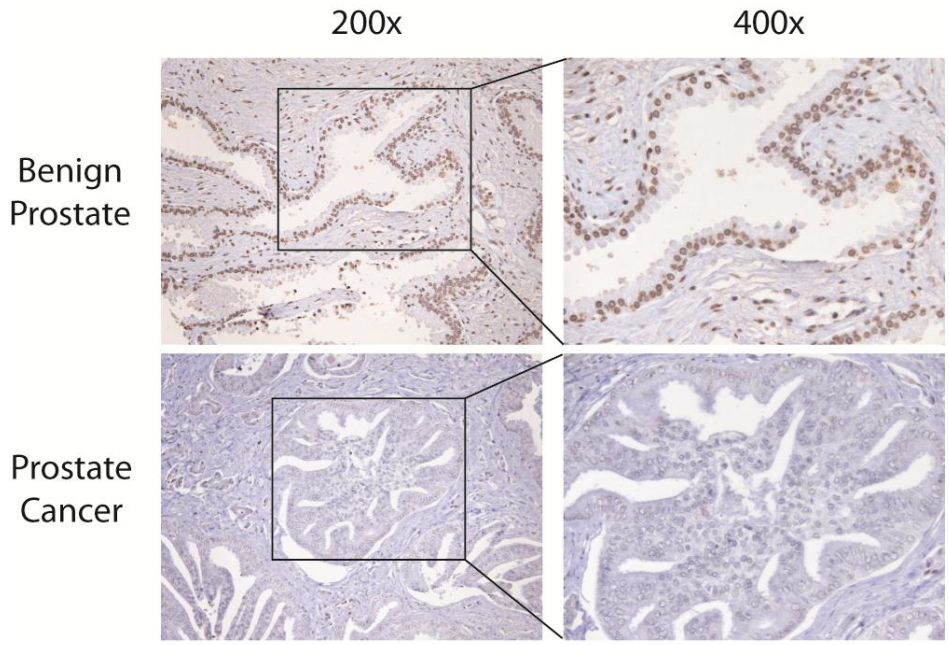

Figure 8: PPP2R2C protein expression is downregulated in primary prostate tumors. IHC for PPP2R2C was performed on the VM-TMA, and benign prostate epithelia and primary prostate were photographed at 200x and 400x original magnification. Benign prostate tissue exhibited robust nuclear expression, while primary prostate cancer expressed low levels of PPP2R2C.

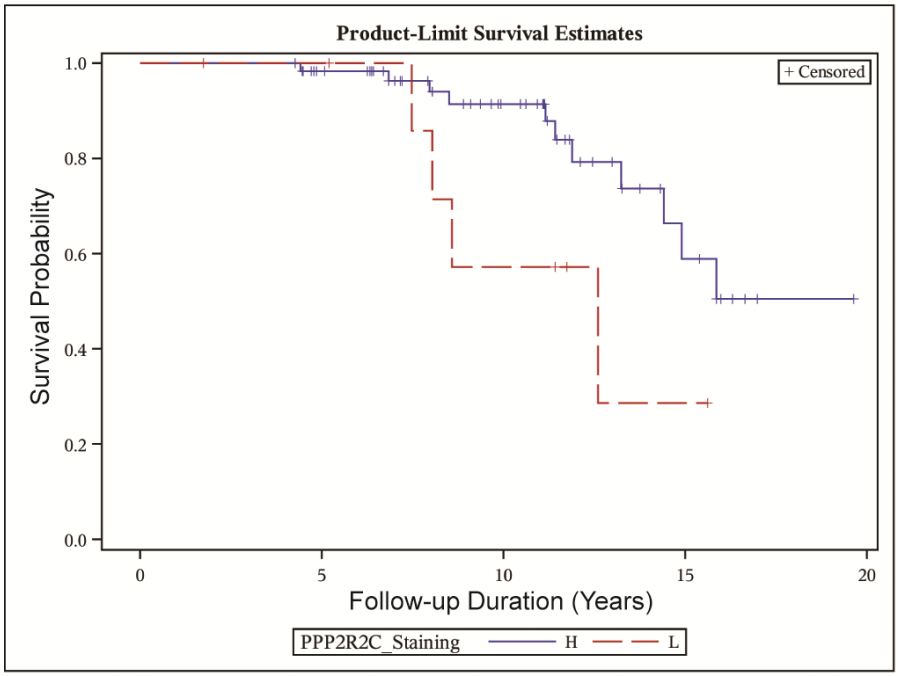

Figure 9: Kaplan-Meier analysis of post-surgical survival. Patients were subdivided into groups based on the mean nuclear intensity (MNI) staining of PPP2R2C in representative tumor cores on the VM-TMA. Kaplan-Meier survival estimates from patients with high PPP2R2C expression (MNI≥1; H, blue) and those patients with low PPP2R2C expression (MNI<1; L, Red) were compared using a log-rank test. There was a statistically significant difference in survival (p=0.0452) between the two populations.

Table 1: Clinico-pathological parameters

Mean Nuclear Staining Intensity	0+ (n = 11) *n (%) or mean (median; range)*	1+ (n = 14) *n (%) or mean (median; range)*	2+ (n = 24) *n (%) or mean (median; range)*	3+ (n = 29) *n (%) or mean (median; range)*	All patients (n =78) *n (%) or mean (median; range)*
Age at surgery (years)	65.2 (67.0; 51.7-73.5)	63.4 (65.9; 53.4-73.3)	63.7 (64.4; 44.0-76.0)	66.2 (67.3; 52.3-75.0)	64.8 (65.5; 44.0-76.0)
Pre-operative PSA					
Total PSA value (ng/ml)	11 (7; 1-32)*	11 (8; 2-41)*	14 (10; 5-40)*	19 (12; 2-90)*	15 (10; 1-90)*
PSA ≤ 10 ng/ml	3 (60.0)	8 (66.7)	8 (53.3)	9 (45.0)	28 (53.8)
PSA > 10 ng/ml	2 (40.0)	4 (33.3)	7 (46.7)	11 (55.0)	24 (46.2)
Follow-up (years)	9.2 (8.6; 1.7-15.7)	10.7 (10.5; 6.4-16.9)	9.4 (10.0; 2.6-19.6)	9.9 (9.7; 4.4-16.8)	9.8 (9.5; 1.7-19.6)
Gleason sum	6 (7; 5-8)	7 (7; 5-9)	7 (7; 5-10)	7 (7; 4-9)	7 (7; 4-10)
GS ≤ 6	5 (45.5)	5 (35.7)	6 (25.0)	7 (29.1)	23 (29.5)
GS = 7	4 (36.4)	5 (35.7)	8 (33.3)	14 (48.3)	33 (42.3)
GS = 3+4	3 (27.3)	6 (42.9)	8 (33.3)	14 (48.3)	31 (39.7)
GS = 4+3	1 (9.1)	1 (7.1)	0 (0.0)	0 (0.0)	2 (2.6)
GS ≥ 8	2 (18.2)	2 (14.3)	10 (41.7)	8 (27.6)	22 (28.2)
Pathologic stage					
pT2	2 (18.2)	6 (42.9)	4 (16.7)	12 (41.4)	24 (30.8)
pT3a	9 (81.8)	6 (42.9)	14 (58.3)	12 (41.4)	41 (52.6)
pT3b	0 (0.0)	0 (0.0)	3 (12.5)	2 (6.9)	5 (6.4)
pT3c	0 (0.0)	1 (7.1)	1 (4.2)	3 (10.3)	5 (6.4)
pT4	0 (0.0)	1 (7.1)	2 (8.3)	0 (0.0)	3 (3.8)
Tumor volume, ml^3	7 (7; 2-15)*	5 (4; 1-14)*	10 (8; 1-35)*	8 (5; 1-23)*	8 (6; 1-35)*
Lymph node involvement					
Yes	0 (0.0)*	1 (11.1)*	2 (12.5)*	1 (5.8)*	4 (8.7)*
No	4 (100.0)*	8 (88.9)*	14 (87.5)*	16 (94.1)*	42 (91.3)*
Extracapsular extension					
Yes	9 (81.8)	8 (57.1)	20 (83.3)	17 (60.7)*	54 (70.1)*
No	2 (18.2)	6 (42.9)	4 (16.7)	11 (39.3)*	23 (29.9)*
Surgical margin involvement					
Yes	7 (63.6)	8 (57.1)	13 (54.2)	15 (51.7)	43 (55.1)
No	4 (36.4)	6 (42.9)	11 (45.8)	14 (48.3)	35 (44.9)
Adjuvant treatment post-RP					
Endocrine therapy alone	4 (36.4)	6 (42.9)	3 (12.5)	7 (29.1)	20 (25.6)
Radiotherapy alone	0 (0.0)	0 (0.0)	1 (4.2)	1 (3.4)	2 (2.6)
Radiotherapy + endocrine	0 (0.0)	0 (0.0)	1 (4.2)	1 (3.4)	2 (2.6)
Biochemical recurrence					
Yes	5 (45.5)	6 (42.9)	7 (29.2)	11 (37.9)	29 (37.2)*
No	6 (54.5)	8 (57.1)	17 (70.8)	18 (62.1)	49 (62.3)*
Local recurrence					
Yes	1 (9.1)	0 (0.0)	0 (0.0)	2 (7.4)	3 (3.8)
No	10 (90.9)	14 (100.0)	24 (100.0)	27 (93.1)	75 (96.2)
Distant metastases					
Yes	5 (45.5)	6 (42.9)	5 (20.8)	8 (27.6)	24 (30.8)
No	6 (54.5)	8 (57.1)	19 (79.2)	21 (72.4)	54 (69.2)
Overall death					
Yes	9 (81.8)	3 (21.4)	5 (20.8)	10 (34.5)	27 (34.6)
No	2 (18.2)	11 (78.6)	19 (79.2)	19 (65.5)	51 (65.4)
Prostate Cancer Specific Mortality					
Yes	5 (45.5)	3 (21.4)	3 (12.5)	5 (17.2)	16 (20.5)
No	6 (54.5)	11 (78.6)	21 (87.5)	24 (82.8)	62 (79.5)

* Not all cases have available information

Table 2: PPP2R2C Expression in Benign Prostate and Primary Prostate Cancer

Clinical Outcome	PPP2R2C Nuclear Staining					Mean Nuclear Intensity	p-value
	-	+	++	+++	Total Cores		
Benign	22	26	90	79	217	2.04	p=0.001
Cancer	24	42	88	40	194	1.74	

Table 3: Multivariate Analysis of VM-TMA Patient Outcomes

Clinical Outcome	Mean PPP2R2C Nuclear Intensity	p-value
Biochemical Relapse		
No	2.25	p=0.006
Yes	1.74	
Distant Metastases		
No	2.32	p<0.001
Yes	1.55	
PCSM		
No	2.21	p=0.048
Yes	1.79	

Table 4: Chapter 2 siRNA Sequences

Gene	Oligo Name	Sense Sequence (5'-3')	Antisense Sequence (5'-3')
siUNI	siRNA Universal Negative Control #1	Proprietary	Proprietary
Kif11 #1	SASI_Hs01_00161697	CAUUGACAGUGGCCGAUAA[dT][dT]	UUAUCGGCCACUGUCAAUG[dT][dT]
Kif11 #2	SASI_Hs01_00161696	CUGUACUACAGGAAUUGAU[dT][dT]	AUCAAUUCCUGUAGUACAG[dT][dT]
Kif11 #3	SASI_Hs01_00161689	CAACAAGGAUGAAGUCUAU[dT][dT]	AUAGACUUCAUCCUUGUUG[dT][dT]
PPP2R2C #1	SASI_Hs01_00070843	CCAACAACCUGUACAUCUU[dT][dT]	AAGAUGUACAGGUUGUUGG[dT][dT]
PPP2R2C #2	SASI_Hs01_00070844	CUCUGACAUGCACUAGGUA[dT][dT]	UACCUAGUGCAUGUCAGAG[dT][dT]
PPP2R2C #3	SASI_Hs01_00070845	CAUGCACUAGGUAUGUGCA[dT][dT]	UGCACAUACCUAGUGCAUG[dT][dT]

Table 5: Chapter 2 PCR primer sequences.

Gene	Forward Primer	Reverse Primer
AR	5'-ATCCTCATATGGCCCAGTGTC-3'	5'-GCTCTCTAAACTTCCCGTGGC-3'
PSA	5’-GCATGGGATGGGGATGAAGTAAG-3’	5’-CATCAAATCTGAGGGTTGTCTGGA-3’
PPP2R2C	5’-AGAGCTGATGACCTCACCGTTGTT-3’	5’-ATCAGATGAGGACACAGGCACACA-3’
RPL13a	5’-CCTGGAGGAGAAGAGGAAAGA-3’	5’-TTGAGGACCTCTGTGTATTTG-3’

Chapter 3: Total suppression of androgen receptor signaling selects for a novel, non-neuroendocrine, androgen receptor-deficient prostate cancer cell line that relies on autocrine fibroblast growth factor 8 signaling for proliferation.

Introduction

Continued importance of androgen receptor (AR) signaling as a growth and survival pathway in most tumors has prompted the development of several new anti-androgen treatments. These drugs - including improved AR antagonists(4, 5, 53), inhibitors of androgen synthesis enzymes (25, 54, 55), and inhibitors of AR expression(56) – have exhibited the potential to substantially impair AR signaling in experimental models and clinical trials. It is likely that monotherapy or combination treatment with these agents will eliminate cells reliant on the genomic program regulated by the AR. Aggressive selective pressure against AR-regulated pathways in metastatic disease will likely generate prostate carcinoma cells reliant on survival pathways distinct from those regulated by AR.

Institutions harvesting prostate tumors through rapid autopsy programs have reported heterogeneous patterns of AR expression in metastases collected from patients treated with sustained androgen deprivation therapy (ADT). Notably, most patients harbor infrequent tumor deposits that do not express AR following conventional ADT (57, 58). While it is true that most AR-null tumors express markers of neuroendocrine differentiation, accumulating molecular evidence suggests that neuroendocrine prostate cancer (NEPCa) exists within a more complex spectrum of anaplastic disease ranging from mixed prostatic adenocarcinomas with neuroendocrine features to pure small-cell NEPCa (59-61). Anaplastic prostate cancer is associated with rapid progression, resistance to chemotherapy, and a poor prognosis (62). Importantly, there are rare reports of metastatic prostate tumors that do not express AR, androgen regulated genes (ARGs), or markers of NEPCa (63).

We subjected a previously reported (64) AR-positive LNCaP line stably transfected with a tetracycline-inducible anti-AR shRNA to extended steroid ligand deprivation and AR suppression, in simulation of Total Androgen Pathway Suppression (TAPS). Extended TAPS generated a novel AR and ARG-null prostate cancer line, derived from an AR-positive progenitor. We refer to this prostate cancer cell line as LNCaP-**A**ndrogen **P**athway **I**ndependent **P**rostate **C**ancer (LNCaP^{APIPC}). LNCaP^{APIPC} relies on an autocrine receptor tyrosine kinase (RTK)-mediated signaling for proliferation and survival, mediated in party by downstream upregulation of the oncogene *inhibitor of DNA-binding 1* (ID1). Surprisingly, LNCaP^{APIPC} does not express histologic markers of neuroendocrine-like disease. Follow-up immunohistochemical screening of a patient-derived tissue microarray identified AR-null, PSA-null, non-neuroendocrine tumors that had been harvested from men with known CRPC. These *in vitro* and *in vivo* data indicate that AR-null, non-neuroendocrine tumors can evolve from metastases treated with extended ADT.

Results

Generation of an androgen-pathway independent prostate cancer model cell line through Total Androgen Pathway Suppression.

We received wildtype LNCaP cells stably transduced with a retroviral tetracycline-inducible anti-AR shRNA (LNCaP^{shAR}) as a gift from Dr. Paul Rennie at the University of British Columbia(64). Nearly all previously-developed castration-resistant LNCaP derivatives continue to rely on AR-mediated transcription for survival and growth (65); to avoid this potential outcome from the extended TAPS experiment, LNCaP^{shAR} were stably transfected with a novel androgen-regulated suicide gene construct. This construct (pATK) encodes a triple-probasin response element-driven herpes thymidine kinase. LNCaP$^{shAR/pATK}$ expresses the thymidine kinase in response to androgen treatment (Figure 10A) and undergoes cell death when co-treated with androgen and the nucleoside analog ganciclovir (Figure 10B).

LNCaP$^{shAR/pATK}$ cultured to near-confluency in RPMI1640+5% fetal bovine serum (FBS) was subjected to increasing rounds of androgen deprivation, mimicking clinical TAPS (Figure 11A). First, androgen-replete FBS was replaced with androgen-depleted 5% charcoal-dextran-stripped FBS (CSS). After two weeks of steroid ligand deprivation, media was supplemented with 1µg/ml doxycycline to induce the TET-on anti-AR shRNA, initiating TAPS. Combined ligand and receptor deprivation resulted in cell death for >99% of the LNCaP$^{shAR/pATK}$ population. After five months of TAPS, a residual population of viable cells remained (Figure 11B). This colony was expanded over the course of 3 months and treated with a two-week course of 50µM ganciclovir to eliminate any cells still transcribing ARGs and the androgen-regulated herpes thymidine kinase. Cells that survived ganciclovir treatment were designated LNCaP-Androgen Pathway Independent Prostate Cancer (LNCaP^{APIPC}).

LNCaP^{APIPC} does not express androgen receptor or prostate specific antigen and is derived from LNCaP$^{shAR/pATK}$.

As previously mentioned, virtually all metastatic tumors and prostate cancer models that relapse from traditional ADT maintain robust AR expression and expression of ARGs (65, 66). Therefore we compared AR and ARG expression in LNCaP$^{shAR/pATK}$ and LNCaP^{APIPC} treated with vehicle (ethanol), 1µg/ml doxycycline, or 1nM R1881. LNCaP$^{shAR/pATK}$ expressed detectable AR and PSA when cultured in androgen-depleted media. When LNCaP$^{shAR/pATK}$ were treated with R1881 or doxycycline, AR expression decreased by 1.9-fold (p=0.01) and 6.2-fold (p=0.006), respectively. As expected, PSA expression in LNCaP$^{shAR/pATK}$ markedly increased in response to R1881 stimulation (14-fold increase, p=0.002) and decreased in response to doxycycline treatment (27-fold decrease, p=0.007). AR and PSA were nearly undetectable in LNCaP^{APIPC} by qRT-PCR; AR expression was 45-fold lower and PSA expression was 30-fold lower than LNCaP$^{shAR/pATK}$ cultured in androgen-depleted conditions (Figure 12A). qRT-PCR results were confirmed by immunoblot. AR and PSA were not detectable in LNCaP^{APIPC} cell lysate (Figure 12B).

To confirm that LNCaP^{APIPC} were derived from LNCaP$^{shAR/pATK}$ and not a result of cell line contamination, we compared the genomic structure of the two cell lines by comparative genomic hybridization (CGH)-array analysis (Figure 13). Genomic analysis confirmed a parent-daughter lineage, with only three small (<325Kb) significant genomic losses in LNCaP^{APIPC} compared to LNCaP$^{shAR/pATK}$ (Table 6).

LNCaP^{APIPC} proliferates in steroid-depleted media, is resistant to antiandrogen treatment, and is more aggressive than LNCaP$^{shAR/pATK}$.

LNCaP$^{shAR/pATK}$ and LNCaP^{APIPC} were treated with ADT *in vitro* and cell growth was assessed with the Cyquant DNA-binding fluorescence assay. As expected, LNCaP^{APIPC} grew robustly in steroid-depleted media. LNCaP$^{shAR/pATK}$ grew robustly in hormone-complete media, while hormone or ligand depletion inhibited growth. Furthermore, treatment of LNCaP$^{shAR/pATK}$ with the potent antiandrogen MDV3100 completely inhibited growth, while LNCaP^{APIPC} was resistant to MDV3100 treatment (Figure 14A).

We quantified the relative aggressiveness of LNCaP$^{shAR/pATK}$ and LNCaP^{APIPC} using transwell migration and invasion assays. Both cell lines successfully migrated across the transwell membrane and invaded through a layer of basement membrane extract. LNCaP^{APIPC} exhibited a statistically significant increase in baseline migration (5%, p=0.019) and invasion (12%, p=0.006) when compared to LNCaP$^{shAR/pATK}$. LNCaP^{APIPC} also responded to a transwell FBS gradient with a higher number of migratory cells (117% vs 108%, p=0.001) and invasive cells (129% vs 121%, p=0.025) than LNCaP$^{shAR/pATK}$(Figures 14B, Figure 14C).

LNCaP^{APIPC} does not express markers of neuroendocrine differentiation.

Previous short-term steroid deprivation or AR suppression experiments in LNCaP have generated transdifferentiated LNCaP cells that resemble NEPCa (67). NEPCa is characterized by low AR and ARG expression; increased expression of chromogranin-A (ChA) and synaptophysin (Syn); and often exhibits small-cell morphology (61, 62). We assessed NEPCa marker expression in LNCaP$^{shAR/pATK}$ and LNCaP^{APIPC}

cultured as subcutaneous xenografts in immunocompromised mice. LNCaP$^{shAR/pATK}$ and LNCaP^{APIPC} did not express detectable levels of the NEPCa markers ChA or Syn by immunohistochemistry (IHC; Figure 15).

Analysis of global gene expression indicates that LNCaP^{APIPC} does not express an androgen-regulated gene signature.

AR signaling represents the dominant growth pathway in advanced prostate cancer (66, 68) yet the LNCaP^{APIPC} phenotype indicated the existence of an alternative growth and survival pathway sufficient to replace AR signaling in prostate tumors. To identify this pathway in LNCaP^{APIPC}, global gene expression was analyzed by hybridizing RNA collected from LNCaP$^{shAR/pATK}$ and LNCaP^{APIPC} to Human 44k Agilent gene expression microarrays. Significance Analysis of Microarrays (SAM) was used to identify significant differentially expressed genes (2-fold expression change, q-value < 5%) for each treatment group when compared to vehicle (ethanol). As expected, LNCaP$^{shAR/pATK}$ demonstrated considerable gene expression changes in response to R1881 treatment and AR-suppression while LNCaP^{APIPC} showed almost no statistically significant gene expression changes in response AR pathway manipulation. Furthermore, a head-to-head comparison of gene expression profiles from LNCaP$^{shAR/pATK}$ and LNCaP^{APIPC} cultured in androgen depleted conditions revealed 1083 differentially expressed genes (Table 7).

Gene Set Enrichment Analysis (GSEA) was used to quantitate the enrichment of a published prostate AR-regulated gene signature(69) in LNCaP$^{shAR/pATK}$ and LNCaP^{APIPC}. LNCaP$^{shAR/pATK}$ exhibited a statistically significant ($p<0.001$) normalized enrichment score (NES) in response to androgen stimulation (Figure 16A). ARG expression was not significantly enriched in LNCaP^{APIPC} treated with R1881 ($p=0.316$; Figure 16B). A comparison of genes expressed in LNCaP$^{shAR/pATK}$ proliferating in response to androgen and LNCaP^{APIPC} proliferating under TAPS (Figure 16C) revealed that ARG expression was enriched in LNCaP$^{shAR/pATK}$ ($p<0.001$). This indicated that LNCaP^{APIPC} proliferation and survival was mediated through

a transcriptional program distinct from AR and ARGs. In an effort to identify other prostate cell lines similar to LNCaP^{APIPC}, we compared the gene expression profiles of 20 other prostate-derived cell lines to LNCaP$^{shAR/pATK}$ and LNCaP^{APIPC} using unsupervised hierarchical clustering. Both LNCaP$^{shAR/pATK}$ and LNCaP^{APIPC} treatment groups clustered with other known LNCaP derivatives, suggesting that LNCaP^{APIPC} retains a LNCaP-derived gene expression profile even while lacking AR-regulated gene expression (Figure 17).

Intracellular signal transduction pathway analysis demonstrates a decrease in PI3K pathway signaling and elevated MAPK pathway signaling in LNCaP^{APIPC}.

Loss of the phosphatase and tensin homolog (PTEN) tumor suppressor, and the corresponding deregulation of the phosphoinositide-3-kinase (PI3K) intracellular signaling pathway, is one of the most common genomic alterations found in primary and metastatic prostate cancer (11). Many prostate cancer cell lines, including LNCaP, are PTEN-deficient. Recent investigation into the relationship between PI3K pathway activation and CRPC revealed that PTEN loss and increased PI3K activity is sufficient to compensate for reduced AR activity in both *in vitro* and *in vivo* prostate cancer models (32, 33). Therefore, we hypothesized that PI3K pathway upregulation was supporting LNCaP^{APIPC} growth. PI3K signaling was assessed in LNCaP$^{shAR/pATK}$ and LNCaP^{APIPC} by probing whole-lysate immunoblots for phospho-AKT (pAKT). Elevated pAKT was observed in LNCaP$^{shAR/pATK}$ following treatment with vehicle or doxycycline compared to R1881. Surprisingly, pAKT was nearly undetectable in LNCaP^{APIPC}, suggesting that PI3K activity was not acting as a survival pathway (Figure 18A).

Increased mitogen-activated protein kinase (MAPK) signaling is also postulated to support CRPC proliferation (70). MAPK signal transduction is activated through a variety of stimuli, and is closely associated with receptor tyrosine kinase (RTK) activity. Activation of some RTKs, such as HER2, can stimulate castration-resistant proliferation and simultaneously inhibit AR expression in LNCaP (34).

MAPK signaling was investigated in LNCaP$^{shAR/pATK}$ and LNCaP^{APIPC} by immunoblotting for phosphorylated downstream mediators MEK and ERK1/2. Phosphorylated-MEK (pMEK) and dually phosphorylated-ERK1/2 (ppERK1/2) were elevated in LNCaP^{APIPC} compared to LNCaP$^{shAR/pATK}$(Figure 18B). These data suggested that increased MAPK signaling may be sustaining AR-independent growth in LNCaP^{APIPC}.

LNCaP^{APIPC} overexpresses bioactive FGF8.

LNCaP$^{shAR/pATK}$ and LNCaP^{APIPC} gene expression data was analyzed for upregulated RTK ligands that could plausibly influence MEK/ERK signaling. Fibroblast growth factor 8 (FGF8) was differentially upregulated in LNCaP^{APIPC} (Table 8). FGF8 is transcribed as eight distinct isoforms (FGF8a-h), although only four isoforms (FGF8a, FGF8b, FGF8e and FGF8f) are translated into active protein in humans (71). Previous investigation into the *in vitro* effects of FGF8 isoform overexpression revealed that FGF8b is the most oncogenic (72). Therefore, it was important to identify the specific isoform(s) upregulated in LNCaP^{APIPC}.

Isoform-specific qRT-PCR was performed on cDNA generated from LNCaP$^{shAR/pATK}$ and LNCaP^{APIPC} RNA. LNCaP$^{shAR/pATK}$ expressed low levels of FGF8a/g and FGF8b and did not express FGFe/f; LNCaP^{APIPC} expressed all active FGF8 isoforms at higher levels (FGF8a/g = 1100-fold, $p<0.001$; FGF8b=600-fold, $p<0.001$) than LNCaP$^{shAR/pATK}$. Visualization of the PCR products via agarose gel electrophoresis confirmed single-isoform specificity (Figure 19A).

Detection of FGF8b protein expression in concentrated serum-free conditioned media (CM) collected from LNCaP^{APIPC}, but not LNCaP$^{shAR/pATK}$, confirmed the qRT-PCR results (Figure 19B). Furthermore, androgen-depleted LNCaP$^{shAR/pATK}$ treated with concentrated LNCaP^{APIPC} CM showed a small (11%), but statistically significant ($p=0.01$) increase in proliferation. Treatment with LNCaP$^{shAR/pATK}$ CM had no effect on proliferation (Figure 19C).

FGF8 stimulation activates MAPK pathway signaling and induces proliferation in androgen and androgen-receptor depleted LNCaP$^{shAR/pATK}$.

Treatment of LNCaP$^{shAR/pATK}$ and LNCaP^{APIPC} with exogenous FGF8b increased ERK1/2 phosphorylation. Increased baseline ERK1/2 phosphorylation observed in LNCaP^{APIPC} was completely ablated by treatment with PD173074 (PD074), a fibroblast growth factor receptor (FGFR)-specific inhibitor (73). PD074 also inhibited ERK1/2 phosphorylation in response to exogenous FGF8b stimulation (Figure 19D). A 96-hour growth assay confirmed that exogenous FGF8 treatment stimulated hormone-depleted proliferation in both LNCaP$^{shAR/pATK}$ (27% increase, $p<0.001$) and LNCaP^{APIPC} (7% increase, $p=0.04$). While treatment of LNCaP$^{shAR/pATK}$ with PD074 resulted in a minor decrease in cell number (11%, $p=0.005$), treatment of LNCaP^{APIPC} with PD074 markedly decreased cell number (27%, $p<0.001$). FGF8-mediated proliferation was completely ablated in both cell lines co-treated with PD074 and exogenous FGF8 (Figure 19E).

To demonstrate that FGF8 treatment was sufficient to induce growth in cells cultured under total androgen pathway suppression, hormone-depleted LNCaP$^{shAR/pATK}$ were co-treated with doxycycline and exogenous FGF8b. FGF8b-mediated proliferation was maintained during TAPS over the course of eight days, albeit at a lower rate than AR-replete LNCaP$^{shAR/pATK}$ (Figure 20A). In a parallel experiment, LNCaP$^{shAR/pATK}$ was cultured in androgen-depleted media and AR expression was suppressed by pre-treatment with 1μg/ml doxycycline for 72 hours. Addition of exogenous FGF8b was sufficient to induce castration resistant proliferation in both AR-suppressed LNCaP$^{shAR/pATK}$ and LNCaP$^{shAR/pATK}$ where AR was re-expressed following removal of doxycycline from the media (Figure 20B). These data verified that FGF8b treatment is sufficient to support both AR-dependent castration-resistant growth and total androgen pathway-independent growth.

FGF8 activation of MAPK signaling upregulates ID1 expression

To identify the downstream transcriptional effects of FGF8 signaling in LNCaP^{APIPC}, gene expression data was analyzed for genes that could plausibly be downstream of MAPK signaling and could play a mechanistic role in supporting growth in cells subjected to TAPS. A known oncogene, ID1, was found to be differentially upregulated in LNCaP^{APIPC} compared to LNCaP$^{shAR/pATK}$(3.5-fold increase, q<0.001; Table 8). ID1 is thought to prevent differentiation by binding cell lineage-specific transcription factors, and is downregulated in most terminally differentiated tissues (74). Overexpression of ID1 has been associated with aggressive, castration-resistant, and poorly differentiated prostate cancer (75, 76) and ID1 expression can be upregulated in tissue culture by exogenous treatment with bone morphogenetic protein 2 (77) or fibroblast growth factor 2 (78) via MAPK pathway activation. Because LNCaP^{APIPC} exhibits a poorly-differentiated morphology and increased MAPK pathway activation compared to LNCaP$^{shAR/pATK}$, we hypothesized that ID1 expression may be downstream of FGF8 signaling.

qRT-PCR analysis of LNCaP$^{shAR/pATK}$ revealed that ID1 expression increased 3-fold (p=0.002) following FGF8 stimulation. FGF8 stimulation of LNCaP^{APIPC} resulted in a 1.2-fold increase in ID1 (p=0.043; Figure 21A). Immunoblotting for ID1 confirmed these results (Figure 21B). ID1 upregulation was also observed in androgen-sensitive 22RV1 cells cultured under androgen-depleted conditions (Figure 21C, Figure 21D), suggesting that ID1 regulation by FGF8 is a conserved mechanism in prostate cancer cells. Activation of specific RTKs is associated with an increase in ligand-independent activation of AR transcription in some models (79, 80), however we did not observe a change in AR or PSA expression during FGF8b stimulation (Figure 21A, Figure 21C), further supporting a mechanism by which FGF8 signaling bypasses AR to maintain prostate cancer cell viability and proliferation.

ID1 expression is required for LNCaP^{APIPC} growth, and repressing ID1 expression partially inhibits FGF8b-induced castration-resistant proliferation in LNCaP$^{shAR/pATK}$.

ID1 overexpression supports serum-free growth in wildtype LNCaP (81), and ID1 knockdown suppresses growth in the AR-null prostate cancer cell line PC3 (82). Therefore, ID1 upregulation might be mediating the growth-promoting effects of FGF8 stimulation in androgen-depleted LNCaP^{APIPC} and LNCaP$^{shAR/pATK}$. To assess this hypothesis, anti-ID1 siRNA was used to inhibit ID1 expression in LNCaP^{APIPC} and LNCaP$^{shAR/pATK}$. ID1 knockdown did not significantly affect LNCaP$^{shAR/pATK}$ growth in androgen-depleted conditions compared to a scrambled control siRNA (siUNI). In contrast, ID1-targeting siRNA #1 and siRNA #2 decreased LNCaP^{APIPC} viability by 32% ($p=0.003$) and 43% ($p<0.001$), respectively (Figure 21E). When LNCaP$^{shAR/pATK}$ were co-treated with siRNA and FGF8, however, ID1 knockdown reduced growth by ~35% ($p<0.001$) compared to LNCaP$^{shAR/pATK}$ co-treated with FGF8 and non-targeting control siRNA. The effect of ID1 knockdown was enhanced in LNCaP^{APIPC}, with ID1 siRNA #1 decreasing growth by 39% ($p<0.001$) and siRNA #2 decreasing growth by 50% ($p<0.001$) when compared to LNCaP^{APIPC} co-treated with exogenous FGF8 and a non-targeting control siRNA (Figure 21E). These experiments were replicated in androgen-depleted 22RV1 with similar results, providing further evidence of ID1 expression functioning as a downstream mediator of castration resistant growth in cells stimulated by FGF8 (Figure 21F).

ID1 expression is anti-correlated with PSA expression in CRPC.

Data collected from *in vitro* experiments suggested that FGF8-mediated upregulation of ID1 was sufficient to induce growth in androgen-depleted conditions. Therefore, we hypothesized that *in vivo* CRPC may adapt to low levels of AR signaling by upregulating ID1. To test this hypothesis, cDNA generated from 68 CRPC samples was analyzed for expression of AR, PSA, and ID1 via qRT-PCR. The relationship between AR and PSA expression in CRPC was assessed by calculating a Pearson Product-

Moment Correlation Coefficient (PPMCC). As expected, there was a statistically significant correlation between AR and PSA expression ($r=0.6541$, $p<0.0001$; Figure 22A). A PPMCC calculated to compare AR and ID1 expression revealed no significant association ($r=0.066$, $p=0.5954$; Figure 22B). However, there was a statistically significant inverse correlation ($r=-0.3307$, $p=0.007$) between the expression of PSA and the expression of ID1 (Figure 22C), suggesting that *in vivo* CRPC may upregulate ID1 to compensate for decreased levels of AR-mediated transcription.

Identification of non-NEPCa AR-null prostate cancer metastases.

LNCaP^{APIPC} represents the first AR-null, non-neuroendocrine prostate cancer cell line to be directly derived from an AR-positive progenitor. In clinical disease, AR-null deposits are common in tumors treated with extended ADT, however these cells typically express some neuroendocrine-like histological markers. However, a previous investigation of 95 suspected NEPCa tumors revealed a small subpopulation of tumors that did not express markers of neuroendocrine differentiation (63), similar to LNCaP^{APIPC}. In an attempt to identify additional examples of AR-null and non-neuroendocrine metastases, we performed IHC on CRPC metastases to assess PSA, AR, Chromogranin, and Synaptophysin expression. Out of 184 CRPC metastases collected from 43 patients, five tumors from two patients were identified that did not express PSA, AR, Chromogranin A, or Synaptophysin (PACS-null). Surprisingly, in addition to being histologically PACS-null, these tumors appear to exhibit a cellular morphology more similar to AR-positive adenocarcinoma and LNCaP^{APIPC} subcutaneous xenografts than small cell NEPCa (Figure 23).

Discussion

LNCaP^{APIPC} is the first example of a non-NEPCa androgen pathway-independent prostate cancer model derived directly from an AR-positive progenitor. Complete androgen pathway independence was achieved in LNCaP^{APIPC} via elevated FGF8 autocrine signaling. FGF8 stimulation increased expression of

downstream effector gene ID1, which was required for castration-resistant growth in both LNCaP$^{shAR/pATK}$ and LNCaP^{APIPC}. Furthermore, LNCaP^{APIPC} cells cultured as subcutaneous xenografts histologically and morphologically resembled rare PACS-null tumors obtained from men who were treated with sustained ADT. These data confirm that AR-positive prostate tumors treated with aggressive AR-pathway inhibition may escape AR pathway dependence by upregulating existing signal transduction pathways. Furthermore, the identification of PACS-null tumors in samples collected from clinical CRPC – by our group and by other investigators (63)- indicates that a rare subset of tumors already bypass AR pathway dependence *in vivo*, and that AR loss does not always induce neuroendocrine differentiation. This suggests that alternative signaling mechanisms (such as FGF8/ERK/ID1) may bypass pathways promoting traditional AR-null neuroendocrine differentiation, instead promoting a more anaplastic prostate cancer phenotype.

MAPK signaling has been shown to promote poorly-differentiated tumor growth in models of prostate cancer (83) and constitutive ERK1/2 activity is associated with castration resistance (84-86). Signaling mediated by PI3K, another pathway that supports CRPC and AR-independent growth (32, 33), was decreased in LNCaP^{APIPC}. However, these results may intrinsic to FGF8 signaling in prostate cancer biology. In a conditional PTEN-deficient and FGF8b overexpressing mouse model of prostate cancer, both PTEN loss and FGF8 upregulation was required for tumor initiation, however PI3K signaling was markedly decreased in the progression from prostatic intraepithelial neoplasia (PIN) to more advanced adenocarcinoma (87).

FGF signaling proteins primarily function as autocrine and paracrine signaling molecules and exert a high affinity for the glycosaminoglycan side-chains of cell surface proteoglycans. Therefore, they can be found sequestered near the site of their export (88). FGF8 is mitogenic in both prostate and non-prostate cancer models (87, 89-91), and is detectable by IHC in 50% of primary prostate tumors and 80%

of CRPC metastases (92). While initial studies found FGF8 expression to be transcriptionally regulated by the AR (93, 94), we did not observe FGF8 to be AR-regulated in LNCaP$^{shAR/pATK}$ or LNCaP^{APIPC} (Table 8). Other non-AR-mediated mechanisms of FGF8 transcriptional regulation have been identified in embryogenesis and *in vitro* tissue culture models (95, 96).

The mechanisms by which RTK/MAPK signaling promotes CRPC proliferation are diverse and remain poorly defined (34, 85, 97). While there is some evidence suggesting that MAPK activity functions to stimulate ligand-independent ARG expression (97), FGF8/MAPK signaling did not promote the re-expression of ARGs in LNCaP$^{shAR/pATK}$ and LNCaP^{APIPC}, but instead upregulated the expression of ID1. ID1 expression is downstream of FGF2-mediated signaling in non-prostate models (78), however this is the first example of FGF8-mediated ID1 regulation in prostate cancer. Furthermore, this is the first model demonstrating that AR protein expression is not required for FGF8-mediated proliferation, or ID1-mediated proliferation, in the progression from AR-dependent to AR-pathway independent prostate cancer (81, 98, 99). The role of ID1 expression in sustaining proliferation during TAPS is a topic of ongoing investigation.

It is a well-established phenomenon that LNCaP cells can undergo reversible neuroendocrine transdifferentiation following ADT and other small molecule treatments (67, 100-103), and expression of the AR may prevent the development of a NEPCa-like phenotype (102). However, some forms of ADT that reduce AR protein expression – such as Hsp90 inhibitors – do not induce LNCaP neuroendocrine transdifferentiation (103), suggesting that AR loss alone is not sufficient for neuroendocrine transdifferentiation. By using TAPS to generate the AR-null, ARG-null, non-neuroendocrine cell line LNCaP^{APIPC} we confirmed this hypothesis, although it is still unclear as to why LNCaP^{APIPC} avoided a neuroendocrine-like fate. Because LNCaP cells are a naturally heterogeneous population (65), one explanation may be that the multiple rounds of selection involved in generating LNCaP$^{shAR/pATK}$ selected

against slowly-proliferating NE-like cells (67) naturally existing in the population. More investigation into the mechanisms regulating the development of NEPCa will be critical to understanding how extended ADT affects prostate cancer progression and differentiation.

Ongoing molecular and histopathologic analyses indicate that anaplastic prostate carcinomas exist within a spectrum of AR-null subtypes – including rare carcinoid prostate tumors, small cell anaplastic prostate cancer, large cell neuroendocrine disease - and there is existing IHC evidence of rare tumors that do not express AR or markers of NEPCa (59, 60). Given that anaplastic and neuroendocrine tumors are more common following sustained ADT and likely arise from adenocarcinoma *in vivo* (61), we expect to see an increase in the incidence of AR-pathway independent anaplastic tumors with the use of more potent ADT in patients with CRPC. A molecular analysis of metastases in men treated with more potent forms of ADT – as monotherapy or combined AR/steroid production blockade – will be required to identify those tumors that completely escape AR pathway dependence. Because anaplastic disease is characterized by de-differentiated morphology, we believe that simultaneous inhibition of AR-regulated pro-differentiation transcription and inhibition of pathways promoting de-differentiation (such as ID-family genes) will provide a therapeutic advantage in preventing CRPC recurrence. An improved understanding of ID-family targets, mechanisms regulating classical neuroendocrine differentiation, and processes mediating epithelial-neuronal transdifferentiation must be a priority to further understand and treat the emerging clinical spectrum of ADT-driven anaplastic prostate cancer.

Materials and Methods

Tissue Culture. LNCaP cells stably transfected with a tetracycline-inducible anti-AR shRNA, as previously described (64), were obtained as a gift from Dr. Paul S. Rennie and grown in RPMI1640 (Life Technologies) +5%FBS(Gibco) +1% PenStrep (Gibco)+2.5µg/ml Blasticidin (Life Technologies)+1µg/ml Puromycin (Life Technologies). These cells were further modified via Lipofectamine 2000 (Life Technologies) transfection of a plasmid encoding a triple-probasin-driven herpes thymidine kinase (HSV-

TK) and a Zeocin resistance cassette. A clonal population of this cell line derived from Zeocin (Life Technologies) selection and serial dilution in a 96-well plate, which we refer to as LNCaP$^{shAR/pATK}$, was subjected to TAPS. For two weeks the cells were grown in RPMI1640+5%CSS (Gemini). At week 3, media was supplemented with 1mg/ml doxycycline (Clontech). Media was changed every 3-4 days and P-LNCaP was maintained under TAPS for five months. A surviving colony of proliferating cells emerged. Following a 3-month expansion, this population of cells was treated with 50μM ganciclovir (GCV; InvivoGen) for two weeks to eliminate any cells still robustly expressing an androgen-dependent transcriptional program. We referred to the surviving population as LNCaP^{APIPC}. LNCaP$^{shAR/pATK}$ is maintained in RPMI1640 + 5%FBS +1% PenStrep+2.5μg/ml blasticidin+1μg/ml puromycin+25μg/ml Zeocin. LNCAP^{APIPC} is maintained in RPMI1640 + 5%CSS +1% PenStrep+2.5μg/ml blasticidin+1μg/ml puromycin+25μg/ml Zeocin+1μg/ml doxycycline.

Migration and Invasion Assays. Migration and invasion assays were performed as per protocol in Cultrex 96-well cell invasion/migration transwell plates (R&D Systems). RPMI1640+/-10%FBS was added to the lower chamber and 100,000 cells suspended in serum-free RPMI1640 were added to the top chamber. For invasion assays, membranes were coated with 0.2x BME. Fluorescence was measured on a BioTek Synergy2 multiwell plate reader and normalized to P-LNCaP RPMI1640 serum-free control.

Growth Assays. Cell growth was assayed by plating 5000 cells per well in a TC-treated 96-well black-sided, clear bottom plate (Corning). Media was changed every 48 hours and plates were collected at the reported timepoints and stored at -80C. Plates for each experiment were assayed in batches using Cyquant (Life Technologies) to estimate cell viability as per protocol. Cells were treated with FGF8b (25ng/ml; eBioscience) and PD173074 (1μM; Tocris). MDV3100 (5μM) was received as a gift from Medivation Inc.

Conditioned Media. Serum-free phenol red-free Optimem (Life Technologies) was added to 80% confluent LNCaP^{APIPC} and LNCaP$^{shAR/pATK}$ cultured in a tissue culture-treated T75 flask (Corning). 24 hours later, media was collected and centrifuged for 5 minutes at 5000RPM to pellet cellular debris. The supernatant was added to an Amnicon Ultracel 3K centrifugal filter (Millipore) and concentrated as per manufacturer's instructions.

siRNA Transfection. Cells were plated at 5000 cells/well in a 96-well plate in 100µl of phenol red-free Optimem supplemented with either 3%FBS or 3%CSS +1%PenStrep. 24 hours after cell plating, cells were transfected with siRNA (Sigma) using RNAiMax lipofectamine reagent (Life Technologies) in 20ul total volume. Cell viability was estimated 96 hours after transfection by adding Cell Titer-Glo (Promega) and measuring luminescence (RLUs) as per protocol on a BioTek Synergy2 multiwell plate reader. Luminescence measurements from wells transfected with an equimolar pool of 3xKif11 siRNAs was used to estimate transfection efficiency. Transfections performed in 6-well plates for RNA collection used scaled-up conditions from 96-well experiments, and cells were harvested 24 hours after transfection as described below. siRNA sequences can be found in Table 9.

Human tissue acquisition. Human metastatic prostate tissues were obtained via the University of Washington Medical Center Prostate Cancer Donor Autopsy Program as previously described (104). All human subjects signed informed consent, and all procedures relating to human subjects and tissue were approved by the Institutional Review Board of the University of Washington Medical Center. Harvested tumors were either immediate embedded in OCT (TissueTek OCT Compound), snap frozen, and stored at -80C or formalin-fixed and paraffin-embedded. Human TMAs were constructed for IHC analyses from fixed paraffin-embedded tissues from 43 rapid autopsy patients (consisting of 4 tissue microarray blocks with 2 replicate cores per block). 184 individual metastases were included on the TMAs.

RNA collection and Quantitative Real-Time PCR (qRT-PCR). CRPC total RNA was obtained from metastases harvested by the University of Washington Rapid Autopsy program as previously described by Holcomb, *et al* (50). Cancerous tissue from OCT-embedded tumors was laser capture-microdissected, and RNA was collected and amplified as described previously (105). Cell culture total RNA was isolated from 6-well plates using an RNEasy kit (Qiagen) as per protocol. qRT-PCR reactions were performed in triplicate using an Applied Biosystems 7900 sequence detector with SYBR Green PCR master mix (Life Technologies). Primers were designed using PrimerQuest (IDT, San Diego, CA, USA), and all reactions were normalized to the expression of the housekeeping gene Rpl13a. A water negative control did not produce significant amplification product. PCR primer sequences can be found in Table 10. Statistical analysis was performed using an unpaired two-sided Student's T-test using Welch's correction to determine significance.

Protein Collection and Immunoblotting.

Protein was collected from tissue culture by lysing adherent cells with a cell lysis buffer (1.5M Urea, 1%SDS, 1%NP-40, 2%Tween20, 250nM NaCl, PBS) supplemented with 1x phosphatase inhibitors (PhosStop, Roche Diagnostics) and a 1x protease inhibitor cocktail (Complete Mini, Roche Diagnostics, Basel, Switzerland). Protein was quantified per protocol using a bicinchoninic acid assay (Thermo Scientific). Normalized cell lysates were loaded onto a 12% NuPAGE Bis-Tris gel (Life Technologies) in MES buffer. Protein was transferred to nitrocellulose membranes using a semi-dry transfer apparatus and Tris/CAPS buffer. Immunoblots were probed with primary antibodies targeting AKT (Cell Signaling, #9272), phospho-AKT (Ser473; Cell Signaling, #4058), AR (Santa Cruz, sc-816, N-terminal), Erk1/2 (Sigma, M5670), diphosphorylated-Erk1/2 (Sigma, M9692), FGF8b (R&D Systems, MAB323), ID1(Biocheck, Inc., #195-14), MEK1/2 (Sigma, M5795), phospho-MEK1(Ser298; Upstate, #07-339), or PSA (Dako, A0562). Horseradish-peroxidase conjugated secondary antibodies (Thermo Scientific) were used in conjugation

with Supersignal West Pico Chemiluminescent substrate (Thermo Scientific) to visualize protein targets. Membranes were then stripped for 15 minutes in Stripping Buffer (Thermo Scientific) and re-probed with anti-Actin antibody (Santa Cruz Biotechnology, Santa Cruz, CA; sc-1616) as a loading control.

Gene Expression Microarrays. LNCaP$^{shAR/pATK}$ and LNCaP^{APIPC} were grown in RPMI1640/5%CSS +/- 1µg/ml doxycycline. After 48 hours cells were treated with either vehicle (ethanol) or 1nM R1881. Total RNA was collected 24 hours after R1881 treatment as described above. A reference standard RNA for use in two-color oligo arrays was prepared as described previously(106). Total RNA from triplicate preparations of LNCaP$^{shAR/pATK}$ and LNCaP^{APIPC} cells as well as reference total RNA samples were amplified and hybridized to Agilent 44K whole human genome expression oligonucleotide microarray slides as previously described (107). Spots of poor quality or average intensity levels <300 were removed from further analysis. The Statistical Analysis of Microarray (SAM) program (108) was used to analyze expression differences between groups using unpaired, two-sample t tests. Differentially expressed genes were identified as those with a false-discovery rate q-value$\leq$5% and fold-expression change $\geq$2.

Comparative Genomic Hybridization. 3.5E6 LNCaP$^{shAR/pATK}$ or LNCaP^{APIPC} cells were harvested and genomic DNA was obtained using the DNEasy kit (Qiagen). 1.5ug of genomic DNA was hybridized against Human Gold Standard genomic DNA (Promega G1471) on a Dana Farber Agilent SurePrint G3 2x415K custom CGH array (AMID: 023364). Analysis of raw data was performed on Nexus Copy Number software (v6.0).

P-LNCaP/APIPC Xenograft Tumors. NOD-scid IL2Rgamma^{null} mice were purchased from the Fred Hutchinson Cancer Research Center animal facility. P-LNCaP and APIPC cells were resuspended 1:1 in Matrigel (BD Biosciences) to a final concentration of 5x10^6 cells/ml and 100µl of cells were injected subcutaneously into the flank of each mouse. All xenografts were measured every 2 days. Animals implanted with LNCaP^{APIPC} xenografts were maintained on a diet supplemented with doxycycline

(200mg/Kg, Harlan). When tumors reached a total volume of 500mm^3 animals were enrolled into treatment arms consisting of +/- surgical bilateral orchiectomy (LNCaP^{APIPC} and LNCaP$^{shAR/pATK}$) and +/- doxycycline-supplemented feed (LNCaP$^{shAR/pATK}$). Each treatment group was composed of 8 animals. Animals were sacrificed when tumors reached a volume of 1500mm^3. All xenografts experiments were approved by the Fred Hutchinson Institutional Animal Care And Use Committee (File#1671).

Immunohistochemistry. IHC using anti-Chromogranin A (Dako M0869) and anti-Synaptophysin (Dako, SY38) antibodies was performed by the University of Washington Medical Center Anatomic Pathology Laboratory. IHC using anti-AR (BioGenex, MU256-UC) and anti-PSA (Dako, A0562) antibodies was performed as previously described(20). Briefly, formalin-fixed paraffin-embedded (FFPE) tissue was deparraffinized and rehydrated. 3% Hydrogen peroxide was used to quench endogenous tissue peroxidases and an avidin/biotin blocking system (Dako) was used to quench endogenous avidin/biotin. Antigen retrieval was performed with 10mM citrate buffer, pH=6.0 in a pressure cooker. Tissue was blocked with normal serum specific to the secondary antibody and the primary antibody was applied for 30 min at room temp, followed by biotinylated secondary antibodies (Dako) and ABC reagent (Vector Laboratires). DAB (Dako) was used as the chromogen and the TMA was counterstained with Meyer's hematoxylin. Immunostaining on the human TMAs was assessed by a genitourinary pathologist as 0 for no stain, 1 for faint/equivocal stain, and 2 for intense staining

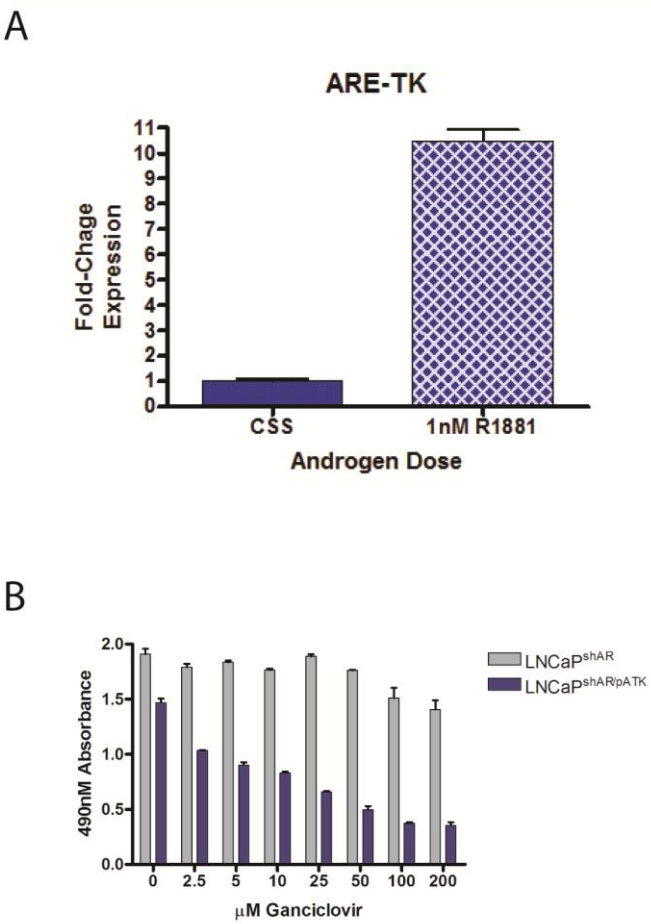

Figure 10: An androgen-regulated herpes thymidine kinase induces androgen and ganciclovir-dependent toxicity in LNCaP$^{shAR/pATK}$. (A) R1881 treatment increases HSV-TK expression in LNCaP$^{shAR/pATK}$. (B) Ganciclovir induces dose-dependent death in LNCaP$^{shAR/pATK}$ cultured in androgen-replete media, but not in LNCaP^{shAR}.

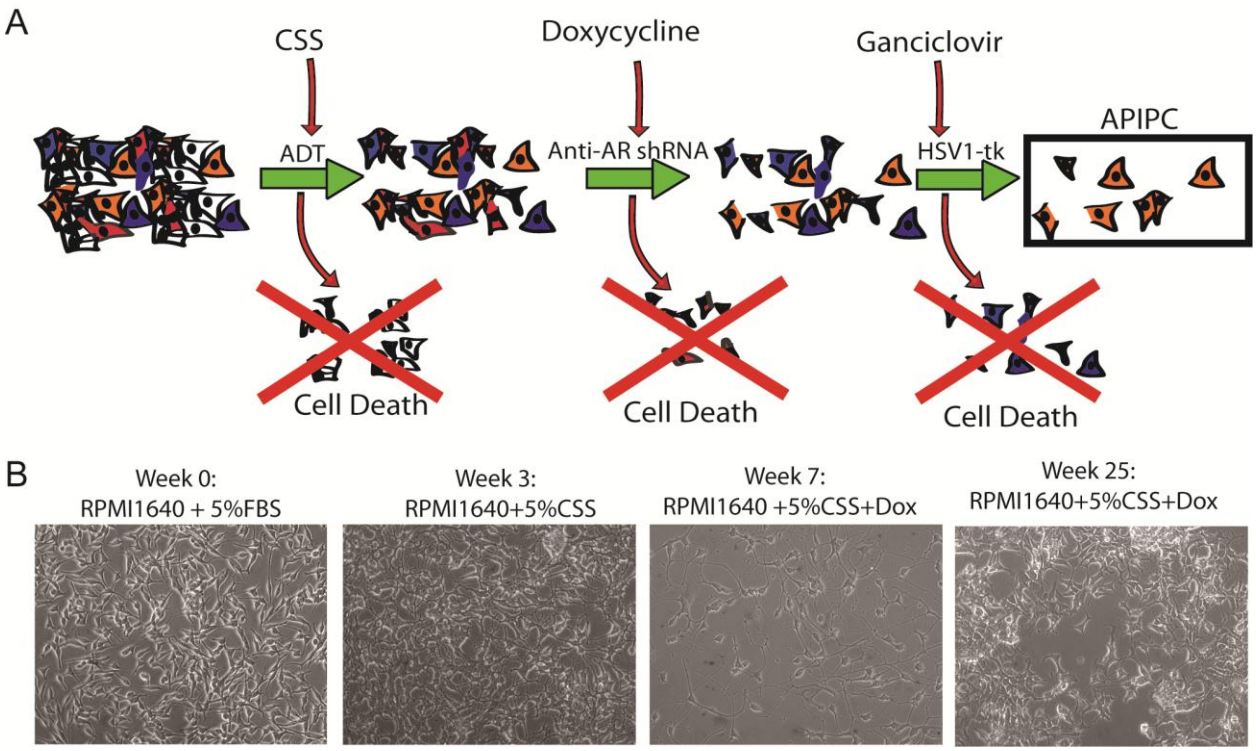

Figure 11: Total Androgen Pathway Suppression. (A) A depiction of TAPS treatment in LNCaP$^{shAR/pATK}$ and the development of LNCaP^{APIPC}. (B) P-LNCaP underwent morphological changes associated with androgen withdrawal in LNCaP cells (week 3), and most cells were non-viable by week 7. Following a massive apoptotic event, a small surviving population regrew from TAPS therapy (week 25). We refer to these cells as LNCaP^{APIPC}.

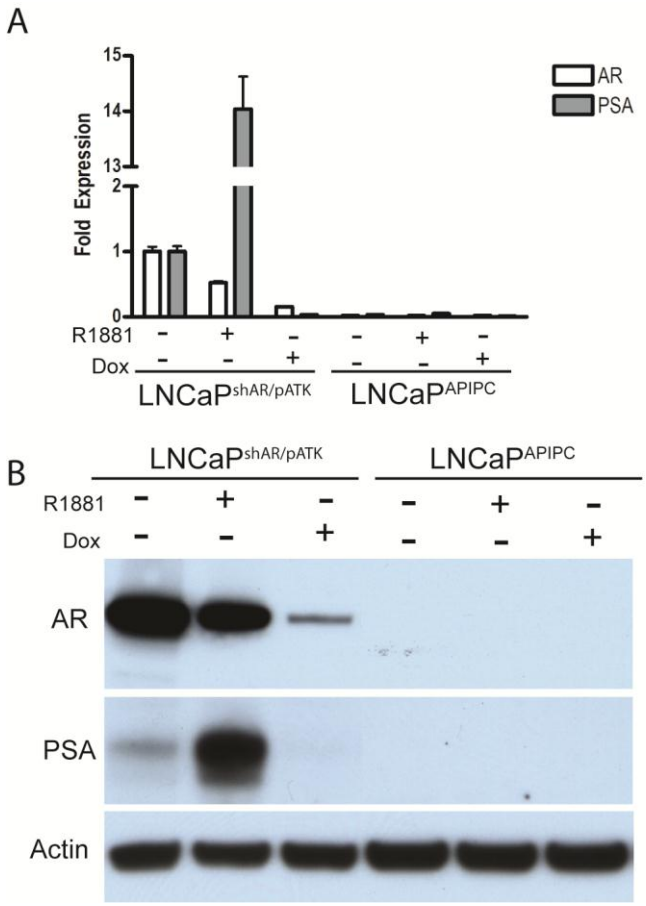

Figure 12: LNCaPAPIPC does not express AR or PSA. (A)qRT-PCR analysis of cDNA generated from LNCaP$^{shAR/pATK}$ shows the expected pattern of AR and PSA expression in response to treatment with 1nM R1881 or 1µg/ml doxycycline. AR and PSA were nearly undetectable by qRT-PCR analysis of cDNA generated from LNCaP^{APIPC}. (B) Cell lysates were collected from LNCaP$^{shAR/pATK}$ and LNCaP^{APIPC} cultured in androgen deprived conditions and treated with +/-R1881 and +/-doxycycline. Immunoblots for AR and PSA confirmed the qRT-PCR results.

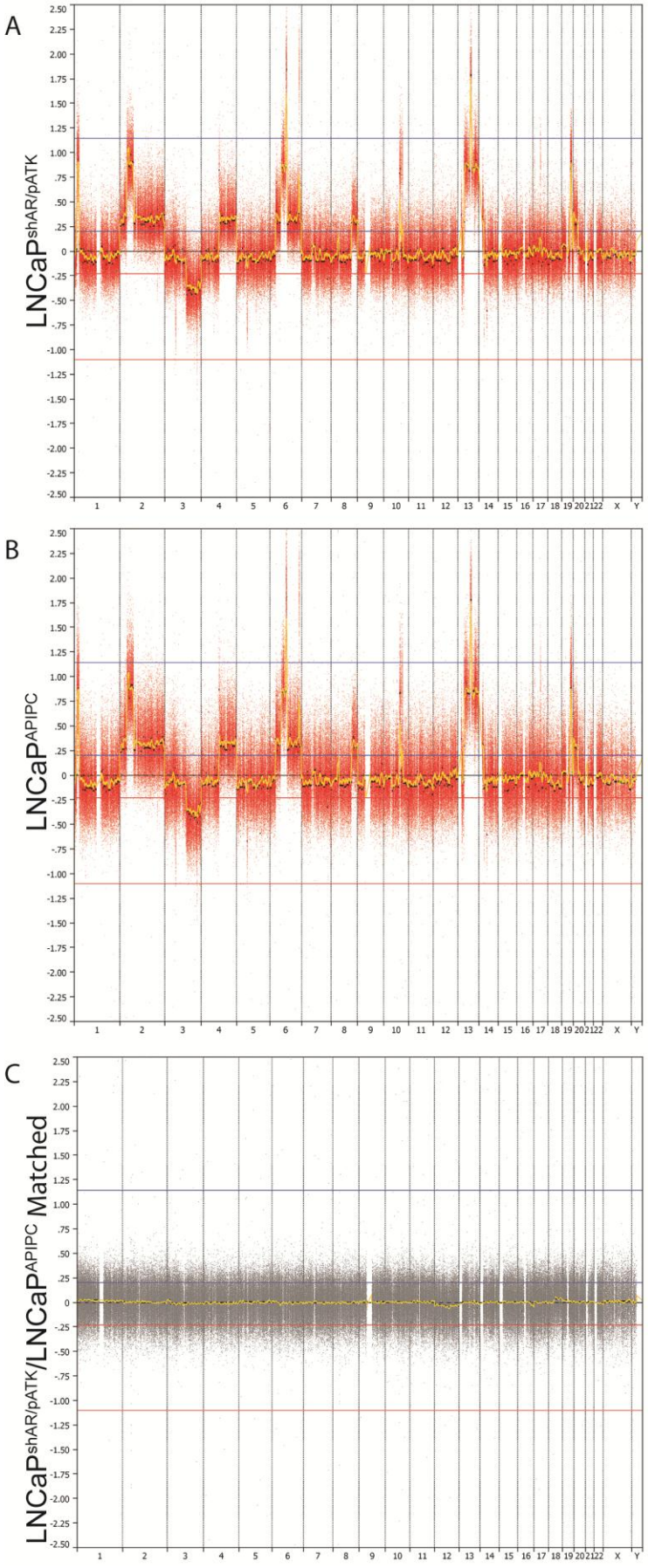

Figure 13: CGH confirms that LNCaP^{APIPC} is derived from LNCaP$^{shAR/pATK}$. CGH analysis of LNCaP$^{shAR/pATK}$ (A) and LNCaP^{APIPC} (B) compared to a Human Gold Standard genomic DNA pool reveals distinct genomic aberrations. (C) Subtraction of LNCaP^{APIPC} CGH data from LNCaP$^{shAR/pATK}$ CGH data confirms nearly 100% overlap in genomic aberrations, confirming a parent-daughter lineage.

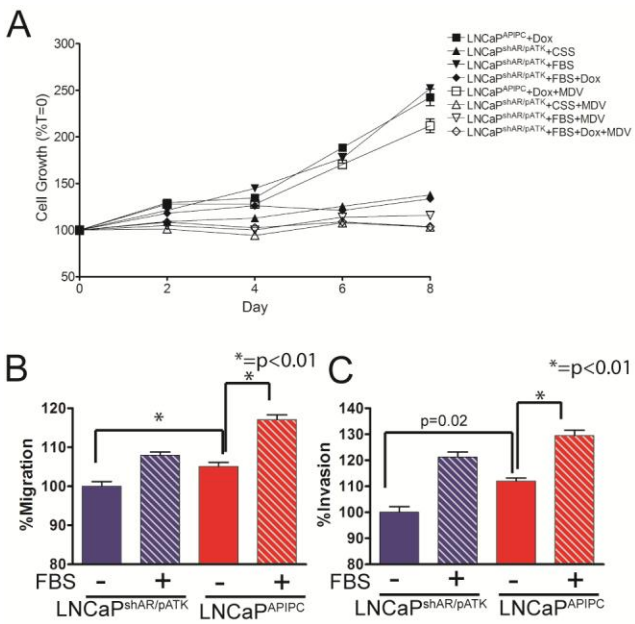

Figure 14: LNCaP^{APIPC} is resistant to ADT and more aggressive than LNCaP$^{shAR/pATK}$. (A) LNCaP^{APIPC} was grown in ligand and receptor depleted conditions and treated with vehicle (DMSO) or 5µM MDV3100. Growth was compared to LNCaP$^{shAR/pATK}$ growth in CSS, Serum, or Serum +1µg/ml doxycycline +/- MDV3100. MDV3100, ligand deprivation, and AR depletion completely inhibited LNCaP$^{shAR/pATK}$ growth. LNCaP^{APIPC} showed only minor growth inhibition when treated with MDV3100. Filled symbols, +DMSO; Open symbols, +MDV3100. Transwell migration (B) and invasion (C) assays demonstrated that LNCaP^{APIPC} is more aggressive than LNCaP$^{shAR/pATK}$ at baseline (no FBS gradient), and has a more robust migratory/invasive response to FBS. *= p<0.01.

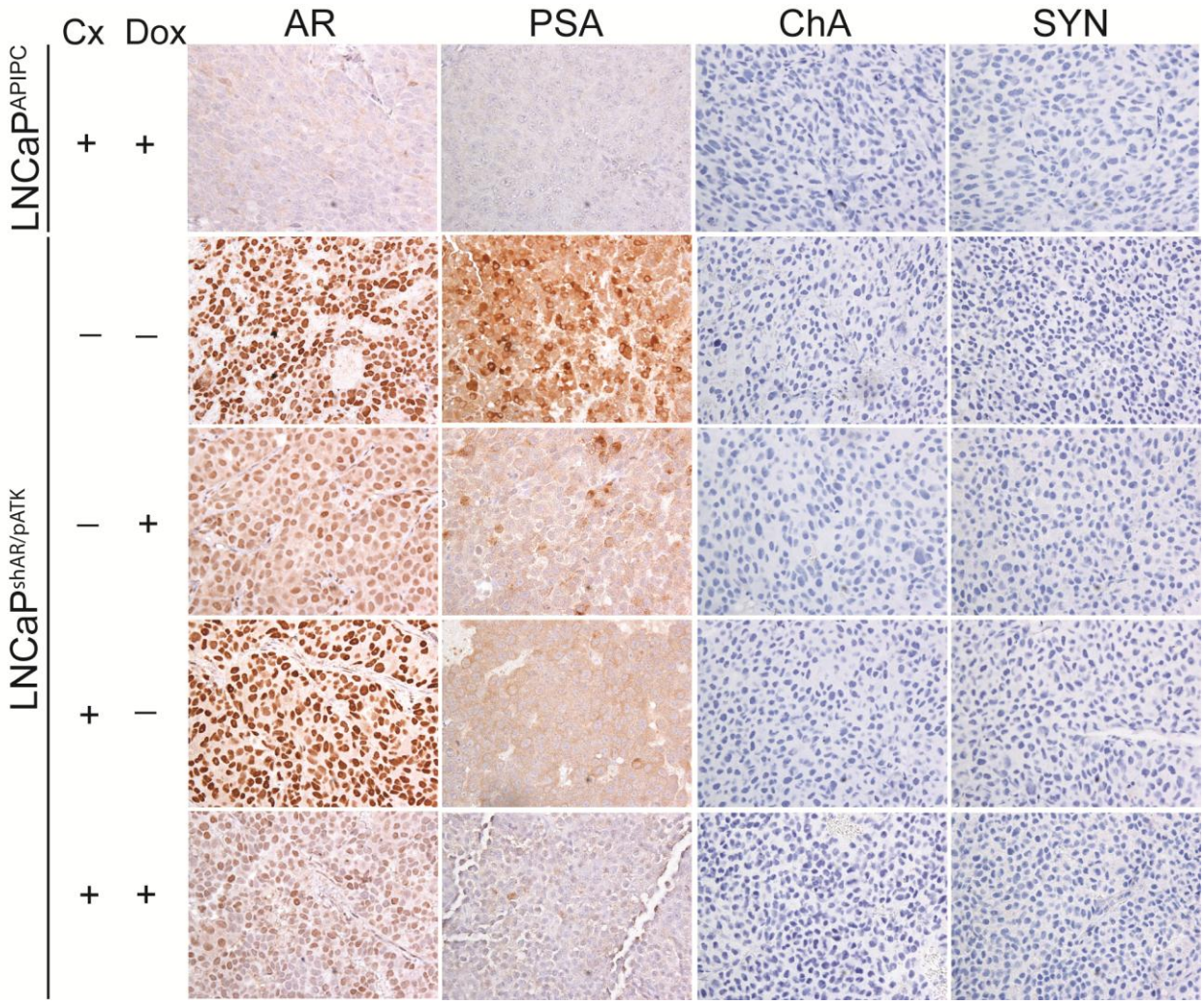

Figure 15: LNCaP^{APIPC} and LNCaP$^{shAR/pATK}$ xenografts do not express markers of NEPCa differentiation. LNCaP^{APIPC} and LNCaP$^{shAR/pATK}$ were grown as subcutaneous xenografts in immunocompromised mice. Mice received no treatment, or ADT in the form of castration or doxycycline-supplemented feed. IHC for AR, PSA, ChA, and SYN was performed on harvested tumors. Neither xenograft line expressed markers of neuroendocrine differentiation. LNCaP^{APIPC} did not express AR or PSA. The *in vivo* LNCaP$^{shAR/pATK}$ response to ADT was similar to the *in vitro* response, although those tumors treated with both doxycycline and castration still maintained AR-regulated gene expression. Cx = castration, Dox = doxycycline.

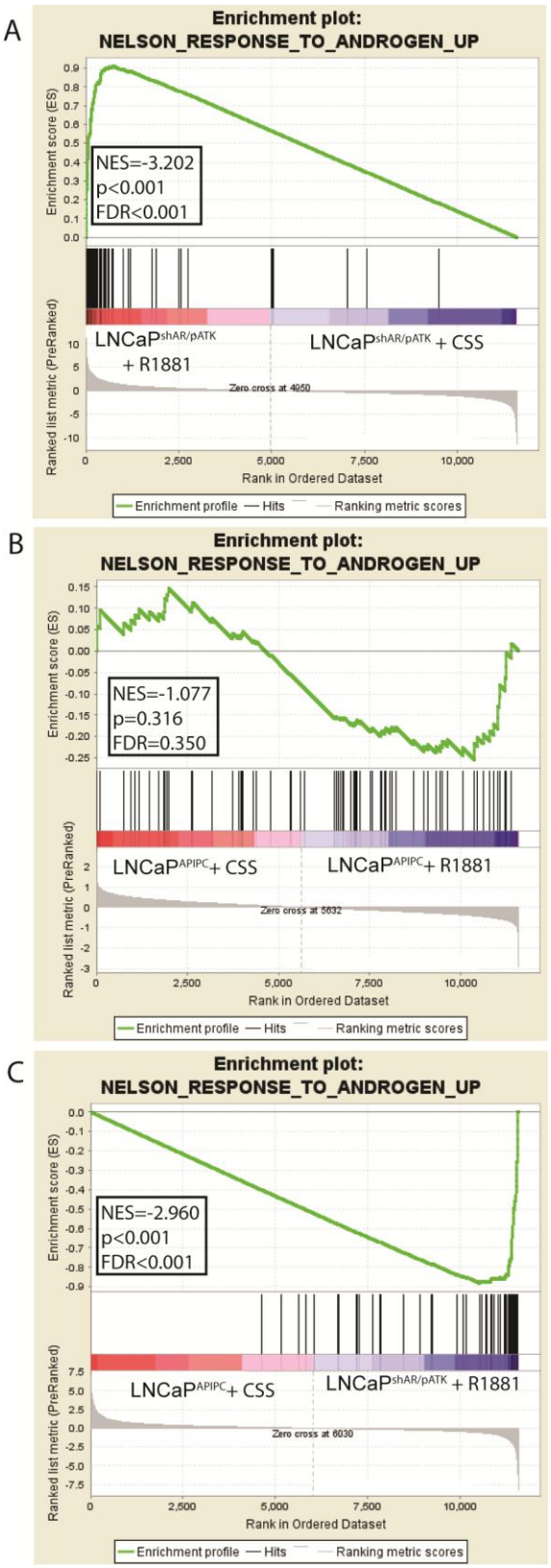

Figure 16: LNCaP^{APIPC} does not express an AR-mediated transcriptional program. LNCaP$^{shAR/pATK}$ and LNCaP^{APIPC} were grown in androgen-depleted media +/- 1µg/ml doxycycline for 48 hours. Cells were then treated with +/-1nM R1881 or vehicle (ethanol) for 24 hours and RNA was collected for gene expression analysis. (A and B) GSEA was used to quantify ARG enrichment in (A) LNCaP$^{shAR/pATK}$ and (B) LNCaP^{APIPC} stimulated with R1881 compared to androgen deprivation. (C) Gene expression in proliferating cells (LNCaP$^{shAR/pATK}$ in response to R1881, LNCaP^{APIPC} in androgen-depleted conditions) confirms an enrichment in androgen-regulated genes in LNCaP$^{shAR/pATK}$. This confirms that LNCaP^{APIPC} does not rely on the re-expression of ARGs for proliferation.

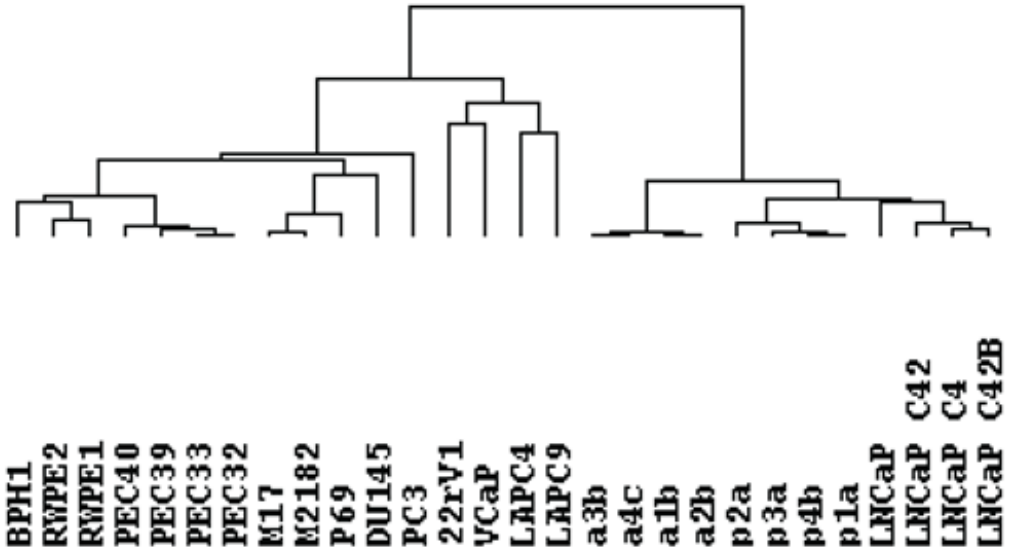

Figure 17: LNCaP^{APIPC} retains a LNCaP-derived gene expression profile. The top 500 expressed genes in each cell line was used to perform unsupervised hierarchical in LNCaP$^{shAR/pATK}$ and LNCaP^{APIPC} treatment groups and 20 other prostate cell lines. Both LNCaP$^{shAR/pATK}$ and LNCaP^{APIPC} cluster with other known LNCaP derivatives. a1-a4= LNCaP^{APIPC}. p1=p4= LNCaP$^{shAR/pATK}$. 1=CSS, 2=CSS+R1881, 3=CSS+Doxycycline, 4=CSS+R1881+Doxycycline.

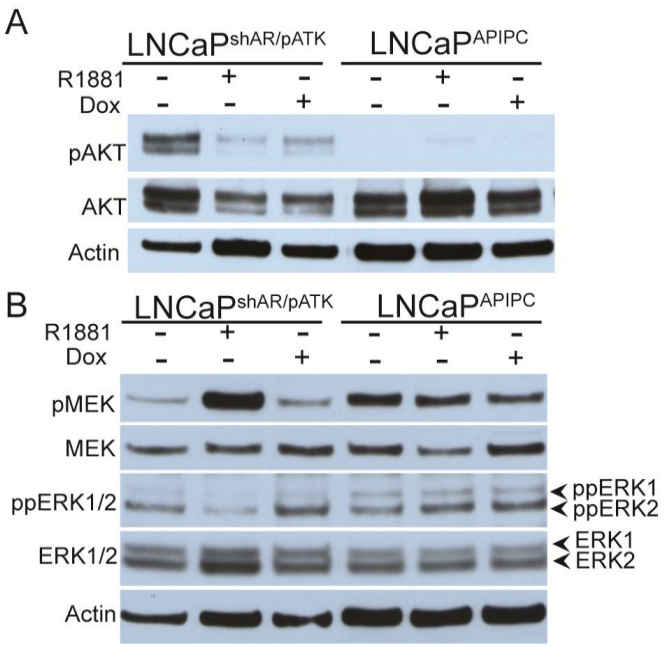

Figure 18: ERK1/2 signaling is upregulated in LNCaP^{APIPC}. LNCaP$^{shAR/pATK}$ and LNCaP^{APIPC} were cultured in androgen depleted media treated with +/-1nM R1881 and +/-1µg/ml doxycycline. Total cell lysates probed via immunoblot for intracellular pathway activation. (A) PI3K pathway signaling was evaluated by relative levels of pAKT. (B) MAPK pathway signaling was assessed through pMEK and ppERk1/2 levels.

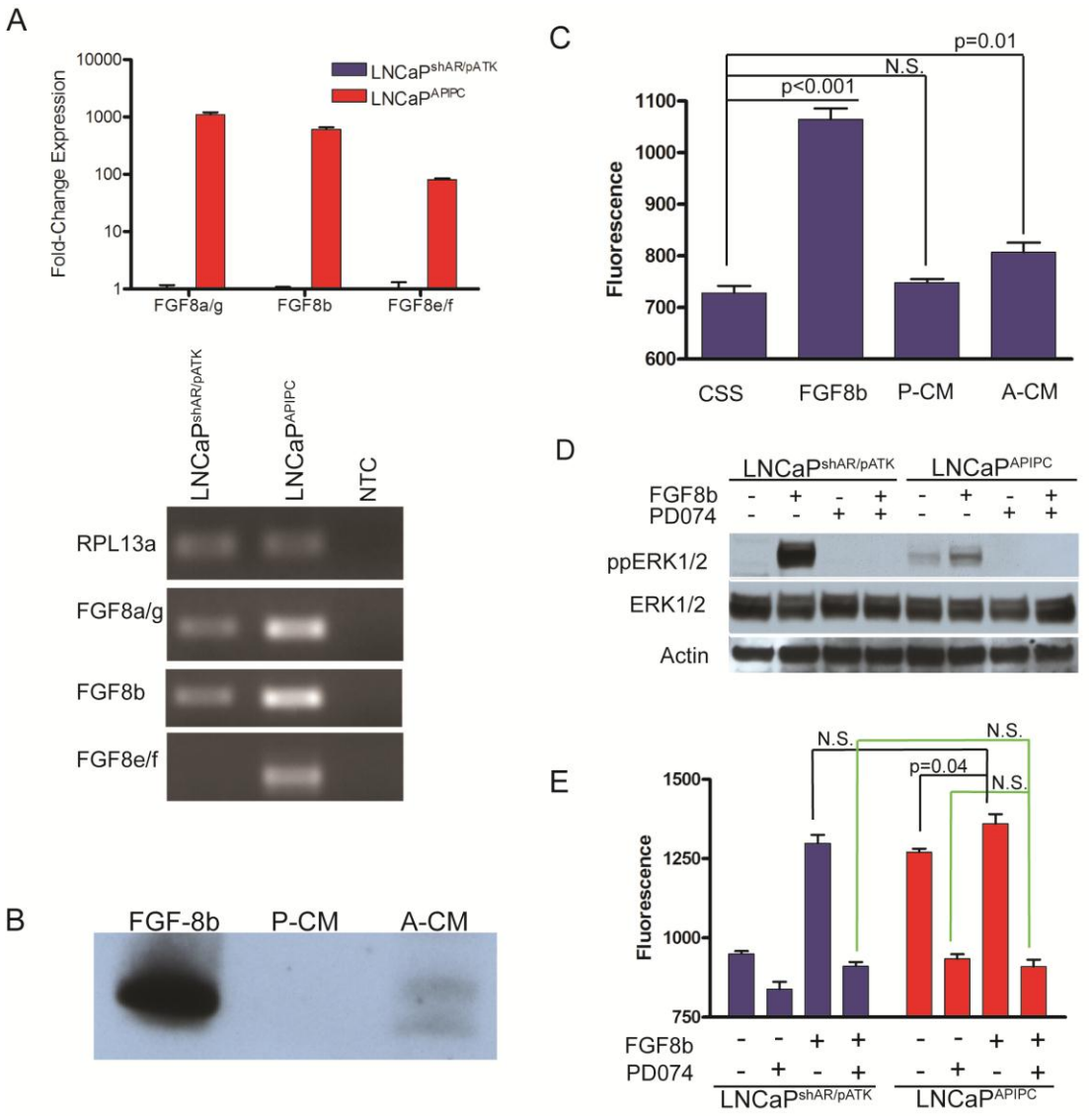

Figure 19: FGF8 signaling functions as an autocrine growth pathway in LNCaP^{APIPC}. (A) qRT-PCR detects FGF8 isoforms expressed by LNCaP$^{shAR/pATK}$ and LNCaP^{APIPC}, but not in a template-null control (NTC). qRT-PCR reaction products, visualized by agarose gel electrophoresis, confirms single-band amplification by each primer. (B) Nearly-confluent LNCaP$^{shAR/pATK}$ and LNCaP^{APIPC} were cultured in serum-free media for 24 hours. Conditioned media (LNCaP$^{shAR/pATK}$ (P-CM) and LNCaP^{APIPC} (A-CM)) were collected, concentrated 20-fold, and equivalent volumes were visualized versus an FGF8b positive control by immunoblotting with an FGF8b-specific antibody. (C) LNCaP$^{shAR/pATK}$ cultured for four days in androgen-depleted media were treated with 25ng/ml FGF8b, P-CM diluted 1:20, or A-CM diluted 1:20. Cell number was approximated using Cyquant. (D) LNCaP$^{shAR/pATK}$ and LNCaP^{APIPC} cultured for 15 hours in serum-free Optimem and treated for 9 hours with +/-1μM PD074. One hour later +/-25ng/ml FGF8 was added. Cell lysates were evaluated for MAPK signaling via immunoblot for ppERK1/2. FGF8b treatment increased MAPK signaling in LNCaP$^{shAR/pATK}$ and LNCaP^{APIPC}. Constitutive ppERK1/2 in LNCaP^{APIPC} is ablated following treatment with PD074. PD074 also completely inhibits ERK1/2 phosphorylation induced by exogenous FGF8b treatment. (E) LNCaP$^{shAR/pATK}$ and LNCaP^{APIPC} were cultured in androgen-deprived conditions and treated with +/-25ng/ml FGF8b and +/-1μM PD074. Cell number was approximated using Cyquant. N.S. = not significant.

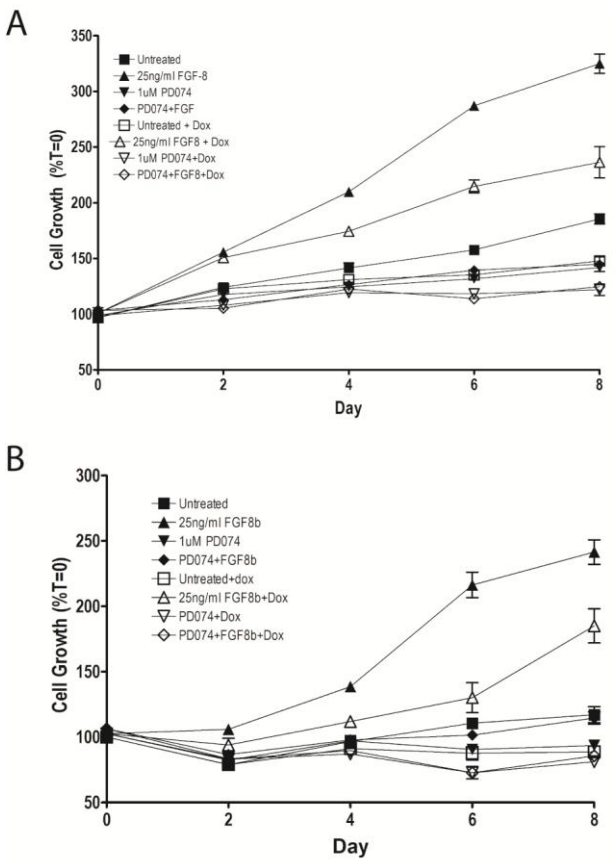

Figure 20: FGF8b treatment promotes growth in LNCaP$^{shAR/pATK}$ cultured under androgen-depleted and AR-suppressed conditions. (A) LNCaP$^{shAR/pATK}$ was cultured in androgen-depleted media +/- 25ngml FGF8, +/-1µM PD074, +/-1µg/ml doxycycline. Doxycycline was added on day 0 (A) or 72 hours prior to FGF8b treatment (B). Closed symbols, -doxycycline; open symbols +doxycycline. Cell number was estimated using Cyquant, and values were normalized to Day 0 (T=0).

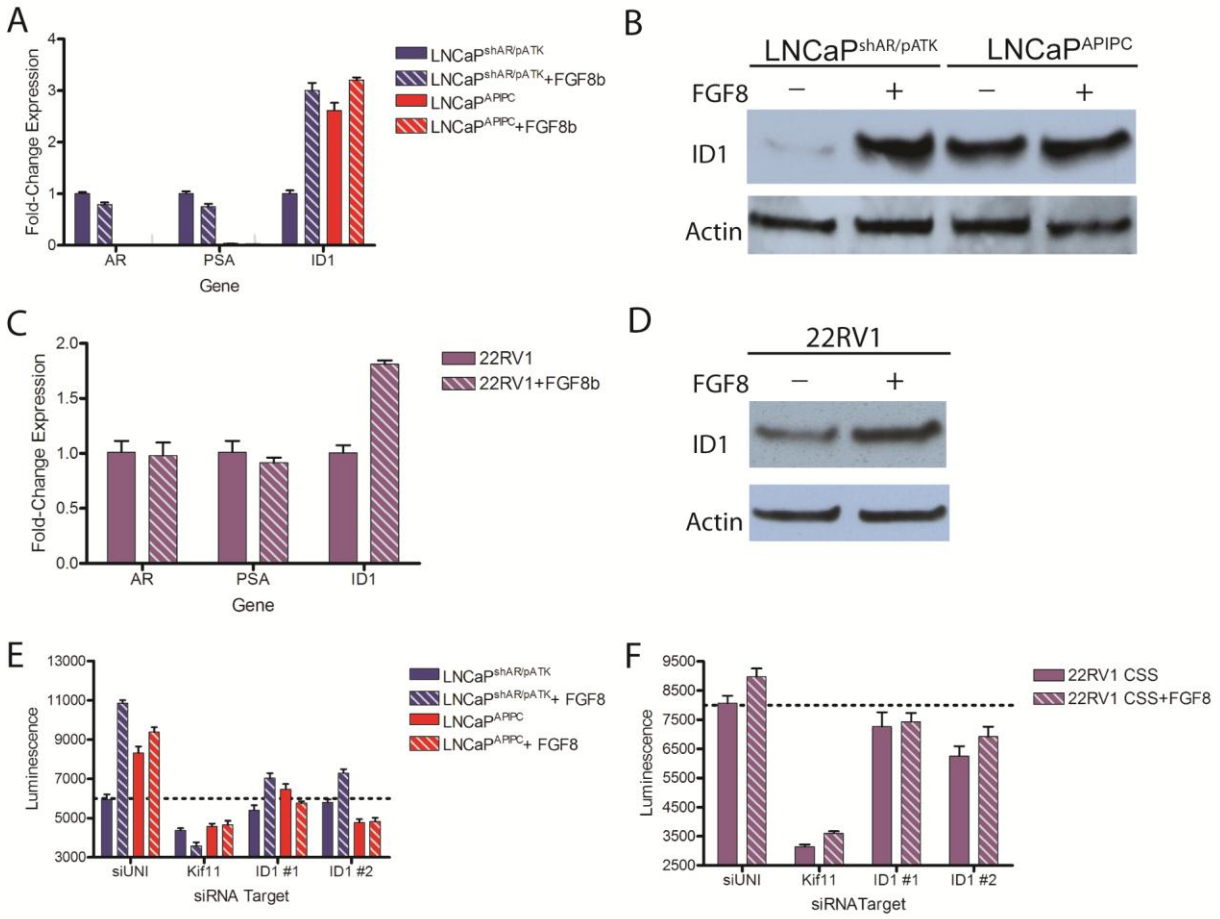

Figure 21: FGF8b-mediated proliferation is facilitated through the upregulation of ID1. (A) qRT-PCR was performed on cDNA generated from LNCaP$^{shAR/pATK}$ and LNCaP^{APIPC} cultured for 16 hours in serum-free Optimem and treated for 8 hours +/-25ng/ml FGF8. FGF8 stimulation upregulated ID1 but did not affect AR or PSA expression. (B) ID1 upregulation was confirmed via immunoblot. (C) qRT-PCR shows FGF8 mediated ID1 upregulation in 22RV1 cells. AR and PSA expression did not change. (D) ID1 upregulation in 22RV1s was confirmed by immunoblot. (E) LNCaP$^{shAR/pATK}$ and LNCaP^{APIPC} cultured in androgen-depleted media were transfected with siRNA specific for target genes and treated with +/-25ng/ml FGF8. ID1 knockdown abrogates FGF8-mediated proliferation. (F) 22RV1s cultured in androgen-depleted media were transfected with siRNA specific for target genes and co-treated with +/-25ng/ml FGF8. ID1 knockdown inhibits FGF8-mediated growth. siUNI, non-targeting control siRNA; Kif11, equimolar mixture of three siRNAs targeting Kif11 and a positive control for transfection efficiency; ID1 #1 and ID1 #2 are siRNAs targeting ID1. Relative cellular number was measured with the Cell Titer Glo luminescence assay. Dashed lines indicate the mean luminescence measured in unstimulated LNCaP$^{shAR/pATK}$ or 22RV1 controls.

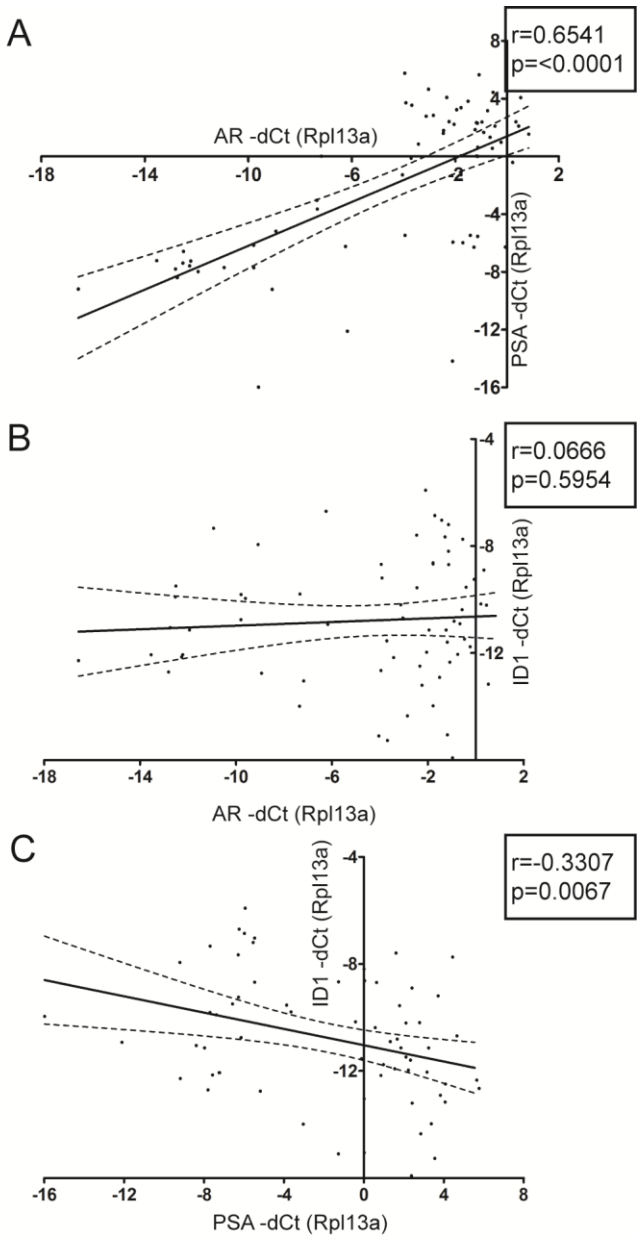

Figure 22: ID1 expression is inversely correlated with PSA expression in CRPC. (A) qRT-PCR was performed on cDNA obtained from 68 castration-resistant metastases. A Pearson Product-Moment Correlation Coeffcient (PPMCC) was calculated to assess the relationship between AR and PSA expression. As expected, AR and PSA expression were significantly correlated. (B) The expression of AR and ID1 expression were not correlated. (C) A PPMCC calculated to compare PSA and ID1 expression indicates a statistically significant inverse association.

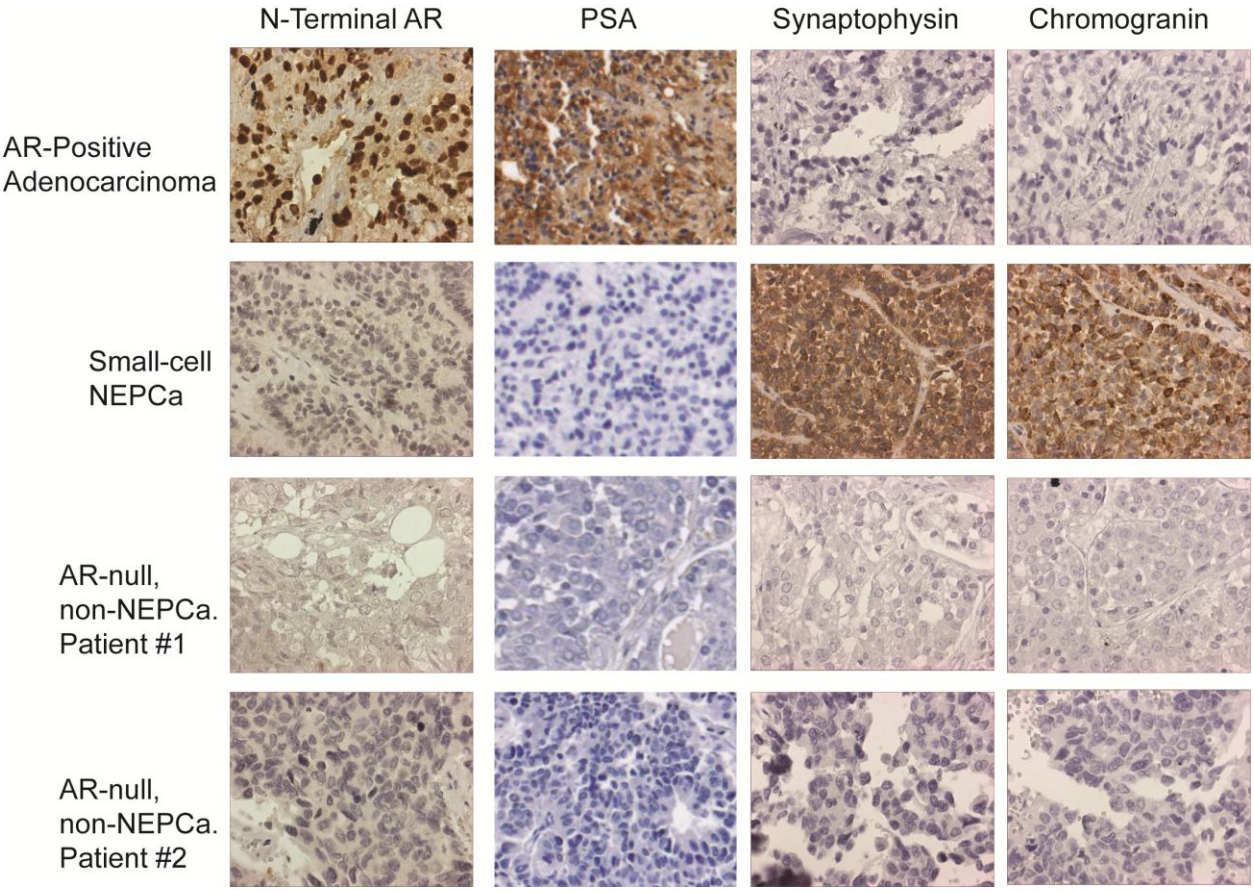

Figure 23: Immunohistochemistry of PACS-null metastases. A prostate metastasis TMA was stained for N-terminal AR, PSA, Synaptophysin and Chromogranin. Representative examples of an AR-positive adenocarcinoma metastasis (AR+, PSA+, ChA-, Syn-) and NEPCa metastasis (AR-, PSA-, ChA+, Syn+) are compared to two PACS-null metastases (AR-, PSA-, ChA-, Syn-) obtained from different patients. Original magnification =400x.

Table 6: Genomic changes in the development of LNCaP^{APIPC}.

Chromosome	Gain/Loss	Start	End	Length (bp)	Affected Genes
Chr3	Loss	37,126,398	37,252,856	123,736	LRRFIP2
Chr5	Loss	162,846,862	163,172,210	325,348	HMMR, BCO35392, MAT2B, tgr
Chr10	Loss	88,737,847	88,946,183	208,336	AGAP11, KIAA1975, FAM25A, GLUD1, FAM35A

Table 7: Gene expression changes in response to androgen pathway manipulation in LNCaP^{APIPC} and LNCaP$^{shAR/pATK}$.

Array Comparison		Gene Expression Change		
Array 1	Array 2	Up	Down	Total
LNCaP$^{shAR/pATK}$+CSS	LNCaP$^{shAR/pATK}$+R1881	456	424	880
	LNCaP$^{shAR/pATK}$+Dox	27	198	225
	LNCaP$^{shAR/pATK}$+R1881+Dox	10	0	10
LNCaP^{APIPC}+CSS	LNCaP^{APIPC}+R1881	3	0	3
	LNCaP^{APIPC}+Dox	2	1	3
	LNCaP^{APIPC}+R1881+Dox	2	1	3
LNCaP^{APIPC}+CSS	LNCaP$^{shAR/pATK}$+CSS	586	497	1083

Table 8: Top 250 genes upregulated in LNCaP^{APIPC}+CSS compared to LNCaP$^{shAR/pATK}$+CSS (mean-centered log2).

Rank	Probe	GeneSymbol	LNCaP$^{shAR/pATK}$ CSS vs LNCaP^{APIPC} CSS q-value(%)	LNCaP$^{shAR/pATK}$ CSS vs LNCaP^{APIPC} CSS Fold Change	LNCaP$^{shAR/pATK}$ CSS	LNCaP$^{shAR/pATK}$ R1881	LNCaP$^{shAR/pATK}$ Dox	LNCaP$^{shAR/pATK}$ R1881+ Doxycycline	LNCaP^{APIPC} CSS	LNCaP^{APIPC} R1881	LNCaP^{APIPC} Doxycycline	LNCaP^{APIPC} R1881+ Doxycycline
1	A_23_P413641	PREX1	0.00	531.42	-4.75	-3.96	-2.92	-4.84	4.30	4.27	3.95	3.94
2	A_24_P941359	FAM65B	0.00	379.55	-4.82	-3.73	-4.53	-4.45	3.74	3.70	3.49	3.47
3	A_23_P91390	THBD	0.00	224.49	-4.03	-4.25	-3.50	-3.71	3.78	3.85	3.93	3.93
4	A_24_P215069	C8orf84	0.00	206.33	-3.88	-3.93	-3.47	-3.53	3.81	3.50	3.86	3.63
5	A_24_P55295	GJA1	0.00	202.59	-4.10	-3.82	-3.78	-3.73	3.56	3.53	3.56	3.42
6	A_23_P24332	MUC15	0.00	184.02	-3.85	-3.92	-3.71	-3.49	3.67	3.54	4.09	3.67
7	A_23_P349566	CCDC85A	0.00	157.23	-3.92	-3.71	-3.16	-3.28	3.37	3.26	3.78	3.66
8	A_23_P358394	FAM65B	0.00	150.35	-3.75	-3.29	-3.38	-3.26	3.49	3.61	3.33	3.25
9	A_23_P427645	TLL1	0.00	141.99	-3.73	-4.08	-2.33	-3.15	3.42	3.19	3.37	3.31
10	A_23_P171074	ITM2A	0.00	139.67	-3.36	-4.17	-3.57	-4.05	3.77	4.21	3.42	3.75
11	A_23_P35725	ANO3	0.00	86.98	-3.14	-3.06	-3.29	-3.25	3.30	3.12	3.41	2.91
12	A_23_P57658	HRASLS	0.00	86.76	-3.46	-2.99	-2.43	-2.92	2.98	2.97	2.95	2.88
13	A_23_P211727	FGF12	0.00	84.11	-3.15	-4.45	-2.46	-2.79	3.25	3.26	3.14	3.20
14	A_23_P163195	LRFN5	0.00	82.90	-3.30	-2.54	-3.18	-2.99	3.07	3.10	2.78	3.06
15	A_32_P199551	C3orf57	0.00	74.51	-3.17	-2.90	-2.96	-3.26	3.05	3.13	2.97	3.14
16	A_23_P420442	SEMA6D	0.00	71.07	-3.52	-1.03	-3.22	-2.96	2.63	2.57	2.79	2.74
17	A_23_P169437	LCN2	0.00	70.94	-3.38	-2.76	-3.16	-2.96	2.77	2.76	3.42	3.32
18	A_23_P154235	NMI	0.00	69.33	-2.96	-3.43	-3.40	-3.35	3.15	3.24	3.40	3.36
19	A_23_P411723	PLAG1	0.00	68.04	-3.14	-3.93	-2.49	-2.68	2.95	3.03	3.19	3.06
20	A_32_P30649	ETV5	0.00	65.67	-3.12	-3.90	-2.37	-2.61	2.92	2.90	3.09	3.08
21	A_32_P57292	LANCL3	0.00	42.79	-2.70	-3.41	-2.22	-2.71	2.72	2.89	2.70	2.72
22	A_23_P94501	ANXA1	0.00	42.68	-2.81	-1.96	-2.59	-2.87	2.60	2.52	2.52	2.60
23	A_23_P170649	C8orf84	0.00	41.65	-2.64	-3.40	-2.58	-2.98	2.74	2.89	2.69	3.29
24	A_23_P139704	DUSP6	0.00	41.05	-2.64	-3.18	-2.29	-2.41	2.72	2.69	2.63	2.47
25	A_23_P80918	ART3	0.00	40.50	-2.52	-2.60	-2.62	-2.51	2.82	2.44	2.63	2.35
26	A_24_P252364	NRCAM	0.00	38.87	-2.50	-2.44	-2.21	-1.74	2.78	1.77	2.32	2.01
27	A_23_P214821	EDN1	0.00	36.75	-2.48	-2.35	-3.09	-2.85	2.72	2.66	2.74	2.66
28	A_23_P58676	C5orf23	0.00	36.54	-2.76	-2.23	-2.82	-2.68	2.43	2.73	2.57	2.76
29	A_23_P327451	NPR3	0.00	35.81	-2.50	-1.91	-3.26	-3.00	2.66	3.00	2.55	2.46
30	A_23_P96302	SPANXA1	0.00	35.01	-2.57	-2.40	-2.60	-2.57	2.56	2.93	2.45	2.19
31	A_23_P73097	RGS20	0.00	31.98	-2.57	-3.08	-1.82	-2.40	2.43	2.42	2.53	2.48
32	A_23_P83838	CA8	0.00	31.39	-2.48	-2.71	-2.10	-2.37	2.49	2.20	2.56	2.40

Table 8 Continued.

33	A_23_P51376	NKAIN1	0.00	27.34	-2.60	-0.58	-2.96	-2.84	2.17	2.74	2.05	2.03
34	A_23_P61406	SHC3	0.00	26.97	-2.55	-3.34	-1.69	-1.39	2.21	2.30	2.21	2.25
35	A_24_P49199	GLDN	0.00	26.11	-2.34	-3.99	-1.31	-2.04	2.37	2.19	2.65	2.46
36	A_23_P124619	S100A14	0.00	25.31	-2.19	-3.57	-1.67	-2.03	2.47	2.51	2.15	2.33
37	A_24_P586712	TPRG1	0.00	23.61	-1.54	-3.95	-2.83	-3.34	3.02	3.02	3.05	2.57
38	A_24_P158536	RHOBTB1	0.00	23.48	-2.24	-1.41	-2.49	-2.30	2.31	2.10	2.11	1.93
39	A_23_P106194	FOS	0.00	23.19	-2.50	-1.37	-2.51	-2.45	2.04	2.37	2.22	2.20
40	A_23_P218928	FAM198B	0.00	22.96	-1.94	-4.62	-1.96	-2.22	2.58	2.62	2.84	2.72
41	A_23_P215634	IGFBP3	0.00	22.17	-2.57	-1.14	-2.05	-2.05	1.90	1.79	1.97	2.15
42	A_23_P23048	S100A9	0.00	22.14	-2.12	-2.62	-1.85	-2.22	2.35	2.29	2.06	2.11
43	A_24_P331704	KRT80	0.00	21.24	-2.02	-2.26	-2.66	-2.18	2.39	2.26	2.22	2.25
44	A_23_P134835	CSGALNACT1	0.00	20.67	-3.05	1.95	-3.31	-2.45	1.32	1.38	1.51	1.55
45	A_24_P339429	KCNJ12	0.00	20.49	-1.83	-3.98	-2.35	-2.24	2.53	2.68	2.57	2.61
46	A_23_P30126	FGFBP1	0.00	20.15	-1.93	-2.66	-2.30	-2.15	2.40	2.32	2.18	2.14
47	A_23_P158593	COL5A1	0.00	19.63	-2.25	-1.97	-2.35	-1.88	2.04	2.09	2.11	2.20
48	A_23_P253536	NPR3	0.00	18.86	-2.09	-1.49	-2.56	-2.60	2.15	2.23	2.15	2.21
49	A_23_P92929	PRR16	0.00	18.08	-2.32	-1.23	-1.88	-2.15	1.85	1.96	1.89	1.89
50	A_23_P128319	ATP2B1	0.00	17.68	-2.24	-2.69	-1.44	-1.38	1.90	1.96	1.92	1.97
51	A_23_P163697	SYT17	0.00	17.21	-2.03	-2.48	-1.82	-1.86	2.07	2.05	2.05	2.03
52	A_23_P208030	SYT4	0.00	16.60	-2.21	-2.17	-1.68	-1.72	1.84	1.82	2.07	2.04
53	A_23_P327551	CPNE4	0.00	16.24	-2.53	-2.37	-1.01	-1.04	1.50	1.74	1.98	1.71
54	A_23_P210210	EPAS1	0.00	16.19	-2.12	-2.22	-1.48	-1.69	1.90	1.79	1.97	1.85
55	A_23_P6771	LMCD1	0.00	16.12	-1.97	-1.78	-2.05	-2.09	2.04	2.03	1.96	1.88
56	A_23_P204286	MGP	0.00	15.34	-1.86	-1.88	-2.68	-2.47	2.08	2.32	2.19	2.31
57	A_23_P69810	AGPAT9	0.00	15.01	-1.98	-1.59	-1.89	-2.09	1.92	1.75	1.95	1.92
58	A_24_P320699	IGFBP3	0.00	14.31	-2.24	-0.83	-1.92	-1.89	1.60	1.68	1.62	1.98
59	A_23_P31064	MOXD1	0.00	14.20	-2.02	-2.29	-1.53	-1.66	1.81	1.86	1.89	1.95
60	A_32_P125338	FAM43B	0.00	13.97	-1.87	-2.48	-1.99	-1.64	1.93	2.14	2.00	1.91
61	A_23_P201551	VAV3	0.00	13.64	-1.69	-3.98	-0.98	-1.71	2.08	2.08	2.13	2.07
62	A_23_P257583	DENND2A	0.00	13.53	-1.67	-1.78	-1.74	-1.84	2.09	1.87	1.61	1.45
63	A_23_P215913	CLU	0.00	13.11	-1.75	-1.88	-1.97	-2.04	1.96	1.93	1.85	1.90
64	A_23_P46829	FGF8	0.00	13.05	-1.88	-1.96	-1.54	-1.72	1.83	1.88	1.69	1.71
65	A_23_P65278	NBEA	0.00	13.01	-2.06	-2.14	-1.20	-1.45	1.64	1.69	1.81	1.73
66	A_24_P246710	CADPS2	0.00	12.98	-2.06	0.16	-2.45	-2.08	1.64	1.68	1.53	1.57
67	A_23_P94754	TNFSF15	0.00	12.62	-1.52	-3.40	-1.61	-1.82	2.14	1.99	2.19	2.04
68	A_23_P251412	SCGN	0.00	12.61	-1.78	-1.27	-2.14	-2.03	1.88	1.85	1.75	1.74
69	A_23_P31407	AGR2	0.00	12.40	-1.65	-0.37	-2.72	-2.51	1.99	2.01	1.58	1.67
70	A_23_P215566	AHR	0.00	11.76	-1.79	-1.91	-1.59	-1.68	1.76	1.66	1.79	1.75
71	A_23_P166929	SERPINI1	0.00	11.53	-1.63	-2.81	-1.46	-1.58	1.89	1.89	1.82	1.88
72	A_23_P51487	GBP3	0.00	11.49	-1.67	-3.09	-1.16	-1.53	1.86	1.73	2.02	1.85
73	A_23_P52207	BAMBI	0.00	11.40	-1.64	-3.00	-0.95	-1.50	1.87	1.86	1.71	1.65

Table 8 Continued.

74	A_32_P99100	PTPRK	0.00	11.39	-1.79	-2.92	-0.85	-1.10	1.72	1.65	1.94	1.90
75	A_23_P431776	ETV4	0.00	11.36	-1.65	-1.66	-1.84	-1.88	1.86	1.90	1.64	1.64
76	A_23_P40108	COL9A3	0.00	11.08	-1.42	-2.33	-2.20	-2.27	2.05	2.17	1.99	2.02
77	A_23_P65307	SLITRK6	0.00	10.89	-2.04	-0.52	-1.38	-1.85	1.41	1.39	1.59	1.40
78	A_23_P500741	CBFA2T3	0.00	10.87	-1.66	-2.54	-1.41	-1.44	1.78	1.47	1.80	2.01
79	A_32_P169505	KIAA2022	0.00	9.76	-1.94	-1.41	-1.23	-0.89	1.34	1.46	1.29	1.38
80	A_23_P157865	TNC	0.00	9.62	-1.63	-1.58	-1.82	-1.63	1.63	1.77	1.55	1.71
81	A_23_P112798	CRIP2	0.00	9.38	-1.90	-1.19	-1.45	-1.36	1.33	1.54	1.47	1.56
82	A_24_P940426	QKI	0.00	9.19	-1.79	-2.65	-0.68	-0.96	1.41	1.32	1.71	1.66
83	A_24_P411749	GPR126	0.00	9.01	-1.56	-2.64	-1.14	-1.17	1.61	1.75	1.55	1.60
84	A_23_P82929	NOV	0.00	8.85	-1.28	-3.87	-0.47	-0.92	1.87	1.85	1.38	1.45
85	A_23_P94403	TYRP1	0.00	8.73	-1.90	-2.17	-0.51	-0.27	1.23	1.17	1.16	1.28
86	A_23_P209578	GAD1	0.00	8.72	-1.50	-1.79	-1.71	-1.66	1.63	1.79	1.55	1.69
87	A_24_P20746	PRR16	0.00	8.60	-1.72	-0.81	-1.23	-1.66	1.39	1.34	1.32	1.37
88	A_24_P280983	HOXA11-AS1	0.00	8.51	-1.41	-3.30	-0.65	-1.05	1.67	1.47	1.66	1.60
89	A_23_P161659	SYT13	0.00	8.24	-1.51	-2.37	-0.94	-1.46	1.54	1.68	1.49	1.58
90	A_23_P92499	TLR2	0.00	8.16	-1.35	-2.94	-1.40	-1.43	1.68	1.74	1.90	1.81
91	A_23_P108751	FHL2	0.00	8.13	-1.40	-0.84	-1.80	-2.04	1.62	1.54	1.50	1.42
92	A_32_P33576	OPRK1	0.00	8.12	-1.45	-4.89	-0.16	-0.53	1.57	1.80	1.62	2.04
93	A_23_P170050	RIT2	0.00	8.11	-1.56	-1.86	-1.27	-1.42	1.46	1.54	1.44	1.66
94	A_24_P419250	RASAL2	0.00	8.08	-1.50	-1.82	-1.25	-1.18	1.52	1.46	1.41	1.37
95	A_24_P256722	CNGA1	0.00	7.92	-1.61	-4.43	-0.04	-0.33	1.38	1.69	1.58	1.76
96	A_23_P111724	RUNDC3B	0.00	7.85	-1.54	-2.25	-1.26	-1.28	1.44	1.45	1.65	1.80
97	A_24_P942945	GPR126	0.00	7.47	-1.24	-2.43	-1.46	-1.31	1.66	1.53	1.65	1.59
98	A_23_P49338	TNFRSF12A	0.00	7.22	-1.47	-1.85	-1.19	-1.22	1.38	1.54	1.36	1.46
99	A_23_P11256	MAGEE2	0.00	7.10	-1.46	-2.43	-0.54	-1.27	1.36	1.50	1.42	1.43
100	A_23_P150609	IGF2	0.00	7.09	-1.38	-1.43	-1.60	-1.45	1.44	1.40	1.51	1.51
101	A_24_P376391	PLXND1	0.00	7.07	-1.34	-2.06	-1.57	-1.33	1.48	1.64	1.57	1.60
102	A_23_P116898	A2M	0.00	6.97	-1.04	-2.94	-0.53	-1.22	1.76	1.42	1.20	1.35
103	A_32_P176036	SHC3	0.00	6.93	-1.44	-1.52	-1.17	-1.27	1.35	1.12	1.45	1.47
104	A_32_P135890	LOC401233	0.00	6.90	-1.35	-0.03	-2.18	-1.86	1.43	1.40	1.31	1.29
105	A_23_P394304	PDZK1IP1	0.00	6.88	-1.22	-1.79	-1.59	-1.49	1.56	1.69	1.40	1.45
106	A_23_P10121	SFRP1	0.00	6.86	-1.40	-1.08	-1.58	-1.43	1.38	1.51	1.23	1.37
107	A_23_P14083	AMIGO2	0.00	6.74	-1.30	-4.26	0.06	-0.44	1.45	1.31	1.62	1.56
108	A_23_P10127	SFRP1	0.00	6.63	-1.32	-1.12	-1.40	-1.50	1.40	1.48	1.22	1.24
109	A_24_P321525	RERG	0.00	6.61	-1.31	-1.20	-1.32	-1.44	1.42	1.12	1.50	1.23
110	A_23_P52336	UNC5B	0.00	6.60	-1.47	-2.56	-0.92	-1.26	1.25	1.02	1.81	2.13
111	A_24_P167012	TNFSF15	0.00	6.58	-1.09	-2.56	-1.32	-1.43	1.63	1.46	1.63	1.68
112	A_23_P71328	MATN2	0.00	6.50	-1.40	-3.61	-0.23	-0.45	1.30	1.30	1.52	1.58
113	A_23_P212715	CBLB	0.00	6.46	-1.41	-1.35	-1.07	-1.19	1.29	1.28	1.24	1.21
114	A_23_P47682	NRIP3	0.00	6.42	-1.13	-2.02	-0.98	-1.18	1.56	1.37	1.28	1.11

Table 8 Continued.

115	A_23_P160920	PDZK1IP1	0.00	6.36	-1.10	-1.93	-1.44	-1.78	1.57	1.54	1.62	1.52
116	A_23_P77321	RTF1	0.00	6.26	-1.32	-1.44	-1.49	-1.33	1.33	1.49	1.37	1.40
117	A_23_P61371	TMEM173	0.00	6.20	-1.16	-1.48	-1.47	-1.10	1.48	1.28	1.20	1.25
118	A_23_P17420	BCAS1	0.00	6.14	-1.25	-1.53	-1.32	-0.95	1.37	1.35	1.20	1.14
119	A_23_P101960	ZFP36L2	0.00	6.13	-1.25	-1.53	-1.15	-1.14	1.37	1.20	1.35	1.14
120	A_23_P60599	UGT1A6	0.00	6.13	-1.63	0.01	-1.07	-1.14	0.99	0.82	1.03	0.99
121	A_23_P339240	PLCH1	0.00	6.09	-1.26	-2.53	-0.75	-0.89	1.35	1.37	1.40	1.30
122	A_23_P16722	DOCK10	0.00	6.05	-1.26	-1.11	-1.63	-1.13	1.33	1.22	1.33	1.24
123	A_23_P408996	MBOAT1	0.00	6.04	-1.03	-3.43	-0.99	-0.91	1.56	1.73	1.46	1.61
124	A_32_P117322	LOC100506130	0.00	5.96	-1.06	-2.41	-0.89	-1.23	1.52	1.63	1.24	1.19
125	A_24_P928052	NRP1	0.00	5.95	-1.50	-1.69	-0.94	-0.81	1.08	1.11	1.30	1.46
126	A_23_P75741	UBE2L6	0.00	5.93	-1.27	-1.52	-1.21	-1.31	1.30	1.37	1.30	1.33
127	A_23_P64808	HOXC13	0.00	5.80	-1.41	-2.29	-0.19	-0.80	1.13	1.15	1.16	1.25
128	A_23_P70660	FAM46A	0.00	5.75	-1.29	-1.18	-1.09	-1.21	1.24	1.13	1.21	1.19
129	A_23_P140146	IFI27L2	0.00	5.74	-1.42	-2.25	-0.14	-0.24	1.10	1.04	1.00	0.90
130	A_24_P299474	ODZ2	0.00	5.72	-1.30	-1.45	-0.98	-0.70	1.21	1.20	1.04	0.97
131	A_32_P83784	ARAP2	0.00	5.71	-1.45	-0.47	-1.24	-1.29	1.07	1.02	1.16	1.19
132	A_24_P944437	ARID5B	0.00	5.69	-1.47	-0.31	-1.26	-0.85	1.03	0.85	1.00	1.01
133	A_23_P217832	FAM129A	0.00	5.66	-1.65	-0.24	-1.28	-1.10	0.85	1.01	1.14	1.27
134	A_24_P313993	CAPS	0.00	5.65	-1.34	-1.06	-1.23	-1.34	1.16	1.22	1.25	1.34
135	A_23_P79289	COBLL1	0.00	5.59	-1.47	-1.08	-0.66	-0.90	1.01	0.84	1.15	1.10
136	A_24_P91852	DYNLT3	0.00	5.58	-1.24	-1.23	-0.97	-1.05	1.24	1.22	1.04	0.99
137	A_23_P102454	INSIG2	0.00	5.54	-1.30	-1.48	-0.80	-1.02	1.17	1.15	1.09	1.19
138	A_23_P337262	APCDD1	0.00	5.46	-1.07	-1.76	-1.20	-1.20	1.38	1.36	1.31	1.18
139	A_23_P66481	RTN4RL1	0.00	5.35	-1.34	-1.93	-0.74	-1.31	1.08	1.46	1.33	1.43
140	A_23_P64792	KCNMB4	0.00	5.28	-1.48	-1.01	-0.64	-0.91	0.92	1.06	1.04	1.02
141	A_23_P83388	EPPK1	0.00	5.26	-1.27	-1.90	-0.92	-0.86	1.13	1.45	1.15	1.21
142	A_23_P118722	ASGR1	0.00	5.17	-1.27	-1.42	-0.77	-0.96	1.10	1.04	1.18	1.10
143	A_23_P40880	CMTM8	0.00	5.11	-0.99	-1.22	-1.61	-1.60	1.36	1.30	1.43	1.33
144	A_23_P22143	PDE6B	0.00	5.01	-1.07	-1.60	-1.10	-1.25	1.25	1.60	1.32	0.84
145	A_23_P154526	GRB14	0.00	4.96	-1.06	-1.87	-0.79	-0.98	1.25	1.10	1.17	1.19
146	A_24_P390403	RTF1	0.00	4.88	-1.15	-1.18	-1.07	-1.17	1.14	1.16	1.13	1.14
147	A_24_P100368	DYNLT3	0.00	4.87	-1.06	-1.01	-1.17	-1.30	1.23	1.22	1.04	1.05
148	A_23_P70968	HOXA7	0.00	4.86	-0.67	-2.90	-0.92	-0.86	1.61	1.05	1.36	1.32
149	A_24_P118938	C20orf112	0.00	4.80	-1.20	-1.16	-1.00	-0.89	1.06	1.08	0.94	1.18
150	A_23_P428129	CDKN1C	0.00	4.77	-1.22	-0.33	-1.12	-1.22	1.03	1.12	0.88	0.86
151	A_24_P383450	IER5L	0.00	4.74	-1.17	-1.71	-0.81	-0.86	1.08	1.37	0.95	1.15
152	A_23_P47058	CUZD1	0.00	4.74	-1.20	-1.84	-1.40	-1.34	1.05	1.05	1.88	1.80
153	A_23_P379864	ASRGL1	0.00	4.74	-1.09	-0.31	-1.54	-1.51	1.16	1.20	1.07	1.01
154	A_24_P24848	PSORS1C1	0.00	4.72	-1.20	-1.37	-0.75	-0.69	1.03	1.30	0.67	1.01
155	A_24_P71649	CNTN3	0.00	4.68	-1.55	-0.83	-0.26	-0.11	0.67	0.93	-0.28	1.42

Table 8 Continued.

156	A_23_P65918	ITPKA	0.00	4.65	-0.97	-1.88	-0.96	-1.28	1.24	1.34	1.32	1.19
157	A_24_P52697	H19	0.00	4.64	-0.82	-1.37	-1.31	-1.45	1.39	1.20	1.18	1.18
158	A_23_P106906	PPL	0.00	4.60	-1.10	-1.41	-0.98	-1.07	1.10	1.16	1.18	1.12
159	A_23_P6596	HES1	0.00	4.60	-0.89	-0.76	-1.32	-1.14	1.32	1.06	0.94	0.79
160	A_23_P213141	TRIM2	0.00	4.56	-0.87	-0.82	-2.08	-1.28	1.32	1.42	1.20	1.11
161	A_32_P190737	FNIP2	0.00	4.55	-1.05	-0.81	-1.08	-0.96	1.14	1.02	0.90	0.84
162	A_23_P354387	MYOF	0.00	4.55	-1.29	0.66	-1.43	-1.61	0.89	0.91	0.93	0.93
163	A_24_P191664	GOLIM4	0.00	4.54	-1.11	-1.28	-0.89	-0.83	1.08	0.86	1.15	1.02
164	A_23_P78958	CAPS	0.00	4.53	-1.25	-0.87	-0.86	-1.01	0.92	0.93	1.09	1.06
165	A_23_P120953	SERHL2	0.00	4.53	-1.19	-0.98	-0.77	-0.92	0.99	1.03	0.87	0.96
166	A_23_P73577	DYNLT3	0.00	4.49	-1.08	-1.26	-0.81	-1.08	1.09	1.11	1.04	0.99
167	A_23_P98092	OAT	0.00	4.49	-1.16	-0.66	-1.21	-0.97	1.01	0.94	1.00	1.05
168	A_23_P126266	HLX	0.00	4.49	-1.09	-0.33	-1.22	-1.37	1.08	1.21	0.99	0.73
169	A_23_P96383	SRPX	0.00	4.47	-0.84	-2.50	-0.60	-0.69	1.32	1.35	0.96	1.01
170	A_24_P944458	INSIG2	0.00	4.42	-1.21	-1.61	-0.40	-0.75	0.93	0.91	0.95	1.04
171	A_23_P257993	DNASE1L3	0.00	4.40	-0.83	-1.74	-1.16	-0.98	1.31	1.23	1.03	1.15
172	A_23_P35349	SVIL	0.00	4.38	-1.19	-1.63	-0.75	-0.98	0.94	0.89	1.32	1.41
173	A_23_P8452	LFNG	0.00	4.33	-0.83	-1.94	-0.92	-1.03	1.28	0.94	1.15	1.36
174	A_32_P18440	ARID5B	0.00	4.33	-1.26	-0.49	-0.91	-0.67	0.85	0.84	0.97	0.95
175	A_24_P270460	IFI27	0.00	4.31	-1.15	-1.18	-0.62	-0.89	0.96	0.85	1.03	1.00
176	A_24_P942370	GALNT4	0.00	4.30	-1.02	-1.57	-0.72	-0.84	1.08	0.95	1.16	0.95
177	A_23_P302568	SLC30A3	0.00	4.29	-1.05	-1.32	-0.79	-0.72	1.05	1.21	0.76	0.85
178	A_23_P163251	PAQR5	0.00	4.26	-0.89	-1.31	-1.16	-1.25	1.21	1.15	1.17	1.08
179	A_23_P213424	ENC1	0.00	4.25	-1.05	-1.67	-0.66	-0.41	1.04	0.92	1.03	0.79
180	A_23_P500130	KANK1	0.00	4.24	-1.34	-0.09	-0.61	-0.80	0.74	0.73	0.81	0.79
181	A_23_P250173	CNTN3	0.00	4.20	-1.16	-0.91	-0.60	-0.35	0.91	0.58	0.94	0.58
182	A_23_P414273	C5orf62	0.00	4.19	-0.54	-3.29	-0.61	-1.07	1.53	1.45	1.29	1.24
183	A_23_P137984	S100A10	0.00	4.17	-1.01	-1.16	-0.99	-0.99	1.05	1.10	0.93	1.07
184	A_24_P233786	FAM129A	0.00	4.15	-1.40	-0.15	-0.98	-0.79	0.65	0.67	1.06	0.94
185	A_24_P251962	PCDHB2	0.00	4.09	-1.21	-1.33	-0.57	-0.57	0.82	0.86	1.00	1.00
186	A_23_P133120	TMEM144	0.00	4.09	-0.95	-2.06	-0.65	-0.77	1.08	0.86	1.28	1.21
187	A_23_P107981	SULT2B1	0.00	4.07	-0.95	-1.37	-0.99	-1.15	1.08	1.20	1.01	1.16
188	A_23_P203391	ASRGL1	0.00	4.06	-1.00	-0.13	-1.18	-1.20	1.02	0.90	0.84	0.75
189	A_23_P254790	TAF9B	0.00	4.02	-1.08	-0.72	-0.88	-0.67	0.93	0.92	0.72	0.79
190	A_23_P380181	LMO4	0.00	3.99	-0.89	-1.61	-0.82	-0.94	1.10	1.02	1.13	1.00
191	A_23_P435636	DAND5	0.00	3.93	-0.90	-1.47	-0.83	-1.04	1.08	1.17	1.07	0.93
192	A_24_P130952	KIAA1804	0.00	3.91	-1.03	-0.45	-1.16	-1.16	0.94	0.96	0.96	0.94
193	A_24_P944570	PXDN	0.00	3.90	-1.01	-0.79	-1.06	-0.79	0.96	1.02	0.81	0.85
194	A_23_P160433	C1orf115	0.00	3.89	-0.82	-1.50	-0.73	-0.78	1.14	1.05	0.76	0.86
195	A_23_P32861	NMD3	0.00	3.89	-1.08	-0.73	-0.73	-0.71	0.88	0.70	0.88	0.80
196	A_23_P365267	SNED1	0.00	3.88	-1.02	-1.92	-0.42	-0.53	0.94	0.95	0.94	1.06

Table 8 Continued.

197	A_23_P47614	PHLDA2	0.00	3.87	-0.87	-0.60	-1.30	-1.24	1.08	1.09	0.95	0.90
198	A_24_P391431	TAF9B	0.00	3.84	-1.02	-1.14	-0.58	-0.66	0.92	0.82	0.88	0.77
199	A_23_P400580	FNIP2	0.00	3.82	-0.96	-0.72	-1.14	-1.00	0.98	0.97	0.96	0.90
200	A_23_P56978	PTK6	0.00	3.81	-0.97	-1.62	-0.63	-0.78	0.96	0.98	1.08	0.99
201	A_24_P316257	NHLRC4	0.00	3.81	-0.93	-1.53	-0.65	-0.71	1.00	1.08	0.49	1.25
202	A_32_P170736	FLJ36031	0.00	3.78	-1.20	-0.98	-0.60	-0.84	0.72	0.82	1.09	1.00
203	A_23_P21457	NMD3	0.00	3.78	-1.07	-0.43	-0.81	-0.83	0.85	0.66	0.81	0.81
204	A_23_P45361	GLUD2	0.00	3.77	-1.13	-0.43	-1.08	-0.81	0.79	0.88	0.90	0.87
205	A_23_P64617	FZD4	0.00	3.75	-0.99	-1.58	-0.66	-0.84	0.92	0.84	1.19	1.12
206	A_24_P240187	LRRN1	0.00	3.74	-0.77	-3.70	0.10	-0.19	1.14	1.04	1.24	1.14
207	A_24_P95029	TAX1BP1	0.00	3.73	-1.17	-0.68	-0.62	-0.68	0.73	0.75	0.85	0.82
208	A_23_P389281	HOXA13	0.00	3.73	-0.88	-3.06	0.16	-0.14	1.01	0.89	1.08	0.94
209	A_23_P147245	OSBPL10	0.00	3.71	-0.93	-0.13	-1.43	-1.56	0.96	0.87	0.86	0.88
210	A_24_P374943	CXADR	0.00	3.69	-0.93	-0.95	-0.88	-0.87	0.95	0.80	0.92	0.96
211	A_23_P138665	GLUD1	0.00	3.69	-1.09	-0.26	-0.85	-0.69	0.80	0.72	0.79	0.84
212	A_24_P380734	SDC2	0.00	3.69	-0.90	-1.61	-0.57	-0.48	0.98	0.89	0.85	0.84
213	A_24_P69095	ENC1	0.00	3.67	-0.97	-1.64	-0.44	-0.59	0.90	0.98	0.82	0.94
214	A_23_P71316	RBPMS	0.00	3.67	-0.82	-0.77	-1.13	-0.97	1.05	1.12	0.75	0.77
215	A_23_P112004	LRRC6	0.00	3.64	-0.95	-1.08	-0.60	-0.64	0.92	0.80	0.80	0.75
216	A_23_P77031	PTPN21	0.00	3.64	-1.42	2.07	-1.31	-1.15	0.45	0.28	0.56	0.52
217	A_23_P48513	IFI27	0.00	3.64	-1.03	-1.06	-0.63	-0.84	0.83	0.90	0.92	0.91
218	A_24_P13041	RTKN2	0.00	3.64	-0.58	-0.81	-1.90	-1.65	1.28	1.27	1.29	1.09
219	A_23_P97871	ARID5B	0.00	3.64	-0.95	-0.37	-1.22	-1.27	0.91	1.01	0.98	0.91
220	A_23_P143845	TIPARP	0.00	3.62	-1.15	0.45	-0.98	-1.06	0.70	0.74	0.64	0.67
221	A_24_P161725	CXADRP3	0.00	3.62	-0.98	-0.92	-0.75	-0.71	0.87	0.70	0.91	0.89
222	A_23_P130995	FXYD5	0.00	3.62	-0.89	-1.64	-0.64	-0.71	0.97	1.09	0.98	0.85
223	A_23_P4536	EPB41L3	0.00	3.60	-0.87	-0.90	-1.48	-1.25	0.98	0.92	1.00	1.10
224	A_32_P218707	LOC100132330	0.00	3.58	-0.67	-0.88	-1.28	-1.34	1.17	1.08	0.94	0.97
225	A_32_P11451	NMD3	0.00	3.56	-0.95	-0.69	-0.55	-0.67	0.88	0.67	0.82	0.78
226	A_24_P104407	SYNM	0.00	3.54	-0.86	-1.47	-0.83	-0.75	0.97	0.89	1.00	1.04
227	A_23_P36888	FAM113B	0.00	3.54	-0.77	-2.65	-0.12	-0.67	1.05	1.00	1.11	1.04
228	A_24_P336728	LPGAT1	0.00	3.52	-0.95	-1.17	-0.71	-0.80	0.86	0.87	1.01	0.90
229	A_23_P133902	PSORS1C1	0.00	3.52	-0.91	-1.17	-0.58	-0.65	0.90	0.84	0.76	0.80
230	A_23_P254363	PRRG1	0.00	3.50	-0.91	-0.69	-0.91	-0.79	0.89	0.75	0.86	0.79
231	A_23_P23669	PALMD	0.00	3.50	-0.78	-1.08	-1.42	-1.07	1.03	1.07	1.13	1.12
232	A_23_P11800	CAMK2N1	0.00	3.48	-0.62	-3.89	0.04	-0.42	1.18	1.20	1.29	1.21
233	A_23_P252306	ID1	0.00	3.48	-1.13	-1.34	-0.30	-0.30	0.67	0.64	0.76	0.99
234	A_23_P211910	PLOD2	0.00	3.48	-0.08	1.65	-2.75	-2.77	1.72	1.41	0.00	-0.10
235	A_24_P273143	NCRNA00152	0.00	3.48	-0.80	-0.74	-1.04	-1.08	0.99	0.94	0.95	0.77
236	A_24_P321919	IQGAP1	0.00	3.46	-1.03	-0.53	-0.69	-0.61	0.75	0.64	0.77	0.70
237	A_24_P170667	ARID5B	0.00	3.45	-1.08	-0.20	-1.07	-0.74	0.71	0.68	0.88	0.82

Table 8 Continued.

238	A_23_P143885	ARHGEF3	0.00	3.45	-1.01	-0.85	-0.54	-0.73	0.78	0.76	0.84	0.76
239	A_23_P160318	COL16A1	0.00	3.45	-0.80	-2.76	-0.13	-0.37	0.98	0.93	1.09	1.05
240	A_24_P6921	LOC541471	0.00	3.44	-0.88	-0.71	-1.08	-1.02	0.90	0.84	0.90	0.72
241	A_23_P17811	SEC14L2	0.00	3.44	-1.09	-0.87	-0.37	-0.73	0.70	0.79	0.81	0.76
242	A_24_P294842	ATXN1	0.00	3.44	-1.26	-0.78	-0.29	-0.44	0.52	0.38	0.91	0.96
243	A_23_P425681	CCK	0.00	3.43	-1.20	0.27	-1.48	-0.75	0.58	0.93	0.65	0.99
244	A_24_P938293	HES1	0.00	3.43	-0.78	-0.84	-0.91	-1.02	0.99	1.13	0.67	0.75
245	A_23_P110531	FST	0.00	3.43	-0.88	-0.86	-0.90	-0.94	0.90	0.82	0.98	0.87
246	A_23_P323930	TSPAN5	0.00	3.41	-0.84	-1.49	-0.74	-0.68	0.94	0.82	0.97	1.02
247	A_23_P364544	C12orf60	0.00	3.41	-0.70	-1.32	-0.87	-1.02	1.07	1.05	0.98	0.80
248	A_23_P338912	PHLDA1	0.00	3.41	-0.70	-0.27	-1.07	-1.33	1.06	0.80	0.83	0.68
249	A_24_P314159	APP	0.00	3.38	-1.12	-0.56	-0.48	-0.67	0.63	0.75	0.75	0.69
250	A_23_P136246	COX7B2	0.00	3.38	-0.92	-0.76	-0.63	-0.51	0.84	0.73	0.63	0.62

Table 9: Chapter 3 siRNA Sequences

Gene	Oligo Name	Sense Sequence (5'-3')	Antisense Sequence (5'-3')
siUNI	siRNA Universal Negative Control #1	Proprietary	Proprietary
Kif11 #1	SASI_Hs01_00161697	CAUUGACAGUGGCCGAUAA[dT][dT]	UUAUCGGCCACUGUCAAUG[dT][dT]
Kif11 #2	SASI_Hs01_00161696	CUGUACUACAGGAAUUGAU[dT][dT]	AUCAAUUCCUGUAGUACAG[dT][dT]
Kif11 #3	SASI_Hs01_00161689	CAACAAGGAUGAAGUCUAU[dT][dT]	AUAGACUUCAUCCUUGUUG[dT][dT]
ID1 #1	SASI_Hs01_00057899	CCUCUCUGCACACCUACUA[dT][dT]	UAGUAGGUGUGCAGAGAGG[dT][dT]
ID1 #2	SASI_Hs01_00246329	GGGCGCUCCUCUCUGCACA[dT][dT]	UGUGCAGAGAGGAGCGCCC[dT][dT]

Table 10: Chapter 3 PCR Primers

Gene	Forward Primer	Reverse Primer
AR	5'-ATCCTCATATGGCCCAGTGTC-3'	5'-GCTCTCTAAACTTCCCGTGGC-3'
HSV-TK	5’-CACGTTATTTACCCTGTTTCGGGC-3’	5’-AGGATAAAGACGTGCATGGAACGG-3’
ID1	5’-AGGTAAACGTGCTGCTCTACG-3’	5’-TGTAGTCGATGACGTGCTGGA-3’
PSA	5’-GCATGGGATGGGGATGAAGTAAG-3’	5’-CATCAAATCTGAGGGTTGTCTGGA-3’
RPL13a	5’-CCTGGAGGAGAAGAGGAAAGA-3’	5’-TTGAGGACCTCTGTGTATTTG-3’
FGF8a/g	5'-CCAAGCCCAGCATGTGAGGGA -3'	5'-TCGGACTCGAACTCTGCTTCCAAA-3'
FGF8b	5'CTCCAAGCCCAGGTAACTGTT-3'	5'-TCGGACTCGAACTCTGCTTCCAAA-3'
FGF8e/f	5'-CTCGCTTCCCTGTTCCGGGCT-3'	5'-TCGGACTCGAACTCTGCTTCCAAA-3'

Chapter 4: Conclusions

The elimination of androgen receptor (AR) signaling remains the major therapeutic goal in treating castration-resistant prostate cancer (CRPC). With the development of more potent and diverse pathway inhibitors, it is likely that single-agent or combination therapy will completely extinguish AR-mediated transcription. If AR-regulated signaling is absolutely essential for *in vivo* CRPC survival, Total Androgen Pathway Suppression (TAPS) will lead to complete disease remission. Alternatively, TAPS will select against cells dependent on AR for survival, allowing for the expansion of those cells utilizing AR-independent growth pathways.

Mounting evidence suggests that alternative signaling pathways will play an important role in CRPC following aggressive androgen deprivation therapy (ADT). As previously mentioned, existing *in vitro* and *in vivo* observations indicate that AR-positive tumors can co-opt PI3K signaling to promote AR-independent growth (32, 33). Observations from clinical CRPC suggests that transdifferentiation of AR-positive adenocarcinoma into a more anaplastic, AR-low/null, neuroendocrine phenotype may enable (or is a marker of) androgen pathway independence (62). In this body of work, we present evidence of additional molecular alterations that enable AR-pathway bypass. In Chapter 2, we demonstrate that the loss of a protein phosphatase 2A (PP2A) regulatory subunit (PPP2R2C) is sufficient to promote *in vitro* prostate cancer growth that is independent of androgens and the AR, and is resistant to antiandrogen treatment. In Chapter 3, we demonstrate that completely suppressing AR signaling in an AR-positive cell line can generate progenitor cells that are AR-null and non-neuroendocrine. These progenitor cells relied on autocrine growth pathways and mitogen-activated protein kinase (MAPK) signaling in lieu of an active AR transcriptional program.

By referencing patient-derived gene expression data and performing immunohistochemistry (IHC) on patient-derived prostate cancer tissue, we found *in vivo* evidence indicating that these *in vitro*

alterations are present in human disease. PPP2R2C was found downregulated in primary and metastatic prostate cancer and significantly correlates with aggressive disease. AR-null, non-neuroendocrine tumors were observed in a cohort of patients with known CRPC. These observations suggest that some populations of *in vivo* CRPC metastases, under selection from conventional ADT, may escape reliance on AR signaling.

Analysis of tissue harvested from men treated with next-generation antiandrogen monotherapy (MDV3100 or Abiraterone) will enable future investigators to identify those molecular alterations sufficient to promote *in vivo* growth under aggressive ADT. However, experiments performed in xenograft models suggest that *de novo* androgen synthesis and maintained AR-dependence will continue to be the dominant mechanism of therapy resistance in cells treated with monotherapy (24). The development and clinical use of N-terminal AR inhibitors that target both wild-type and aberrant AR splicing variants will provide additional selective pressure against AR signaling (5), however successful *in vivo* TAPS will likely require combination therapy targeting multiple nodes of AR biology and androgen ligand production.

By studying the molecular mechanisms of TAPS bypass in a diverse array of experimental models, investigators may identify a common set of deregulated signaling pathways and downstream mediators. Co-targeting these common pathways in addition to aggressive AR inhibition may result in longer disease-free remission, or complete remission in some patients. The results from experiments performed in Chapter 2 and Chapter 3 identify AR bypass mechanisms in the most commonly studied *in vitro* androgen-dependent prostate cancer models, and will serve as a foundation for further investigation into the molecular basis of androgen pathway-independent disease.

References

1. Jemal A, Siegel R, Xu J, Ward E. Cancer Statistics , 2010. CA: A Cancer Journal for Clinicians. 2010;60:277-300.
2. Harris WP, Mostaghel EA, Nelson PS, Montgomery B. Androgen deprivation therapy: progress in understanding mechanisms of resistance and optimizing androgen depletion. Nat Clin Pract Urol. 2009 Feb;6(2):76-85.
3. Attard G, Reid AH, Yap TA, Raynaud F, Dowsett M, Settatree S, et al. Phase I clinical trial of a selective inhibitor of CYP17, abiraterone acetate, confirms that castration-resistant prostate cancer commonly remains hormone driven. J Clin Oncol. 2008 Oct 1;26(28):4563-71.
4. Scher HI, Beer TM, Higano CS, Anand A, Taplin ME, Efstathiou E, et al. Antitumour activity of MDV3100 in castration-resistant prostate cancer: a phase 1-2 study. Lancet. 2010 Apr 24;375(9724):1437-46.
5. Andersen RJ, Mawji NR, Wang J, Wang G, Haile S, Myung JK, et al. Regression of castrate-recurrent prostate cancer by a small-molecule inhibitor of the amino-terminus domain of the androgen receptor. Cancer Cell. 2010 Jun 15;17(6):535-46.
6. Cannata DH, Kirschenbaum A, Levine AC. Androgen deprivation therapy as primary treatment for prostate cancer. J Clin Endocrinol Metab. 2012 Feb;97(2):360-5.
7. Pagliarulo V, Bracarda S, Eisenberger MA, Mottet N, Schroder FH, Sternberg CN, et al. Contemporary role of androgen deprivation therapy for prostate cancer. Eur Urol. 2012 Jan;61(1):11-25.
8. Boccardo F, Rubagotti A, Barichello M, Battaglia M, Carmignani G, Comeri G, et al. Bicalutamide monotherapy versus flutamide plus goserelin in prostate cancer patients: results of an Italian Prostate Cancer Project study. J Clin Oncol. 1999 Jul;17(7):2027-38.
9. Culig Z, Hoffmann J, Erdel M, Eder IE, Hobisch A, Hittmair A, et al. Switch from antagonist to agonist of the androgen receptor bicalutamide is associated with prostate tumour progression in a new model system. Br J Cancer. 1999 Sep;81(2):242-51.
10. Labrie F. Blockade of testicular and adrenal androgens in prostate cancer treatment. Nat Rev Urol. 2011 Feb;8(2):73-85.
11. Taylor BS, Schultz N, Hieronymus H, Gopalan A, Xiao Y, Carver BS, et al. Integrative genomic profiling of human prostate cancer. Cancer Cell. 2010 Jul 13;18(1):11-22.
12. Cai C, He HH, Chen S, Coleman I, Wang H, Fang Z, et al. Androgen receptor gene expression in prostate cancer is directly suppressed by the androgen receptor through recruitment of lysine-specific demethylase 1. Cancer Cell. 2011 Oct 18;20(4):457-71.
13. Sharma A, Yeow WS, Ertel A, Coleman I, Clegg N, Thangavel C, et al. The retinoblastoma tumor suppressor controls androgen signaling and human prostate cancer progression. J Clin Invest. 2010 Dec 1;120(12):4478-92.
14. Heinlein CA, Chang C. Androgen receptor (AR) coregulators: an overview. Endocr Rev. 2002 Apr;23(2):175-200.
15. Wang Q, Li W, Zhang Y, Yuan X, Xu K, Yu J, et al. Androgen receptor regulates a distinct transcription program in androgen-independent prostate cancer. Cell. 2009 Jul 23;138(2):245-56.
16. Dehm SM, Schmidt LJ, Heemers HV, Vessella RL, Tindall DJ. Splicing of a novel androgen receptor exon generates a constitutively active androgen receptor that mediates prostate cancer therapy resistance. Cancer Res. 2008 Jul 1;68(13):5469-77.
17. Sun S, Sprenger CC, Vessella RL, Haugk K, Soriano K, Mostaghel EA, et al. Castration resistance in human prostate cancer is conferred by a frequently occurring androgen receptor splice variant. J Clin Invest. 2010 Aug 2;120(8):2715-30.

18. Watson Pa, Chen YF, Balbas MD, Wongvipat J, Socci ND, Viale A, et al. Constitutively active androgen receptor splice variants expressed in castration-resistant prostate cancer require full-length androgen receptor. Proceedings of the National Academy of Sciences. 2010:1-7.
19. Haelens A, Tanner T, Denayer S, Callewaert L, Claessens F. The hinge region regulates DNA binding, nuclear translocation, and transactivation of the androgen receptor. Cancer Res. 2007 May 1;67(9):4514-23.
20. Zhang X, Morrissey C, Sun S, Ketchandji M, Nelson PS, True LD, et al. Androgen receptor variants occur frequently in castration resistant prostate cancer metastases. PLoS One. 2011;6(11):e27970.
21. Cai C, Chen S, Ng P, Bubley GJ, Nelson PS, Mostaghel EA, et al. Intratumoral de novo steroid synthesis activates androgen receptor in castration-resistant prostate cancer and is upregulated by treatment with CYP17A1 inhibitors. Cancer Res. 2011 Oct 15;71(20):6503-13.
22. Locke JA, Guns ES, Lehman ML, Ettinger S, Zoubeidi A, Lubik A, et al. Arachidonic acid activation of intratumoral steroid synthesis during prostate cancer progression to castration resistance. Prostate. 2010 Feb 15;70(3):239-51.
23. Lubik AA, Gunter JH, Hendy SC, Locke JA, Adomat HH, Thompson V, et al. Insulin increases de novo steroidogenesis in prostate cancer cells. Cancer Res. 2011 Sep 1;71(17):5754-64.
24. Mostaghel EA, Marck BT, Plymate SR, Vessella RL, Balk S, Matsumoto AM, et al. Resistance to CYP17A1 inhibition with abiraterone in castration-resistant prostate cancer: induction of steroidogenesis and androgen receptor splice variants. Clin Cancer Res. 2011 Sep 15;17(18):5913-25.
25. de Bono JS, Logothetis CJ, Molina A, Fizazi K, North S, Chu L, et al. Abiraterone and increased survival in metastatic prostate cancer. N Engl J Med. 2011 May 26;364(21):1995-2005.
26. Hagenbuch B, Meier PJ. The superfamily of organic anion transporting polypeptides. Biochim Biophys Acta. 2003 Jan 10;1609(1):1-18.
27. Yang M, Xie W, Mostaghel E, Nakabayashi M, Werner L, Sun T, et al. SLCO2B1 and SLCO1B3 may determine time to progression for patients receiving androgen deprivation therapy for prostate cancer. J Clin Oncol. 2011 Jun 20;29(18):2565-73.
28. Wright JL, Kwon EM, Ostrander EA, Montgomery RB, Lin DW, Vessella R, et al. Expression of SLCO transport genes in castration-resistant prostate cancer and impact of genetic variation in SLCO1B3 and SLCO2B1 on prostate cancer outcomes. Cancer Epidemiol Biomarkers Prev. 2011 Apr;20(4):619-27.
29. Hamada A, Sissung T, Price DK, Danesi R, Chau CH, Sharifi N, et al. Effect of SLCO1B3 haplotype on testosterone transport and clinical outcome in caucasian patients with androgen-independent prostatic cancer. Clin Cancer Res. 2008 Jun 1;14(11):3312-8.
30. Tamai I, Nezu J, Uchino H, Sai Y, Oku A, Shimane M, et al. Molecular identification and characterization of novel members of the human organic anion transporter (OATP) family. Biochem Biophys Res Commun. 2000 Jun 24;273(1):251-60.
31. Lin HK, Yeh S, Kang HY, Chang C. Akt suppresses androgen-induced apoptosis by phosphorylating and inhibiting androgen receptor. Proc Natl Acad Sci U S A. 2001 Jun 19;98(13):7200-5.
32. Mulholland DJ, Tran LM, Li Y, Cai H, Morim A, Wang S, et al. Cell autonomous role of PTEN in regulating castration-resistant prostate cancer growth. Cancer Cell. 2011 Jun 14;19(6):792-804.
33. Carver BS, Chapinski C, Wongvipat J, Hieronymus H, Chen Y, Chandarlapaty S, et al. Reciprocal feedback regulation of PI3K and androgen receptor signaling in PTEN-deficient prostate cancer. Cancer Cell. 2011 May 17;19(5):575-86.
34. Cai C, Portnoy DC, Wang H, Jiang X, Chen S, Balk SP. Androgen receptor expression in prostate cancer cells is suppressed by activation of epidermal growth factor receptor and ErbB2. Cancer Res. 2009 Jun 15;69(12):5202-9.
35. Nabhan C, Lestingi TM, Galvez A, Tolzien K, Kelby SK, Tsarwhas D, et al. Erlotinib has moderate single-agent activity in chemotherapy-naive castration-resistant prostate cancer: final results of a phase II trial. Urology. 2009 Sep;74(3):665-71.

36. Whang YE, Armstrong AJ, Rathmell WK, Godley PA, Kim WY, Pruthi RS, et al. A phase II study of lapatinib, a dual EGFR and HER-2 tyrosine kinase inhibitor, in patients with castration-resistant prostate cancer. Urol Oncol. 2011 Mar 9.
37. Roudier MP, True LD, Higano CS, Vesselle H, Ellis W, Lange P, et al. Phenotypic heterogeneity of end-stage prostate carcinoma metastatic to bone. Hum Pathol. 2003 Jul;34(7):646-53.
38. Eichhorn PJ, Creyghton MP, Bernards R. Protein phosphatase 2A regulatory subunits and cancer. Biochim Biophys Acta. 2009 Jan;1795(1):1-15.
39. Millward TA, Zolnierowicz S, Hemmings BA. Regulation of protein kinase cascades by protein phosphatase 2A. Trends Biochem Sci. 1999 May;24(5):186-91.
40. Sablina AA, Hahn WC. The role of PP2A A subunits in tumor suppression. Cell Adh Migr. 2007 Jul-Sep;1(3):140-1.
41. Sablina AA, Hector M, Colpaert N, Hahn WC. Identification of PP2A complexes and pathways involved in cell transformation. Cancer Res. 2010 Dec 15;70(24):10474-84.
42. Arroyo JD, Hahn WC. Involvement of PP2A in viral and cellular transformation. Oncogene. 2005 Nov 21;24(52):7746-55.
43. Singh AP, Bafna S, Chaudhary K, Venkatraman G, Smith L, Eudy JD, et al. Genome-wide expression profiling reveals transcriptomic variation and perturbed gene networks in androgen-dependent and androgen-independent prostate cancer cells. Cancer Lett. 2008 Jan 18;259(1):28-38.
44. Mao X, Boyd LK, Yanez-Munoz RJ, Chaplin T, Xue L, Lin D, et al. Chromosome rearrangement associated inactivation of tumour suppressor genes in prostate cancer. Am J Cancer Res. 2011;1(5):604-17.
45. Bhardwaj A, Singh S, Srivastava SK, Honkanen RE, Reed E, Singh AP. Modulation of protein phosphatase 2A activity alters androgen-independent growth of prostate cancer cells: therapeutic implications. Mol Cancer Ther. 2011 May;10(5):720-31.
46. Eichhorn PJ, Creyghton MP, Wilhelmsen K, van Dam H, Bernards R. A RNA interference screen identifies the protein phosphatase 2A subunit PR55gamma as a stress-sensitive inhibitor of c-SRC. PLoS Genet. 2007 Dec;3(12):e218.
47. Kobayashi T, Inoue T, Shimizu Y, Terada N, Maeno A, Kajita Y, et al. Activation of Rac1 is closely related to androgen-independent cell proliferation of prostate cancer cells both in vitro and in vivo. Mol Endocrinol. 2010 Apr;24(4):722-34.
48. Mendiratta P, Mostaghel E, Guinney J, Tewari AK, Porrello A, Barry WT, et al. Genomic strategy for targeting therapy in castration-resistant prostate cancer. J Clin Oncol. 2009 Apr 20;27(12):2022-9.
49. Drake JM, Graham NA, Stoyanova T, Sedghi A, Goldstein AS, Cai H, et al. Oncogene-specific activation of tyrosine kinase networks during prostate cancer progression. Proc Natl Acad Sci U S A. 2012 Jan 31;109(5):1643-8.
50. Holcomb IN, Young JM, Coleman IM, Salari K, Grove DI, Hsu L, et al. Comparative analyses of chromosome alterations in soft-tissue metastases within and across patients with castration-resistant prostate cancer. Cancer Res. 2009 Oct 1;69(19):7793-802.
51. True L, Coleman I, Hawley S, Huang CY, Gifford D, Coleman R, et al. A molecular correlate to the Gleason grading system for prostate adenocarcinoma. Proc Natl Acad Sci U S A. 2006 Jul 18;103(29):10991-6.
52. Page ST, Lin DW, Mostaghel EA, Marck BT, Wright JL, Wu J, et al. Dihydrotestosterone administration does not increase intraprostatic androgen concentrations or alter prostate androgen action in healthy men: a randomized-controlled trial. J Clin Endocrinol Metab. 2011 Feb;96(2):430-7.
53. Tran C, Ouk S, Clegg NJ, Chen Y, Watson PA, Arora V, et al. Development of a second-generation antiandrogen for treatment of advanced prostate cancer. Science. 2009 May 8;324(5928):787-90.
54. Handratta VD, Vasaitis TS, Njar VC, Gediya LK, Kataria R, Chopra P, et al. Novel C-17-heteroaryl steroidal CYP17 inhibitors/antiandrogens: synthesis, in vitro biological activity, pharmacokinetics, and

antitumor activity in the LAPC4 human prostate cancer xenograft model. J Med Chem. 2005 Apr 21;48(8):2972-84.
55. Ang JE, Olmos D, de Bono JS. CYP17 blockade by abiraterone: further evidence for frequent continued hormone-dependence in castration-resistant prostate cancer. Br J Cancer. 2009 Mar 10;100(5):671-5.
56. Butler LM, Agus DB, Scher HI, Higgins B, Rose A, Cordon-Cardo C, et al. Suberoylanilide hydroxamic acid, an inhibitor of histone deacetylase, suppresses the growth of prostate cancer cells in vitro and in vivo. Cancer Res. 2000 Sep 15;60(18):5165-70.
57. Shah RB, Mehra R, Chinnaiyan AM, Shen R, Ghosh D, Zhou M, et al. Androgen-independent prostate cancer is a heterogeneous group of diseases: lessons from a rapid autopsy program. Cancer Res. 2004 Dec 15;64(24):9209-16.
58. Hirano D, Okada Y, Minei S, Takimoto Y, Nemoto N. Neuroendocrine differentiation in hormone refractory prostate cancer following androgen deprivation therapy. Eur Urol. 2004 May;45(5):586-92; discussion 92.
59. Wan X, Liu J, Lu JF, Tzelepi V, Yang J, Starbuck MW, et al. Activation of beta-catenin signaling in androgen receptor-negative prostate cancer cells. Clin Cancer Res. 2012 Feb 1;18(3):726-36.
60. Tzelepi V, Zhang J, Lu JF, Kleb B, Wu G, Wan X, et al. Modeling a lethal prostate cancer variant with small-cell carcinoma features. Clin Cancer Res. 2012 Feb 1;18(3):666-77.
61. Beltran H, Rickman DS, Park K, Chae SS, Sboner A, Macdonald TY, et al. Molecular Characterization of Neuroendocrine Prostate Cancer and Identification of New Drug Targets. Cancer Discov. 2011 Nov;1(6):487-95.
62. Sagnak L, Topaloglu H, Ozok U, Ersoy H. Prognostic significance of neuroendocrine differentiation in prostate adenocarcinoma. Clin Genitourin Cancer. 2011 Dec;9(2):73-80.
63. Wang W, Epstein JI. Small cell carcinoma of the prostate. A morphologic and immunohistochemical study of 95 cases. Am J Surg Pathol. 2008 Jan;32(1):65-71.
64. Cheng H, Snoek R, Ghaidi F, Cox ME, Rennie PS. Short hairpin RNA knockdown of the androgen receptor attenuates ligand-independent activation and delays tumor progression. Cancer Res. 2006 Nov 1;66(21):10613-20.
65. Sobel RE, Sadar MD. Cell lines used in prostate cancer research: a compendium of old and new lines--part 1. J Urol. 2005 Feb;173(2):342-59.
66. Bluemn EG, Nelson PS. The androgen/androgen receptor axis in prostate cancer. Curr Opin Oncol. 2012 May;24(3):251-7.
67. Yuan TC, Veeramani S, Lin MF. Neuroendocrine-like prostate cancer cells: neuroendocrine transdifferentiation of prostate adenocarcinoma cells. Endocr Relat Cancer. 2007 Sep;14(3):531-47.
68. Huggins C, Hodges CV. Studies on prostatic cancer. I. The effect of castration, of estrogen and androgen injection on serum phosphatases in metastatic carcinoma of the prostate. CA Cancer J Clin. 1972 Jul-Aug;22(4):232-40.
69. Nelson PS, Clegg N, Arnold H, Ferguson C, Bonham M, White J, et al. The program of androgen-responsive genes in neoplastic prostate epithelium. Proc Natl Acad Sci U S A. 2002 Sep 3;99(18):11890-5.
70. Ueda T, Bruchovsky N, Sadar MD. Activation of the androgen receptor N-terminal domain by interleukin-6 via MAPK and STAT3 signal transduction pathways. J Biol Chem. 2002 Mar 1;277(9):7076-85.
71. Gemel J, Gorry M, Ehrlich GD, MacArthur CA. Structure and sequence of human FGF8. Genomics. 1996 Jul 1;35(1):253-7.
72. MacArthur CA, Lawshe A, Shankar DB, Heikinheimo M, Shackleford GM. FGF-8 isoforms differ in NIH3T3 cell transforming potential. Cell Growth Differ. 1995 Jul;6(7):817-25.

73. Mohammadi M, Froum S, Hamby JM, Schroeder MC, Panek RL, Lu GH, et al. Crystal structure of an angiogenesis inhibitor bound to the FGF receptor tyrosine kinase domain. Embo J. 1998 Oct 15;17(20):5896-904.
74. Perk J, Iavarone A, Benezra R. Id family of helix-loop-helix proteins in cancer. Nat Rev Cancer. 2005 Aug;5(8):603-14.
75. Leung HY, Dickson C, Robson CN, Neal DE. Over-expression of fibroblast growth factor-8 in human prostate cancer. Oncogene. 1996 Apr 18;12(8):1833-5.
76. Dorkin TJ, Robinson MC, Marsh C, Bjartell A, Neal DE, Leung HY. FGF8 over-expression in prostate cancer is associated with decreased patient survival and persists in androgen independent disease. Oncogene. 1999 Apr 29;18(17):2755-61.
77. Langenfeld EM, Langenfeld J. Bone morphogenetic protein-2 stimulates angiogenesis in developing tumors. Mol Cancer Res. 2004 Mar;2(3):141-9.
78. Passiatore G, Gentilella A, Rom S, Pacifici M, Bergonzini V, Peruzzi F. Induction of Id-1 by FGF-2 involves activity of EGR-1 and sensitizes neuroblastoma cells to cell death. J Cell Physiol. 2011 Jul;226(7):1763-70.
79. Yang L, Wang L, Lin HK, Kan PY, Xie S, Tsai MY, et al. Interleukin-6 differentially regulates androgen receptor transactivation via PI3K-Akt, STAT3, and MAPK, three distinct signal pathways in prostate cancer cells. Biochem Biophys Res Commun. 2003 Jun 6;305(3):462-9.
80. Gregory CW, Whang YE, McCall W, Fei X, Liu Y, Ponguta LA, et al. Heregulin-induced activation of HER2 and HER3 increases androgen receptor transactivation and CWR-R1 human recurrent prostate cancer cell growth. Clin Cancer Res. 2005 Mar 1;11(5):1704-12.
81. Ouyang XS, Wang X, Ling MT, Wong HL, Tsao SW, Wong YC. Id-1 stimulates serum independent prostate cancer cell proliferation through inactivation of p16(INK4a)/pRB pathway. Carcinogenesis. 2002 May;23(5):721-5.
82. Ling YX, Tao J, Fang SF, Hui Z, Fang QR. Downregulation of Id1 by small interfering RNA in prostate cancer PC3 cells in vivo and in vitro. Eur J Cancer Prev. 2011 Jan;20(1):9-17.
83. Mulholland DJ, Kobayashi N, Ruscetti M, Zhi A, Tran LM, Huang J, et al. Pten Loss and RAS/MAPK Activation Cooperate to Promote EMT and Metastasis Initiated from Prostate Cancer Stem/Progenitor Cells. Cancer Res. 2012 Mar 22.
84. Oka H, Chatani Y, Kohno M, Kawakita M, Ogawa O. Constitutive activation of the 41- and 43-kDa mitogen-activated protein (MAP) kinases in the progression of prostate cancer to an androgen-independent state. Int J Urol. 2005 Oct;12(10):899-905.
85. Rodriguez-Berriguete G, Fraile B, Martinez-Onsurbe P, Olmedilla G, Paniagua R, Royuela M. MAP Kinases and Prostate Cancer. J Signal Transduct. 2012;2012:169170.
86. Gioeli D, Mandell JW, Petroni GR, Frierson HF, Jr., Weber MJ. Activation of mitogen-activated protein kinase associated with prostate cancer progression. Cancer Res. 1999 Jan 15;59(2):279-84.
87. Zhong C, Saribekyan G, Liao CP, Cohen MB, Roy-Burman P. Cooperation between FGF8b overexpression and PTEN deficiency in prostate tumorigenesis. Cancer Res. 2006 Feb 15;66(4):2188-94.
88. Turner N, Grose R. Fibroblast growth factor signalling: from development to cancer. Nat Rev Cancer. 2010 Feb;10(2):116-29.
89. Tanaka A, Miyamoto K, Minamino N, Takeda M, Sato B, Matsuo H, et al. Cloning and characterization of an androgen-induced growth factor essential for the androgen-dependent growth of mouse mammary carcinoma cells. Proc Natl Acad Sci U S A. 1992 Oct 1;89(19):8928-32.
90. Song Z, Powell WC, Kasahara N, van Bokhoven A, Miller GJ, Roy-Burman P. The effect of fibroblast growth factor 8, isoform b, on the biology of prostate carcinoma cells and their interaction with stromal cells. Cancer Res. 2000 Dec 1;60(23):6730-6.
91. Maruyama-Takahashi K, Shimada N, Imada T, Maekawa-Tokuda Y, Ishii T, Ouchi J, et al. A neutralizing anti-fibroblast growth factor (FGF) 8 monoclonal antibody shows anti-tumor activity against

FGF8b-expressing LNCaP xenografts in androgen-dependent and -independent conditions. Prostate. 2008 May 1;68(6):640-50.
92. Gnanapragasam VJ, Robinson MC, Marsh C, Robson CN, Hamdy FC, Leung HY. FGF8 isoform b expression in human prostate cancer. Br J Cancer. 2003 May 6;88(9):1432-8.
93. Gnanapragasam VJ, Robson CN, Neal DE, Leung HY. Regulation of FGF8 expression by the androgen receptor in human prostate cancer. Oncogene. 2002 Aug 1;21(33):5069-80.
94. Wang Q, Stamp GW, Powell S, Abel P, Laniado M, Mahony C, et al. Correlation between androgen receptor expression and FGF8 mRNA levels in patients with prostate cancer and benign prostatic hypertrophy. J Clin Pathol. 1999 Jan;52(1):29-34.
95. Armstrong K, Robson CN, Leung HY. NF-kappaB activation upregulates fibroblast growth factor 8 expression in prostate cancer cells. Prostate. 2006 Aug 1;66(11):1223-34.
96. Brondani V, Klimkait T, Egly JM, Hamy F. Promoter of FGF8 reveals a unique regulation by unliganded RARalpha. J Mol Biol. 2002 Jun 7;319(3):715-28.
97. Feldman BJ, Feldman D. The development of androgen-independent prostate cancer. Nat Rev Cancer. 2001 Oct;1(1):34-45.
98. Ling MT, Wang X, Lee DT, Tam PC, Tsao SW, Wong YC. Id-1 expression induces androgen-independent prostate cancer cell growth through activation of epidermal growth factor receptor (EGF-R). Carcinogenesis. 2004 Apr;25(4):517-25.
99. Forootan SS, Wong YC, Dodson A, Wang X, Lin K, Smith PH, et al. Increased Id-1 expression is significantly associated with poor survival of patients with prostate cancer. Hum Pathol. 2007 Sep;38(9):1321-9.
100. Cox ME, Deeble PD, Lakhani S, Parsons SJ. Acquisition of neuroendocrine characteristics by prostate tumor cells is reversible: implications for prostate cancer progression. Cancer Res. 1999 Aug 1;59(15):3821-30.
101. Yuan TC, Veeramani S, Lin FF, Kondrikou D, Zelivianski S, Igawa T, et al. Androgen deprivation induces human prostate epithelial neuroendocrine differentiation of androgen-sensitive LNCaP cells. Endocr Relat Cancer. 2006 Mar;13(1):151-67.
102. Wright ME, Tsai MJ, Aebersold R. Androgen receptor represses the neuroendocrine transdifferentiation process in prostate cancer cells. Mol Endocrinol. 2003 Sep;17(9):1726-37.
103. Frigo DE, McDonnell DP. Differential effects of prostate cancer therapeutics on neuroendocrine transdifferentiation. Mol Cancer Ther. 2008 Mar;7(3):659-69.
104. Roudier MP, True LD, Higano CS, Vesselle H, Ellis W, Lange P, et al. Phenotypic heterogeneity of end-stage prostate carcinoma metastatic to bone. Hum Pathol. 2003 Jul;34(7):646-53.
105. True L, Coleman I, Hawley S, Huang CY, Gifford D, Coleman R, et al. A molecular correlate to the Gleason grading system for prostate adenocarcinoma. Proc Natl Acad Sci U S A. 2006 Jul 18;103(29):10991-6.
106. Morrissey C, True LD, Roudier MP, Coleman IM, Hawley S, Nelson PS, et al. Differential expression of angiogenesis associated genes in prostate cancer bone, liver and lymph node metastases. Clin Exp Metastasis. 2008;25(4):377-88.
107. Koreckij TD, Trauger RJ, Montgomery RB, Pitts TE, Coleman I, Nguyen H, et al. HE3235 inhibits growth of castration-resistant prostate cancer. Neoplasia. 2009 Nov;11(11):1216-25.
108. Tusher VG, Tibshirani R, Chu G. Significance analysis of microarrays applied to the ionizing radiation response. Proc Natl Acad Sci U S A. 2001 Apr 24;98(9):5116-21.

Vita

Eric Bluemn was born in Rock Springs, Wyoming and grew up in Chippewa Falls, Wisconsin. He attended college at the University of Minnesota Duluth where he graduated with a Bachelor of Science in Biology in 2005. Eric began his graduate studies in 2005 with the Medical Scientist Training Program at the University of Washington. He joined the Molecular and Cellular Biology program in 2007, graduating with a Doctorate of Philosophy in 2012.